Supplementary Information

for

Engineering Regioselectivity in the Hydrosilylation of Alkynes using Heterobimetallic Dual-Functional Hybrid Catalysts

Max Roemer, Sinead T. Keaveney, Vinicius R. Gonçales, Jiaxin Lian, Shreedhar Gautam, James E. Downes, J. Justin Gooding, Barbara A. Messerle

Correspondence to:

*max.roemer@sydney.edu.au
*barbara.messerle@mq.edu.au

Table of Contents

1. Syntheses

General

Experiments were conducted under an argon atmosphere unless stated otherwise. Starting materials and solvents were purchased from Sigma-Aldrich, AK Scientific, Honeywell and Merck. Carbon black (VXC72 R) was obtained from Cabot Corporation and used as the solid support for the heterobimetallic hybrid catalysts. THF was purified using an LC Technology Solution Inc. solvent purification system, and further dried by storage over 4 Å molecular sieves. The surface immobilization of the Rh and Ir hybrid catalysts and the catalysis experiments were conducted under an argon atmosphere (high purity Ar). NMR spectra were recorded on Bruker AV NEO 300 MHz and AV 400 MHz spectrometers, and the spectra were referenced to residual solvent signals.[1] All NMR spectra were recorded at 298 K.

Synthesis of the Rh and Ir Complexes

We reported the syntheses of the required ligands and Rh and Ir complexes for immobilization previously. Briefly, the metal precursor $[Rh(CO)_2Cl]_2$, $[RhCp^*Cl_2]_2$ or $[IrCp^*Cl_2]_2$ were reacted with the desired pyrazole-triazole ligand in dichloromethane. This was followed by addition of sodium tetrakis[3,5-bis(trifluoromethyl)phenyl]borate ($NaBAr^F{}_4$), leading to chloride abstraction and formation of the metal complexes used for surface immobilization in near quantitative yield.[2]

2. Surface Immobilization and Characterization

Simultaneous immobilization of Rh and Ir catalysts on carbon black (CB) was conducted as described in the following procedure. A Schlenk flask was charged with the specified amount of Rh- and Ir-based metal complexes and degassed nitromethane (10 mL). The solution was cooled to 0 °C before degassed hydrochloric acid (0.1 M, 0.5 mL) was added slowly under stirring, followed by sodium nitrite (4.8 mg, 0.07 mmol). Stirring was continued for another 10 min. CB (100 mg) was added and the mixture was stirred for 16 h at room temperature. Subsequently, the black mixture was transferred into glass centrifuge tubes and centrifuged for 20 min at 4000 rpm. The liquids were removed and discarded, and the remaining black solids were treated with three subsequent washing and centrifugation steps, with the solvent for washing being firstly methanol, then deionized water (MilliQ, 18 Ω), and finally methanol. Each step utilizes 8 mL for the washing, followed by centrifugation for 20 min at 4000 rpm, and discarding of the liquids. The obtained black solids were allowed to dry overnight at room temperature under air and finally dried under vacuum (~ 2.0 × 10^{-1} mbar), affording the heterobimetallic hybrid catalysts as black powders. The yields varied from 82 - 117 mg for the different batches of hybrid catalysts using 100 mg of CB in the grafting procedure (Table S1).

Table S1. Precursor ratios and isolated yields of the heterobimetallic hybrid catalysts.

Hybrid catalyst	Rh Complex	m [mg]	n [mol]	Ir Complex	m [mg]	n [mol]	CB [mg]	Yield [mg]
Rh/IrC$_{11}$–a	**Rh^{I}C$_{11}$**	50	0.035	**Ir^{III}C$_{11}$**	57	0.035	100	117
Rh/IrC$_{6}$–a	**Rh^{I}C$_{6}$**	48	0.035	**Ir^{III}C$_{6}$**	55	0.035	100	102
Rh/IrC$_{0}$–a	**Rh^{I}C$_{0}$**	44	0.035	**Ir^{III}C$_{0}$**	51	0.035	100	105
Rh/IrC$_{11}$–b	**Rh^{III}C$_{11}$**	54	0.035	**Ir^{III}C$_{11}$**	57	0.035	100	87
Rh/IrC$_{11}$–a2	**Rh^{I}C$_{11}$**	2.5	0.002	**Ir^{III}C$_{11}$**	2.9	0.002	50	35
Rh/IrC$_{11}$–a3	**Rh^{I}C$_{11}$**	2.5	0.002	**Ir^{III}C$_{11}$**	14.3	0.010	100	37

Characterization by X-ray Photoelectron Spectroscopy (XPS)

Characterization by X-ray photoelectron spectroscopy was performed on an ESCALab Xi (Thermo Scientific) spectrometer with a monochromatic Al Kα source. The pressure in the analysis chamber during measurements was < 10^{-8} mbar. The pass energy and step size for narrow scans were 20 eV and 0.1 eV, respectively. The take-off angle was normal to the sample surface. Spectral analysis was performed using Avantage 4.73 software and curve fitting was carried out with a mixture of Gaussian-Lorentzian functions. Peaks were calibrated to the carbon black C–C at 284.5 eV.

XPS survey and narrow band scans are shown in Figure S1 - Figure S5. Narrow band scans were conducted for the elements O, N, C, Rh or Ir, and for a number of measurements Cl and F were also included. We note that inclusion of Cl and F in the elemental composition has only a subtle effect on the overall metal concentration. For the sake of consistency, all metal concentrations are reported without inclusion of Cl and F. Determined elemental compositions are reported in Table S2 - Table S7.

Table S2. Elemental composition of **Rh/IrC$_{11}$–a** from XPS.

Element	Binding Energy [eV]	FWHM [eV]	FWHM [eV]	Atomic %
C1s	284.51	0.92	49240.39	54.29
C1s A	285.20	1.73	26743.58	29.49
C1s B	286.50	1.73	6389.34	7.05
O1s	532.30	2.53	9260.70	3.65
N1s	401.40	1.73	5443.87	3.62
N1s A	402.70	1.73	1158.49	0.77
N1s B	400.30	1.73	440.00	0.29
Ir4f7	63.05	1.47	476.60	0.07
Ir4f5	66.15	1.47	374.91	-
Rh3d5	310.38	2.15	6969.62	0.77
Rh3d3	315.09	2.15	3455.15	-
Ir4d3	313.38	1.92	968.450	-

Rh/IrC$_6$–a

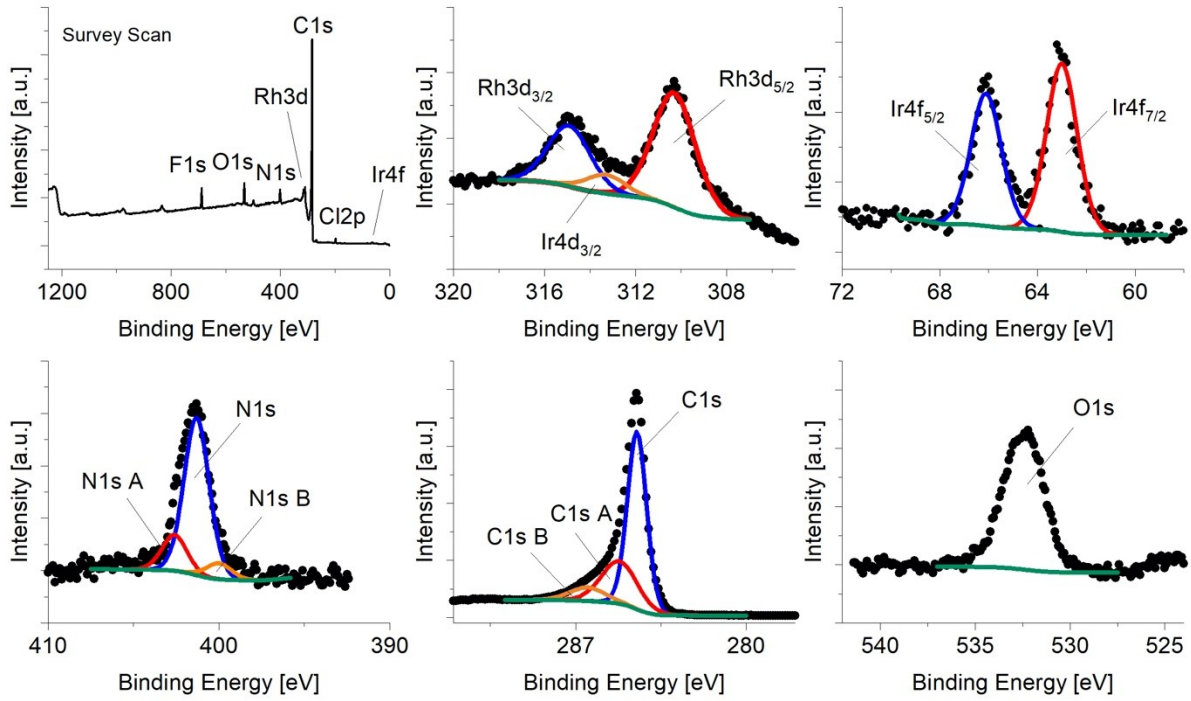

Figure S1. X-ray photoelectron spectra of the heterobimetallic hybrid catalyst **Rh/IrC$_6$–a.** Survey scan, narrow band scans for the $Rh3d_{3/2}$/$Rh3d_{5/2}$ signals, the $Ir4f_{5/2}$/$Ir4f_{7/2}$ signals, the N1s signal, the C1s signal and the O1s signal.

Table S3. Elemental composition of **Rh/IrC$_6$–a** from XPS.

Element	Binding Energy [eV]	FWHM [eV]	FWHM [eV]	Atomic %
C1s	284.48	0.93	62443.42	57.05
C1s A	285.20	1.73	27974.06	25.56
C1s B	286.50	1.73	8882.73	8.12
O1s	532.40	2.48	13125.93	4.29
N1s	401.30	1.73	5633.91	3.11
N1s A	402.60	1.73	1285.41	0.71
N1s B	400.00	1.73	575.04	0.32
Rh3d5	310.29	2.19	8281.83	0.76
Rh3d3	314.93	2.19	4383.75	-
Ir4d3	313.30	2.02	1262.57	-
Ir4f7	63.00	1.48	770.05	0.09
Ir4f5	66.10	1.48	605.75	-

Rh/IrC$_0$–a

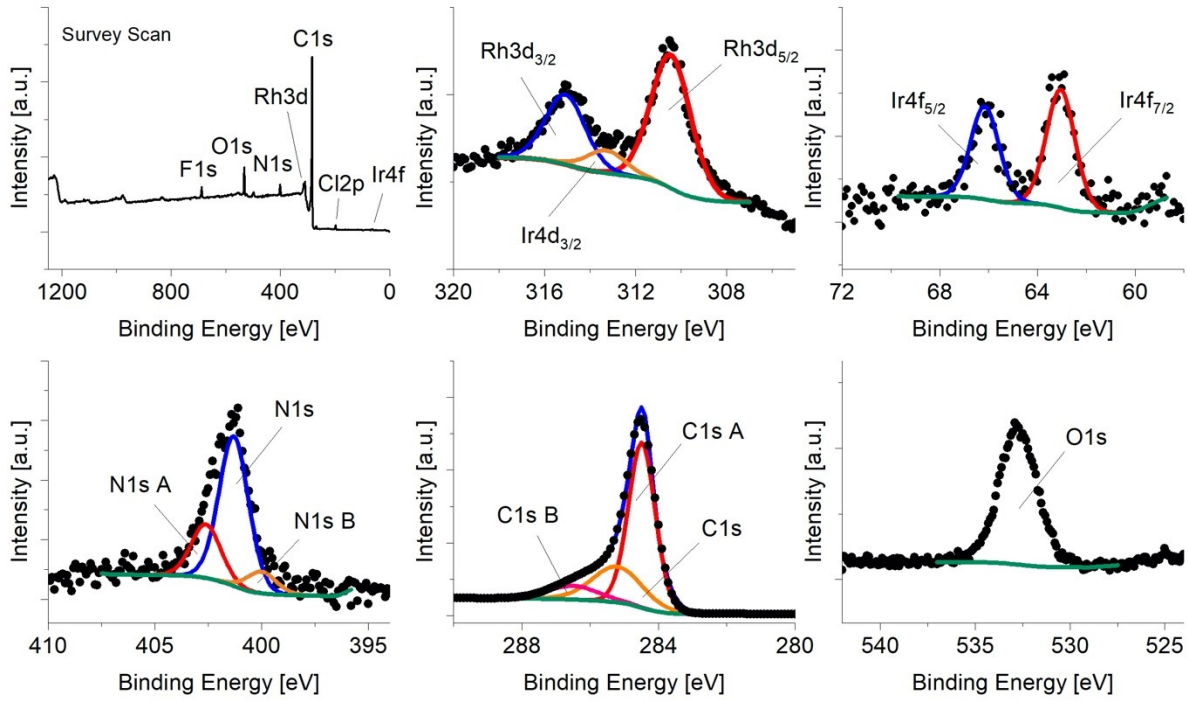

Figure S2. X-ray photoelectron spectra of the heterobimetallic hybrid catalyst **Rh/IrC$_0$–a**. Survey scan, narrow band scans for the Rh3d$_{3/2}$/Rh3d$_{5/2}$ signals, the Ir4f$_{5/2}$/Ir4f$_{7/2}$ signals, the N1s signal, the C1s signal and the O1s signal.

Table S4. Elemental composition of **Rh/IrC$_0$–a** from XPS.

Element	Binding Energy [eV]	FWHM [eV]	FWHM [eV]	Atomic %
C1s	284.49	0.93	22745.92	55.76
C1s A	285.20	1.73	9210.32	22.58
C1s B	286.50	1.73	3555.35	8.72
O1s	532.74	2.32	8110.14	7.11
N1s	401.30	1.63	2217.81	3.28
N1s A	402.60	1.63	795.39	1.18
N1s B	400.00	1.63	318.29	0.47
Rh3d5	310.44	2.06	3405.23	0.83
Rh3d3	315.08	2.06	1777.92	-
Ir4d3	313.30	2.02	568.32	-
F1s	688.68	2.05	3231.29	-
Ir4f7	63.05	1.38	205.8	0.06
Ir4f5	66.15	1.38	161.89	-

Rh/IrC$_{11}$–a2

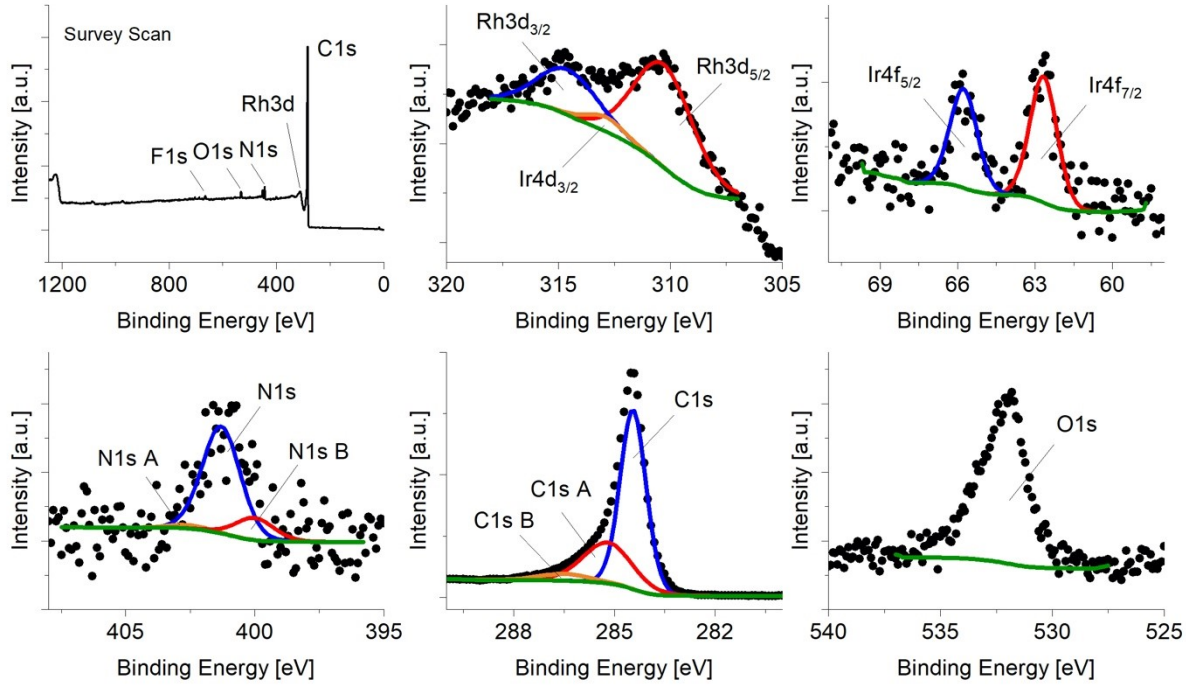

Figure S3. X-ray photoelectron spectra of the heterobimetallic hybrid catalyst **Rh/IrC$_{11}$–a2**. Survey scan, narrow band scans for the Rh3d$_{3/2}$/Rh3d$_{5/2}$ signals, the Ir4f$_{5/2}$/Ir4f$_{7/2}$ signals, the N1s signal, the C1s signal and the O1s signal.

Table S5. Elemental composition of **Rh/IrC$_{11}$–a2** from XPS.

Element	Binding Energy [eV]	FWHM [eV]	FWHM [eV]	Atomic %
C1s	284.43	0.92	32633.69	73.20
C1s A	285.20	1.73	8588.85	19.27
C1s B	286.50	1.73	1725.28	3.87
O1s	532.03	2.55	2823.13	2.26
N1s	401.30	1.73	584.77	0.79
N1s A	402.60	1.73	17.78	0.02
N1s B	400.00	1.73	121.44	0.16
Rh3d5	310.29	3.12	1759.84	0.39
Rh3d3	314.55	3.12	777.59	-
Ir4d3	312.90	2.02	159.73	-
Ir4f7	62.67	1.24	65.86	0.02
Ir4f5	65.77	1.24	51.81	-

Rh/IrC$_{11}$–a3

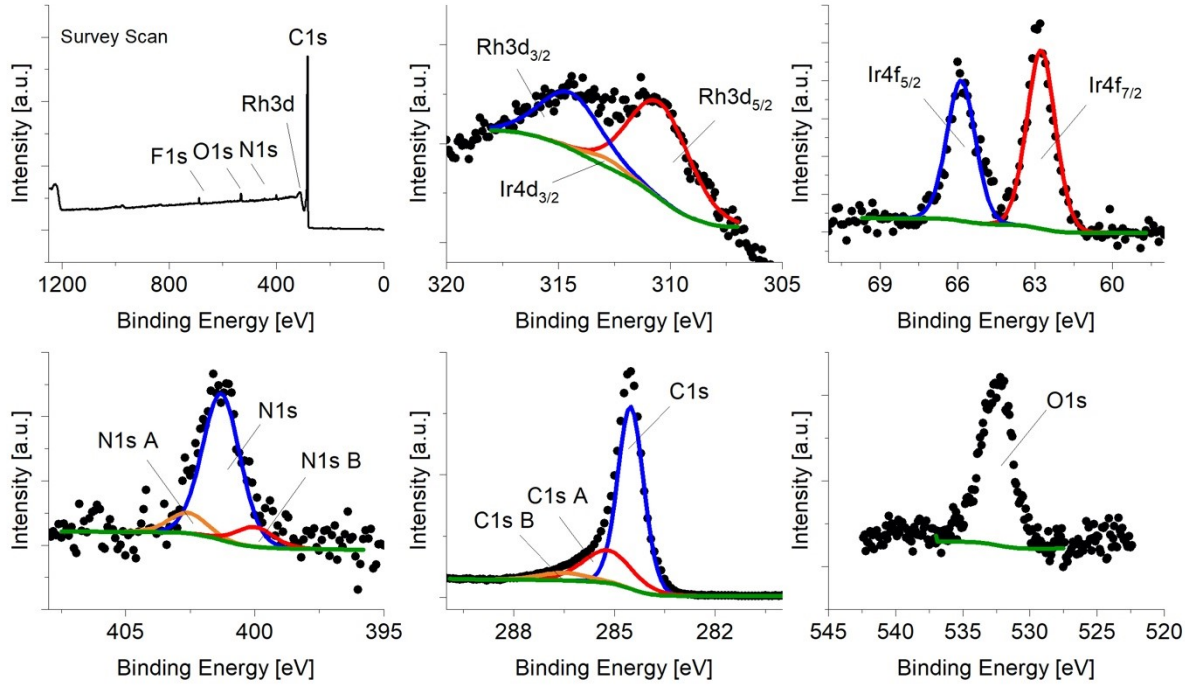

Figure S4. X-ray photoelectron spectra of the heterobimetallic hybrid catalyst **Rh/IrC$_{11}$–a3**. Survey scan, narrow band scans for the Rh3d$_{3/2}$/Rh3d$_{5/2}$ signals, the Ir4f$_{5/2}$/Ir4f$_{7/2}$ signals, the N1s signal, the C1s signal and the O1s signal.

Table S6. Elemental composition of **Rh/IrC$_{11}$–a3** from XPS.

Element	Binding Energy [eV]	FWHM [eV]	FWHM [eV]	Atomic %
C1s	284.51	0.92	29483.11	67.13
C1s A	285.20	1.73	9985.38	22.74
C1s B	286.50	1.73	2310.92	5.26
O1s	532.34	2.67	3562.27	2.9
N1s	401.30	1.72	849.41	1.17
N1s A	402.60	1.72	118.92	0.16
N1s B	400.00	1.72	114.02	0.16
Rh3d5	310.48	3.22	1689.1	0.38
Rh3d3	314.43	3.22	988.75	-
Ir4d3	312.90	2.02	91.94	-
Ir4f7	62.76	1.30	331.85	0.1
Ir4f5	65.86	1.30	261.04	-

Rh/IrC$_{11}$–b

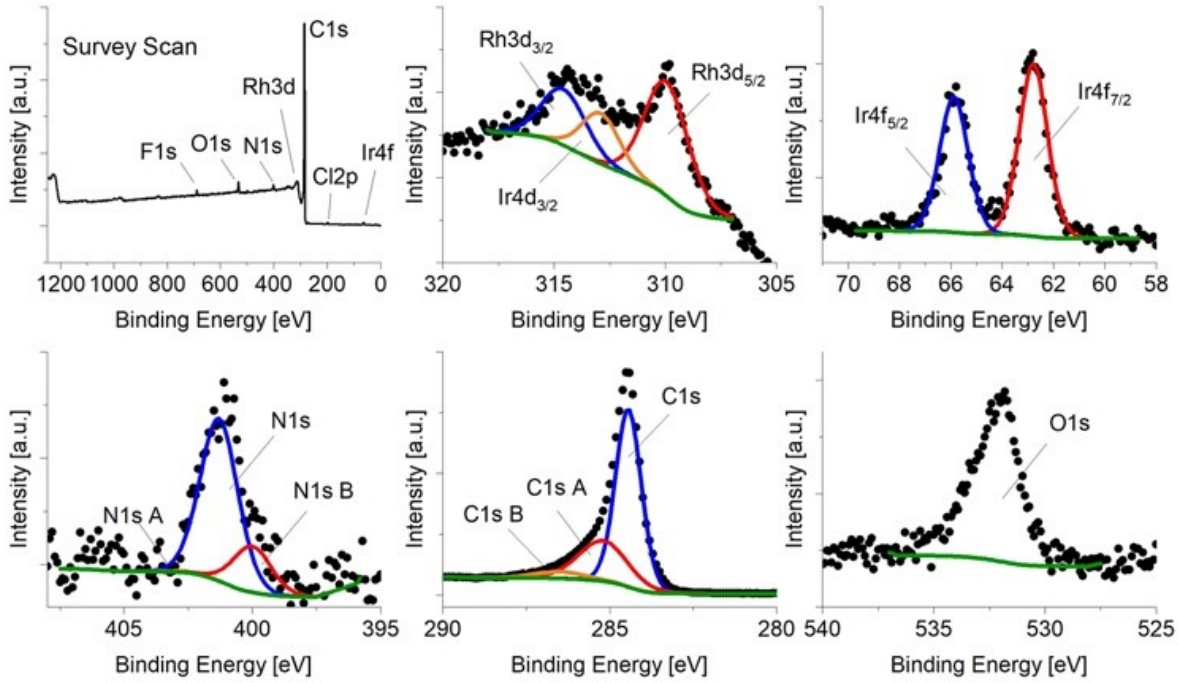

Figure S5. X-ray photoelectron spectra of the hybrid catalyst **Rh/IrC$_{11}$–b**. Survey scan, narrow band scans for the Rh3d$_{3/2}$/Rh3d$_{5/2}$ signals, the Ir4f$_{5/2}$/Ir4f$_{7/2}$ signals, the N1s signal, the C1s signal and the O1s signal.

Table S7. Elemental composition of **Rh/IrC$_{11}$–b** from XPS.

Element	Binding Energy [eV]	FWHM [eV]	FWHM [eV]	Atomic %
C1s	284.44	0.91	28912.16	61.6
C1s A	285.20	1.73	12464.06	26.56
C1s B	286.50	1.73	2052.36	4.37
O1s	532.02	2.29	3950.55	3.01
N1s	401.30	1.73	1432.19	1.84
N1s A	402.60	1.73	9.88	0.01
N1s B	400.00	1.73	406.24	0.52
Rh3d5	309.94	2.32	1686.89	0.36
Rh3d3	314.57	2.32	829.47	-
Ir4d3	312.90	2.02	647.46	-
F1s	688.50	1.87	1895.68	1.1
Cl2p3	198.22	2.12	434.61	0.5
Cl2p1	199.92	2.12	223.06	-
Ir4f7	62.79	1.30	428.74	0.12
Ir4f5	65.89	1.30	337.26	-

Characterization by Energy Dispersive X-ray Spectroscopy (EDX)

SEM/EDX: Scanning electron microscope (SEM) images and EDX spectra were acquired using a Zeiss EVO MA15 Scanning electron microscope equipped with Oxford Instruments Aztec Synergy EDS/EBSD. The hybrid catalyst (~ 1-2 mg), in the form of a black powder, was placed onto a round and flat sample holder equipped with double sided adhesive tape. The sample was pressed onto the tape using a spatula, and any non-attached powder was carefully removed using a gentle stream of air. Sample holders were mounted on a revolving holder disc, which was placed in the chamber and evacuated. Calibration was carried out using a copper standard and the sample to detector distance was 12 mm using an energy of 12.5 keV.

Initially, the sample was screened by SEM and flat areas were identified. For determination of elemental compositions, typically five to six areas were selected and scanned. This was followed by EDX area mapping. Analyses were performed with the Oxford Instruments AZtec software package. Data deconvolution and background removal was performed with AZtec TruMap. Determined elemental concentrations by EDX are reported in Table S8 - Table S19 below.

Table S8. Elemental composition of **Rh/IrC$_{11}$–a** from EDX in atomic %.

Element	Area 1	Area 2	Area 3	Area 4	Area 5	Average
C	95.15	95.54	96.05	95.78	95.41	95.59
O	3.00	2.67	2.22	2.49	2.83	2.64
S	0.40	0.38	0.40	0.36	0.34	0.38
Cl	0.94	0.92	0.94	0.91	0.94	0.93
Rh	0.44	0.42	0.36	0.42	0.41	0.41
Ir	0.06	0.07	0.04	0.03	0.06	0.05

Table S9. Elemental composition of **Rh/IrC$_{11}$–a** from EDX in weight %.

Element	Area 1	Area 2	Area 3	Area 4	Area 5	Average
C	88.25	88.84	90.19	89.58	88.86	89.14
O	3.70	3.31	2.78	3.11	3.52	3.28
S	0.99	0.95	0.99	0.89	0.85	0.93
Cl	2.57	2.51	2.60	2.52	2.60	2.56
Rh	3.53	3.35	2.87	3.38	3.30	3.29
Ir	0.96	1.03	0.57	0.52	0.87	0.79

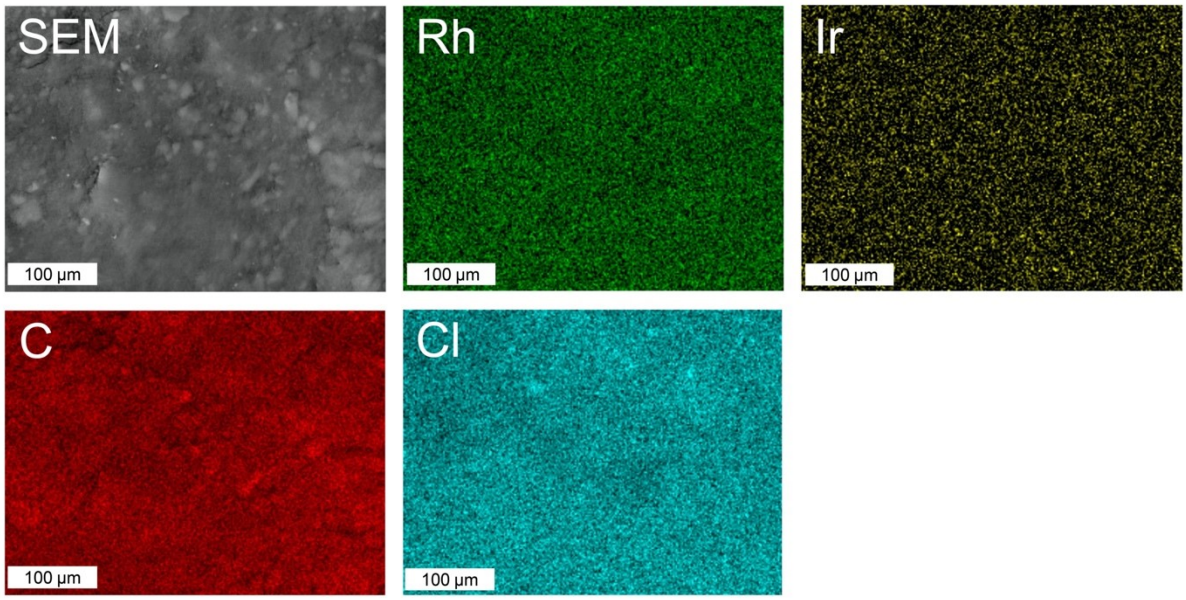

Figure S6. SEM image and EDX maps for Rh, Ir, C and Cl of the heterobimetallic hybrid catalyst **Rh/IrC$_6$–a.**

Table S10. Elemental composition of **Rh/IrC$_6$–a** from EDX in atomic %.

Element	Area 1	Area 2	Area 3	Area 4	Area 5	Average
C	92.96	92.95	93.46	93.14	92.85	92.96
O	5.26	5.33	4.64	5.09	5.48	5.26
S	0.44	0.43	0.47	0.45	0.45	0.44
Cl	0.86	0.82	0.91	0.85	0.79	0.86
Rh	0.41	0.39	0.43	0.41	0.36	0.41
Ir	0.06	0.07	0.08	0.06	0.07	0.06

Table S11. Elemental composition of **Rh/IrC$_6$–a** from EDX in weight %.

Element	Area 1	Area 2	Area 3	Area 4	Area 5	Average
C	85.89	85.99	86.02	86.12	86.06	86.02
O	6.47	6.57	5.69	6.27	6.77	6.35
S	1.09	1.07	1.15	1.11	1.12	1.11
Cl	2.35	2.25	2.47	2.33	2.15	2.31
Rh	3.27	3.06	3.43	3.25	2.85	3.17
Ir	0.93	1.06	1.23	0.92	1.06	1.04

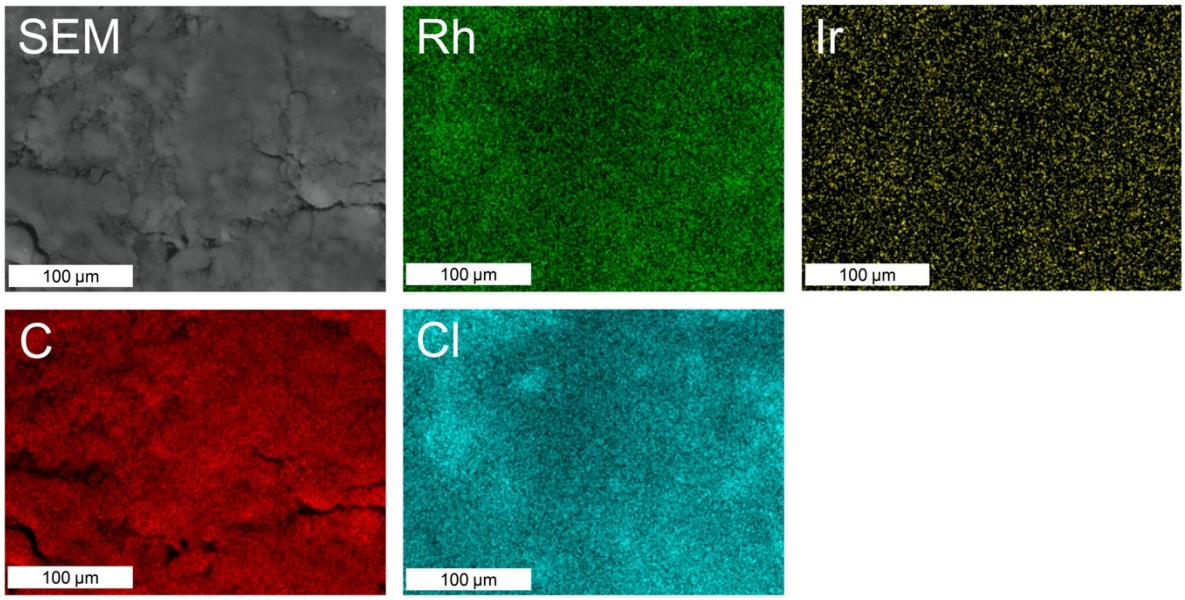

Figure S7. SEM image and EDX maps for Rh, Ir, C and Cl of the heterobimetallic hybrid catalyst **Rh/IrC$_0$–a**.

Table S12. Elemental composition of **Rh/IrC$_0$–a** from EDX in atomic %.

Element	Area 1	Area 2	Area 3	Area 4	Area 5	Average
C	91.46	92.50	93.00	92.79	92.65	92.48
O	6.76	5.51	5.12	5.60	5.35	5.67
S	0.43	0.42	0.43	0.40	0.43	0.42
Cl	0.89	1.04	0.96	0.80	1.04	0.95
Rh	0.39	0.48	0.43	0.35	0.47	0.42
Ir	0.07	0.06	0.06	0.06	0.06	0.06

Table S13. Elemental composition of **Rh/IrC$_0$–a** from EDX in weight %.

Element	Area 1	Area 2	Area 3	Area 4	Area 5	Average
C	84.16	84.80	85.75	86.16	84.97	85.17
O	8.29	6.73	6.29	6.93	6.53	6.95
S	1.05	1.02	1.07	0.99	1.05	1.04
Cl	2.42	2.81	2.62	2.19	2.80	2.57
Rh	3.08	3.74	3.39	2.80	3.71	3.34
Ir	1.00	0.91	0.88	0.94	0.93	0.93

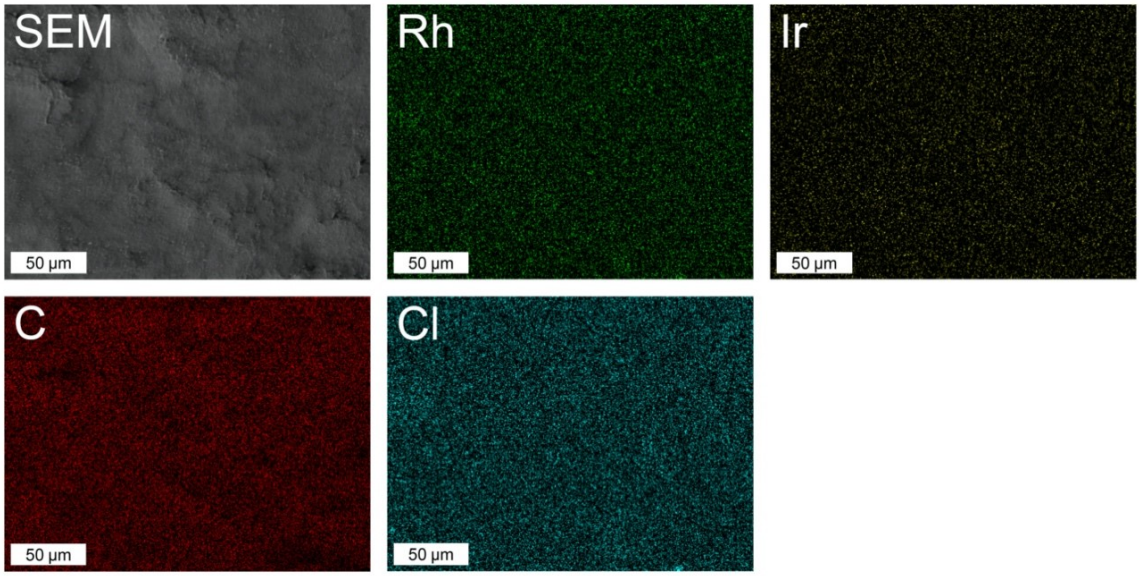

Figure S8. SEM image and EDX maps for Rh, Ir, C and Cl of the heterobimetallic hybrid catalyst **Rh/IrC11–a2.**

Table S14. Elemental composition of **Rh/IrC$_{11}$–a2** from EDX in atomic %.

Element	Area 1	Area 2	Area 3	Area 4	Area 5	Area 6	Area 7	Average
C	94.66	95.46	94.98	94.83	95.16	94.6	95.23	94.99
O	4.4	3.59	4.11	4.21	3.89	4.44	3.84	4.07
S	0.48	0.48	0.47	0.51	0.51	0.49	0.48	0.49
Cl	0.32	0.34	0.32	0.32	0.32	0.35	0.33	0.33
Rh	0.11	0.09	0.1	0.08	0.1	0.1	0.08	0.09
Ir	0.04	0.04	0.03	0.05	0.02	0.03	0.04	0.04

Table S15. Elemental composition of **Rh/IrC$_{11}$–a2** from EDX in weight %.

Element	Area 1	Area 2	Area 3	Area 4	Area 5	Area 6	Area 7	Average
C	90.76	91.83	91.42	91	91.68	90.85	91.65	91.31
O	5.61	4.59	5.27	5.38	5	5.68	4.92	5.21
S	1.23	1.25	1.21	1.3	1.31	1.25	1.24	1.26
Cl	0.9	0.97	0.9	0.92	0.9	0.98	0.93	0.93
Rh	0.87	0.73	0.79	0.69	0.86	0.84	0.69	0.78
Ir	0.61	0.63	0.41	0.72	0.25	0.4	0.56	0.51

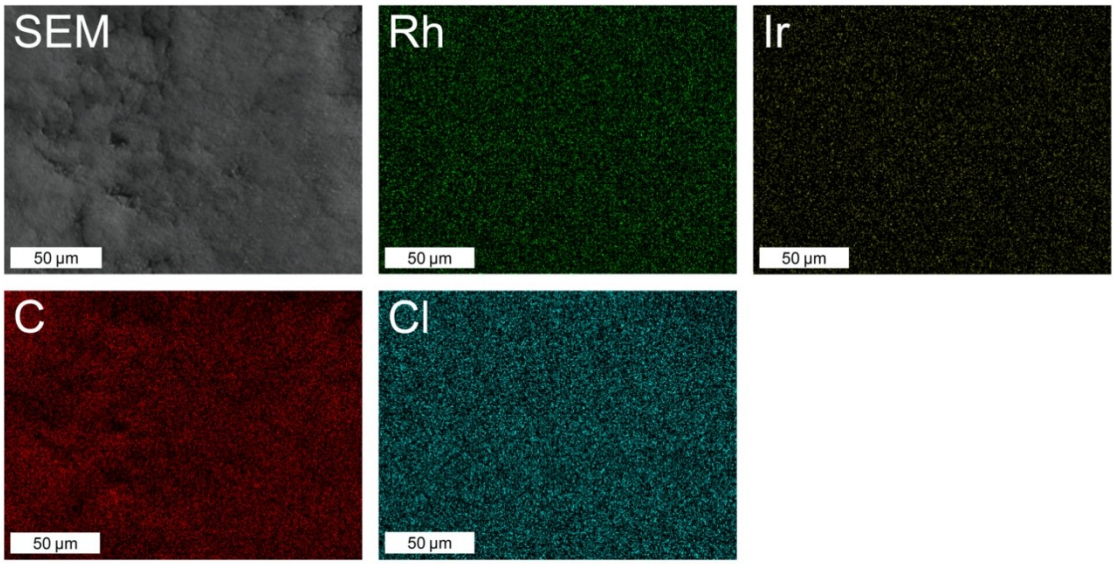

Figure S9. SEM image and EDX maps for Rh, Ir, C and Cl of the heterobimetallic hybrid catalyst **Rh/IrC$_{11}$–a3**.

Table S16. Elemental composition of **Rh/IrC$_{11}$–a3** from EDX in atomic %.

Element	Area 1	Area 2	Area 3	Area 4	Area 5	Average
C	95.61	95.34	95.44	95.64	95.57	95.52
O	3.41	3.43	3.41	3.32	3.24	3.36
S	0.46	0.56	0.51	0.49	0.53	0.51
Cl	0.37	0.47	0.44	0.36	0.48	0.42
Rh	0.05	0.06	0.09	0.07	0.07	0.07
Ir	0.1	0.14	0.1	0.13	0.11	0.12

Table S17. Elemental composition of **Rh/IrC$_{11}$–a3** from EDX in weight %.

Element	Area 1	Area 2	Area 3	Area 4	Area 5	Average
C	91.55	90.3	90.87	91.06	90.92	90.94
O	4.36	4.33	4.33	4.21	4.1	4.27
S	1.19	1.41	1.3	1.25	1.35	1.30
Cl	1.05	1.32	1.25	1.02	1.35	1.20
Rh	0.37	0.51	0.75	0.55	0.54	0.54
Ir	1.48	2.13	1.5	1.91	1.74	1.75

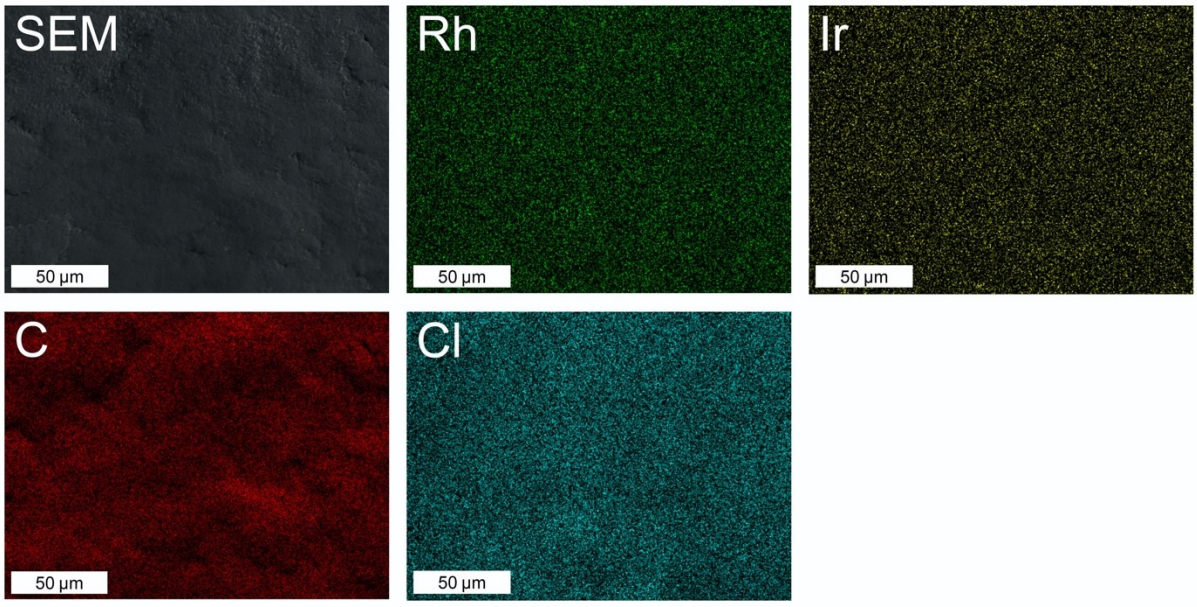

Figure S10. SEM image and EDX maps for Rh, Ir, C and Cl of the heterobimetallic hybrid catalyst **Rh/IrC$_{11}$–b.**

Table S18. Elemental composition of **Rh/IrC$_{11}$–b** from EDX in atomic %.

Element	Area 1	Area 2	Area 3	Area 4	Area 5	Average
C	95.04	95.04	94.96	94.53	94.71	94.86
O	3.03	2.96	3.28	3.83	3.39	3.30
S	0.75	0.77	0.68	0.64	0.74	0.72
Cl	0.73	0.78	0.65	0.61	0.71	0.70
Rh	0.20	0.20	0.19	0.20	0.21	0.20
Ir	0.24	0.25	0.23	0.20	0.23	0.23

Table S19. Elemental composition of **Rh/IrC$_{11}$–b** from EDX in weight %.

Element	Area 1	Area 2	Area 3	Area 4	Area 5	Average
C	87.29	87.17	87.61	87.51	87.01	87.32
O	3.71	3.61	4.04	4.72	4.15	4.05
S	1.85	1.89	1.67	1.58	1.83	1.76
Cl	1.99	2.11	1.78	1.66	1.91	1.89
Rh	1.59	1.56	1.48	1.58	1.65	1.57
Ir	3.58	3.66	3.41	2.95	3.45	3.41

Characterization by X-ray Absorption Spectroscopy (XAS)

XAS measurements were performed at the XAS beamline at the Australian Synchrotron. XANES and EXAFS data were recorded at the Rh-K edge (~23.2 keV) and the Ir L_3 edge (~ 11.2 keV) in separate experiments for the heterobimetallic hybrid catalysts.

Sample Preparation and Measurement

The heterobimetallic hybrid catalysts (~ 70 mg), **Rh/IrC$_{11}$–a**, **Rh/IrC$_6$–a**, **Rh/IrC$_0$–a** and **Rh/IrC$_{11}$–b**, were pressed into a pellet (7 mm) using a hydraulic press with a force of 3t and subsequently mounted on 7 mm sample holders and secured with Kapton tape. The sample holders were mounted on an autosampler, which was placed into the sample chamber of the XAS beamline (Hutch B) and subsequently measured. The Rh samples were measured twice, and the Ir samples were measured once.

Rh- and Ir EXAFS data was recorded on separate freshly prepared pellets for each of the samples. The recorded spectra were aligned to internal Rh and Ir standards, and for data processing and handling the Athena software was used.

Fitting

We fitted the experimental EXAFS data obtained for the heterobimetallic hybrid catalysts versus data obtained from FEFF calculations involving the cationic Rh and Ir fragments of the respective complexes, using the Artemis software package.[3] For this we utilized known crystal structures of each of the complexes,[4, 5] using only the scattering paths with significant overall contributions. These were typically eight paths, involving the nearest neighbouring atoms.

We have established in earlier works that the set of $Ir^{III}C_n$ (n = 11, 6, 0) and **$Rh^{III}C_{11}$** precursor complexes, which bear all the Cp*/Cl co-ligands, do maintain their structure during the immobilization procedure with good fits obtained for all systems before and after immobilization. In contrast, the head-groups of $Rh^{I}C_n$ (n = 11, 6, 0), which bear the CO ligands, are transformed to the $Rh(PyT)_2X_2$ groups, which are a complex mixture of different isomers and co-ligands. We surmise that fitting separately the Ir and Rh sites is a reasonable avenue to analyse the obtained Rh K edge and Ir L_3 edge data of the heterobimetallic complexes.

Firstly, we have fitted the Ir L_3 edge data of the first coordination shell of **Rh/IrC$_{11}$–a** and **Rh/IrC$_0$–a** to the cationic Ir fragments (IrCp*Cl). Starting guess values for the refinement for selected scattering path were: σ^2 = 0.003; Amplitude factor = 1, delr = 0 and E_0 = 0. We implemented for some scattering paths restraints on the Debye-Waller factors (σ^2), which improved the overall quality of the fits. The calculated bond distance from FEFF for the first coordination shell, i.e. the two binding N atoms, five C atoms of the Cp* ring and, the Cl atoms and the fitting parameters are reported in Table S20. N denotes the coordination number for each atom in the relevant scattering path. Fourier transformed EXAFS data (k^2 weighted) for **Rh/IrC$_{11}$–a** and **Rh/IrC$_0$–a** is shown in Figure S11 and Figure S12.

Both fits of R space are of good quality with no indication of significant changes compared to the monometallic catalysts. This suggests that the presence of adjacent surface bound Rh complexes does not affect electronics of the Ir sites, which is perhaps unsurprising given the large through bond distances between each metal centre. Furthermore, through space interactions appear to be absent too, or insignificantly small, as there is no observed difference for the long the chain C_{11}–derivatives and the short tether C_0–derivatives.

Secondly, we fitted the Rh K-edge data of **Rh/IrC$_{11}$–b** using the X-ray data of the cationic RhCp*Cl fragment. We applied the same fitting parameters as above, which resulted again in a good fit, Figure S13. Again, there were no differences to the monometallic analogue,[2] thus leading to the same conclusions as elaborated above.

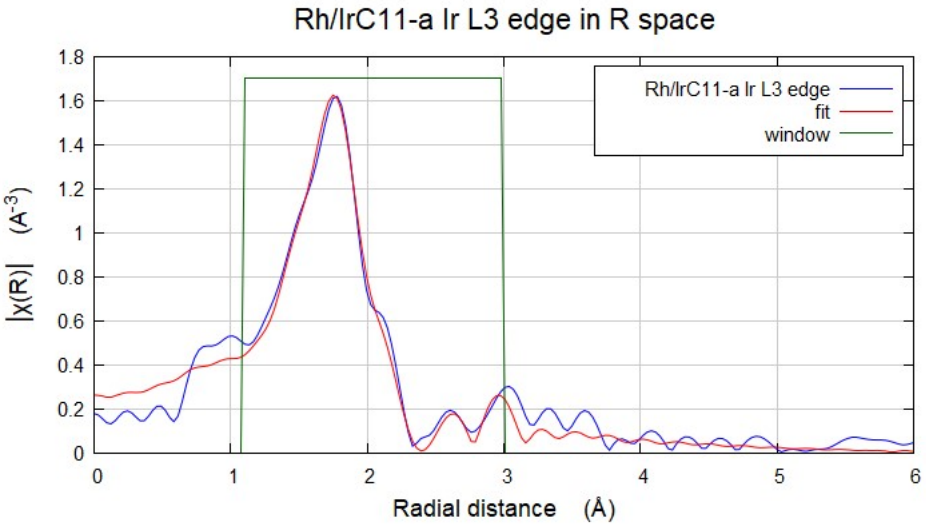

Figure S11. Fourier transformed EXAFS data (k^2 weighted) **Rh/IrC$_{11}$–a** showing the experimental data and obtained fit, and the applied fitting window.

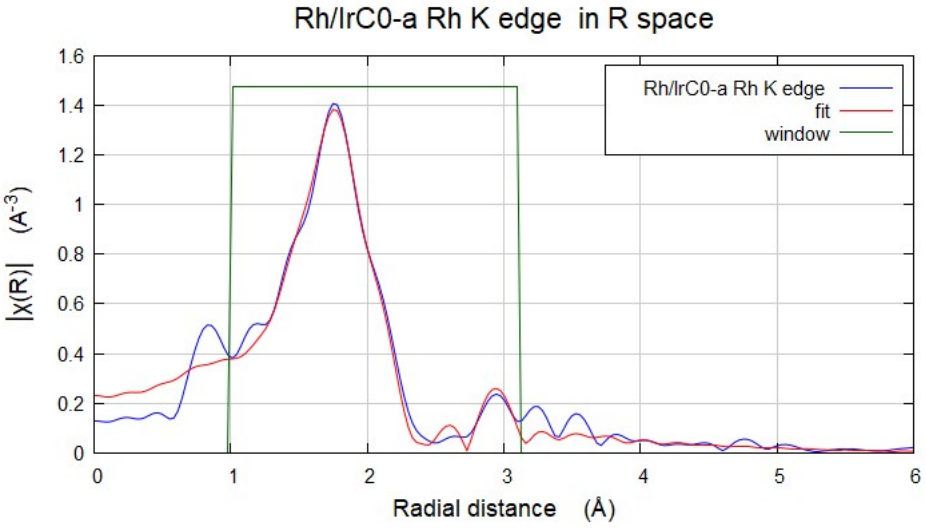

Figure S12. Fourier transformed EXAFS data (k^2 weighted) **Rh/IrC$_0$–a** showing the experimental data and obtained fit, and the applied fitting window.

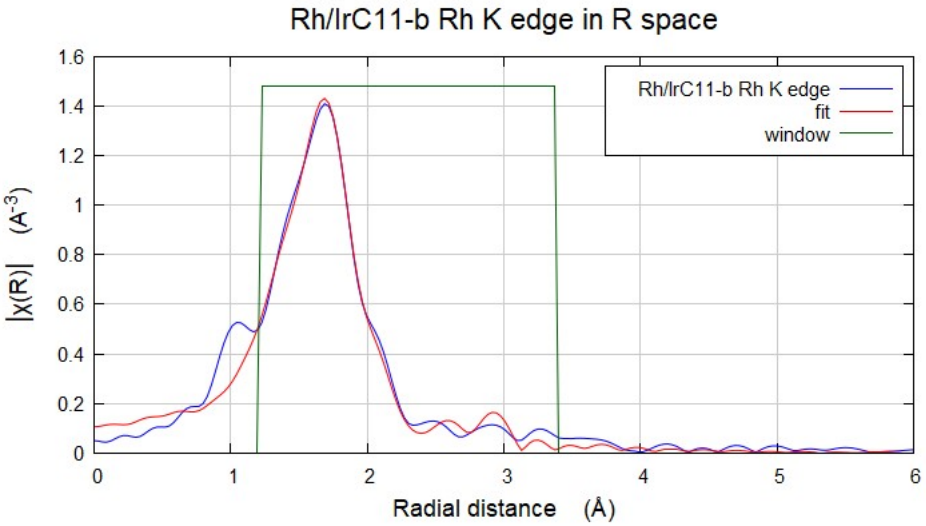

Figure S13. Fourier transformed EXAFS data (k^2 weighted) **Rh/IrC$_{11}$–b** showing the experimental data and obtained fit, and the applied fitting window.

Table S20. Summary of refined parameters for the first coordination shell fit for the heterobimetallic hybrid catalysts Rh/IrC$_n$–a (n = 11, 0) and **Rh/IrC$_{11}$–b** involving the major scattering paths calculated from FEFF and experimental EXAFS data at the Ir L_3 edge and the Rh K-edge.

Hybrid Catalyst	Bond	N	Bond length [Å]	σ^2	E_0 [eV]	R-factor
Ir L_3 edge						
Rh/IrC$_{11}$–a	Ir-N (PyT, 2N)	2	2.094	0.007(4)	9.00 +/- 1.01	0.010
	Ir-C (Cp*, 5C)	5	2.154	0.003(1)		
	Ir-Cl	1	2.379	0.004(2)		
Rh/IrC$_0$–a	Ir-N (PyT, 2N)	2	2.094	0.011(7)	8.54 +/- 0.90	0.010
	Ir-C (Cp*, 5C)	5	2.154	0.004(1)		
	Ir-Cl	1	2.379	0.003(1)		
Rh K edge						
Rh/IrC$_{11}$–b	Rh-N (PyT, 2N)	2	2.093	0.003[a]	-0.30 +/- 1.33	0.020
	Rh-C (Cp*, 5C)	5	2.153	0.004(2)		
	Rh-Cl	1	2.377	0.003(2)		

[a] σ^2 was set to the reported value

Thirdly, we have fitted the Rh sites of the heterobimetallic catalysts of type Rh/IrC$_n$–a. As established previously, the CO ligands are absent in the hybrid catalysts.[2] The samples are composed of two PyT-ligands and two co-ligands (Cl, NO_2, NO_3 or OH) coordinated to one Rh. We have conducted a first shell fitting for the samples, using only the first shell N scattering path with a set amplitude factor of 0.6

for **Rh/IrC$_{11}$–a**, **Rh/IrC$_6$–a** and **Rh/IrC$_0$–a**, and the following guess starting values: σ^2 = 0.003, E_0 = 0, delr = 0 in order to calculate the coordination number. This model ignores the co-ligands X_1/X_2 and only focuses on the first shell possibly explaining the high R factors, while the obtained coordination numbers are six with the chosen starting guess values.

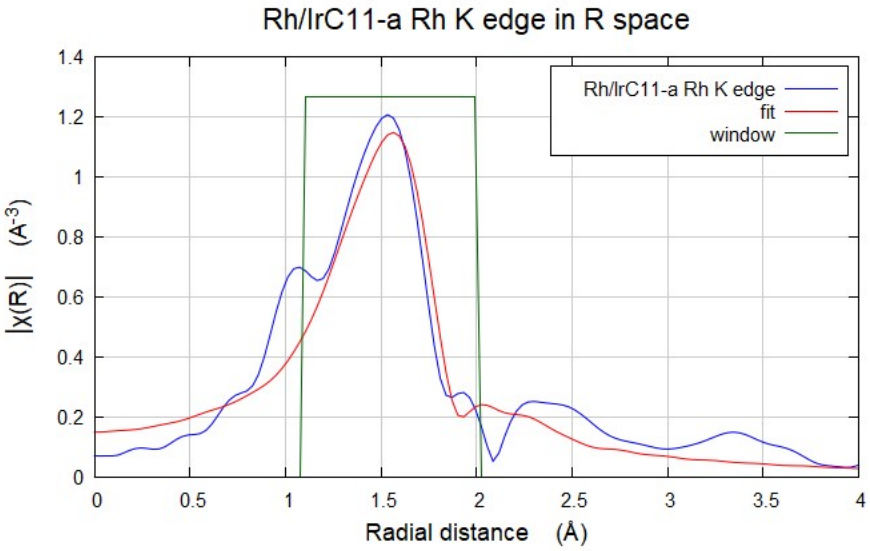

Figure S14. Fourier transformed EXAFS data in R space, Rh K edge (k^2 weighted), **Rh/IrC$_{11}$–a** showing the experimental data and obtained fit, and the applied fitting window.

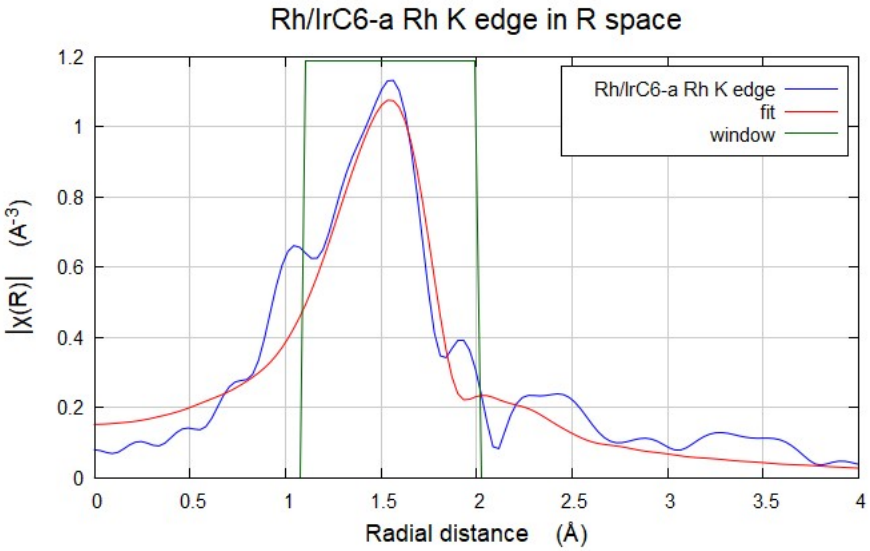

Figure S15. Fourier transformed EXAFS data in R space, Rh K edge (k^2 weighted), **Rh/IrC$_6$–a** showing the experimental data and obtained fit, and the applied fitting window.

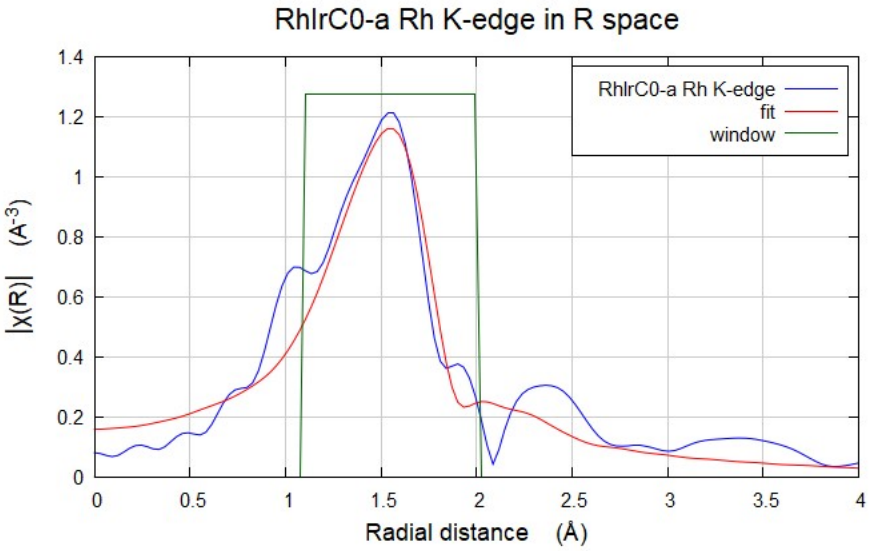

Figure S16. Fourier transformed EXAFS data in R space, Rh K edge (k^2 weighted), **Rh/IrC$_0$–a** showing the experimental data and obtained fit, and the applied fitting window.

Table S21. Summary of refined parameters for the first coordination shell from the fit for Rh/IrC$_n$–a (n = 11, 6, 0) involving the major scattering paths.

Hybrid Catalyst	Bond	Coordination Number	Bond length [Å]	σ^2	E_0 [eV]	S_0^2	R-factor
Rh/IrC$_{11}$–a	Rh-N (PyT, 2N)	5.92 +/- 0.91	2.070	0.007(2)	0.74 +/- 0.87	0.6	0.050
Rh/IrC$_6$–a	Rh-N (PyT, 2N)	6.36 +/- 0.97	2.070	0.009(2)	0.52 +/- 0.81	0.6	0.050
Rh/IrC$_0$–a	Rh-N (PyT, 2N)	6.73 +/- 0.97	2.070	0.008(2)	0.37 +/- 0.78	0.6	0.039

Thermogravimetric Analyses (TGA)

Thermogravimetric analyses were conducted using a TA Instruments thermogravimetric analyzer, equipped with an autosampler. The hybrid catalyst (~ 3 mg) was weighed into a flame treated and tared Pt pan and placed into the TGA analyzer. Each sample was heated from room temperature to 700 °C with a heating rate of 20°C/min under N_2. The weight loss was monitored over time. Data of a control sample of the same batch of CB used in the current study, and treated under grafting conditions under absence of a metal complex, was reported previously.[2]

3. Catalysis Experiments

Catalysis experiments were conducted in custom built centrifugable Schlenk tubes with Young PTFE valves. The tubes were oven dried, equipped with a magnetic stirring bar, evacuated and refilled with Ar before the catalyst was added. This was followed by addition of solvent, the substrate and triethylsilane. The tube was sealed and heated to the specified amount of time under stirring. Subsequently, the tube was allowed to cool down to room temperature and the black suspension was centrifuged at 4000 rpm. For the reactions performed in THF, the clear solution was transferred to a round bottom flask using a glass pipette and concentrated to dryness using a rotary evaporator. The product mixtures were briefly dried under vacuum, dissolved in chloroform-*d* and analysed by ^{1}H NMR spectroscopy. For the reaction runs in toluene-d^{8}, the crude mixture was analysed without solvent removal by ^{1}H NMR spectroscopy.

In addition, several samples were analysed by GC-MS. GC-MS analysis of the catalysis run were conducted on a PerkinElmer Clarus 680 with Clarus SQ 8 C mass spectrometer equipped with EI source. The GC column was a Phenomenex Zebron ZB-5 ms 30 m x 0.25 mm id x 250 μm film thickness. The injected volume was 5μL with 250 °C heating at the injection port. The carrier gas was He with at 1.3 mL/min constant flow with a 10:1 split ratio. The oven program was: 40 °C, held for 5 minutes, and then increased at 50 °C /min to 250 °C, then held for 5 minutes. The MS electron energy was 70 eV in positive EI mode with a solvent delay of 4 min. The MS scan range was 45-620 m/z with a 0.2 s scan time and 0.1 s inter-scan delay.

Hydrosilylation of Phenylacetylene

Reactions in THF

A Schlenk tube was charged with the heterobimetallic hybrid catalyst (2.3 mg for **Rh/IrC$_{11}$-a**, ~ 1 mol% Σ Rh, Ir) and THF (1 mL). Phenylacetylene (9 mg, 0.09 mmol) and triethylsilane (18 mg, 0.16 mol) were added to the vessel under a stream of Ar, which was subsequently sealed. The mixture was stirred for 1 h at 75 °C, allowed to cool down to room temperature and the suspension was centrifuged for 10 min. Analysis was conducted by ^{1}H NMR spectroscopy. The ^{1}H NMR spectral data of the different products, the α–, β(*Z*)– and β(*E*)–vinylsilanes, matched the data of our previous report and that of the literature.[2, 6]

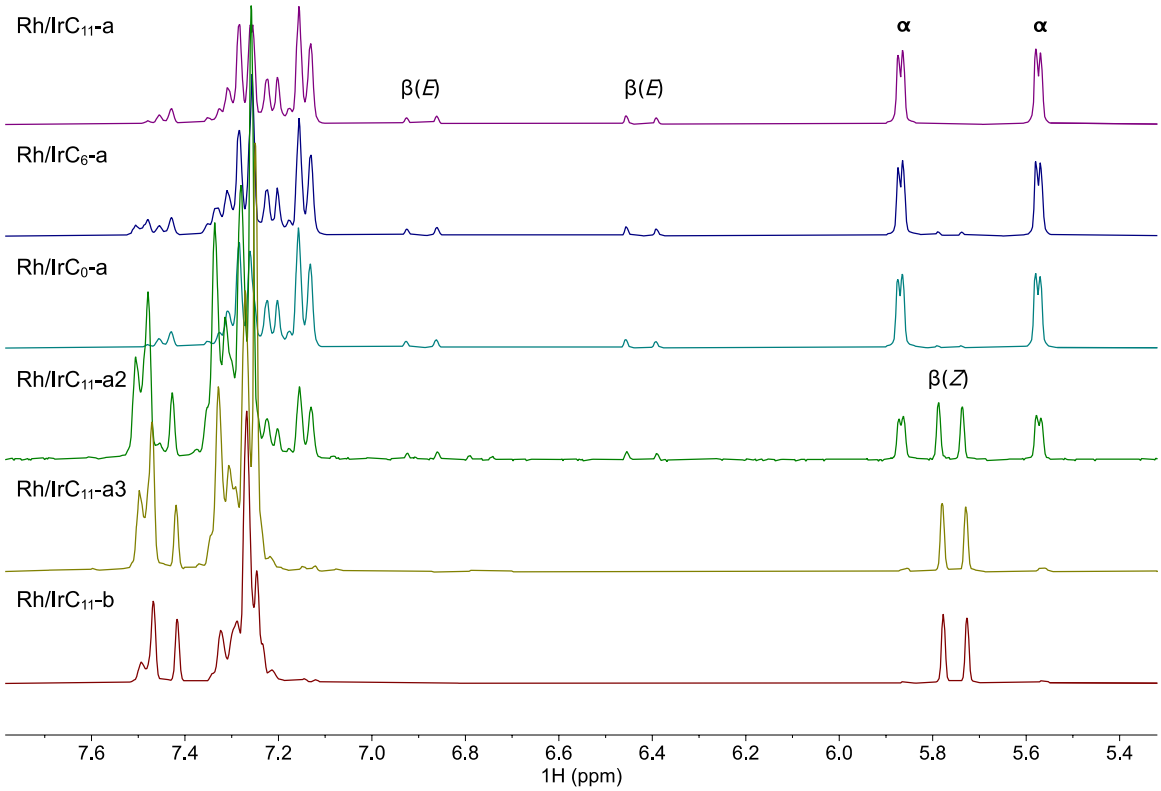

Figure S17. Selected ranges of the different catalysis experiments involving phenylacetylene in THF.

Reactions in Toluene-d^8

The samples were prepared analogously as for the reactions in THF. The mixture was stirred at 120 °C, cooled down to room temperature and centrifuged for a shorter time of only 3 min. The clear solution was transferred to an NMR tube and analysed by ^{1}H NMR spectroscopy.

Hydrosilylation of 1,4-Diethynylbenzene

A Schlenk tube was charged with the heterobimetallic hybrid catalyst **Rh/IrC$_{11}$–a** (4.8 mg, ~ 2.0 mol% Σ Rh, Ir) and 1,4-diethynylbenzene (11 mg, 0.09 mmol). THF (1 mL) was added, followed by addition of triethylsilane (37 mg, 0.31 mmol). The mixture was heated under stirring for the specified amount of time and work-up as described above. The crude product was dried for several minutes under high vacuum, yielding the product mixture as a colourless oil. The yield of the product mixture from Run 3 was 28 mg, which corresponds to a yield of about 90%.

Table S22. Different reaction runs for the hydrosilylation of 1,4-diethynylbenzene.

Run	Hybrid Catalyst	Equiv. Et_3SiH	Time [h]	Solvent	T [°C]	Conversion [%]
1	**Rh/IrC$_{11}$–a**	1.8	1	THF	75	~ 40
2	**Rh/IrC$_{11}$–a**	3.6	15	THF	75	100
3	**Rh/IrC$_{11}$–a**	3.6	24	THF	75	100

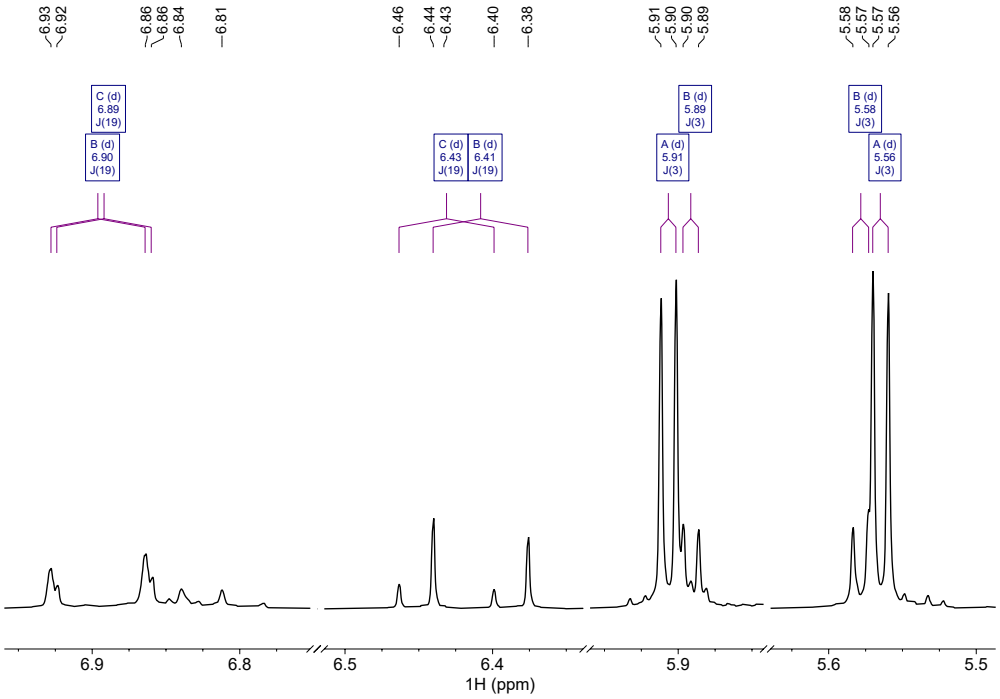

Figure S18. Selected ranges of the ^{1}H NMR spectrum of the crude reaction mixture from hydrosilylation of 1,4-diethynylbenzene. Vinylic $J_{H\text{-}H}$ couplings are assigned as follows: (A) Symmetrical α,α–isomer; $J_{H\text{-}H}$ = 3 Hz. (B) Unsymmetrical $\alpha,\beta(E)$–isomer $J_{H\text{-}H}$ = 3 Hz α–vinylsilane; and $J_{H\text{-}H}$ = 19 Hz for the $\beta(E)$–vinylsilane. (C) Tentatively assigned to the symmetrical $\beta(E)\beta(E)$–isomer; $J_{H\text{-}H}$ = 19 Hz.

1,4-Bis(1-(triethylsilyl)vinyl)benzene: ^{1}H NMR (300 MHz, $CDCl_3$): δ7.09 (s, 4H), 5.90 (d, $J_{H\text{-}H}$ = 3 Hz, 2H), 5.56 (d, $J_{H\text{-}H}$ = 3 Hz, 2H), 0.93 (t, $J_{H\text{-}H}$ = 8 Hz, 9H), 0.68 (q, $J_{H\text{-}H}$ = 8 Hz, 6H) ppm. ^{13}C NMR (75 MHz, $CDCl_3$): δ150.2, 143.4, 128.5, 126.5, 7.5, 3.6 ppm. MS (EI): 358 (92%) $[M]^+$, 329 (100%) $[M - C_2H_5]^+$, 301 (89%) $[M - 2\ C_2H_5]^+$, 273 (77%). The NMR spectroscopic data of the product matches the literature.[7]

GC-MS (EI) analysis of the obtained mixture shows the presence of the other minor components, in addition to the main compounds discussed in the manuscript (Figure S19, S20). These minor components include two species with m/z = 360, which corresponds to $[M + 2H]^+$, likely originating from hydrogenation of different doubly hydrosilylated alkynes (9%). We note that Ir catalysed hydrogenation of silylalkenes with H_2 is known,[8] however the products observed here may also form during GC-MS analysis. Possible H sources are the solvent and excess silane. In addition, a species with the mass of 375 was detected, which corresponds to a hydrolysed product containing an OH group (<1%). Furthermore, a minor amount (<6%) of a triple hydrosilylated product is evident as well (m/z 475, which corresponds to $Ph(C_2H_2SiEt_3)(C_2H_3(SiEt_3)_2)$; and 444, which corresponds to $Ph(C_2H_2SiEt_3)(C_2H_3SiEt_3SiEt_2)$. The latter likely forms through elimination of EtH from $Ph(C_2H_2SiEt_3)(C_2H_3(SiEt_3)_2)$.

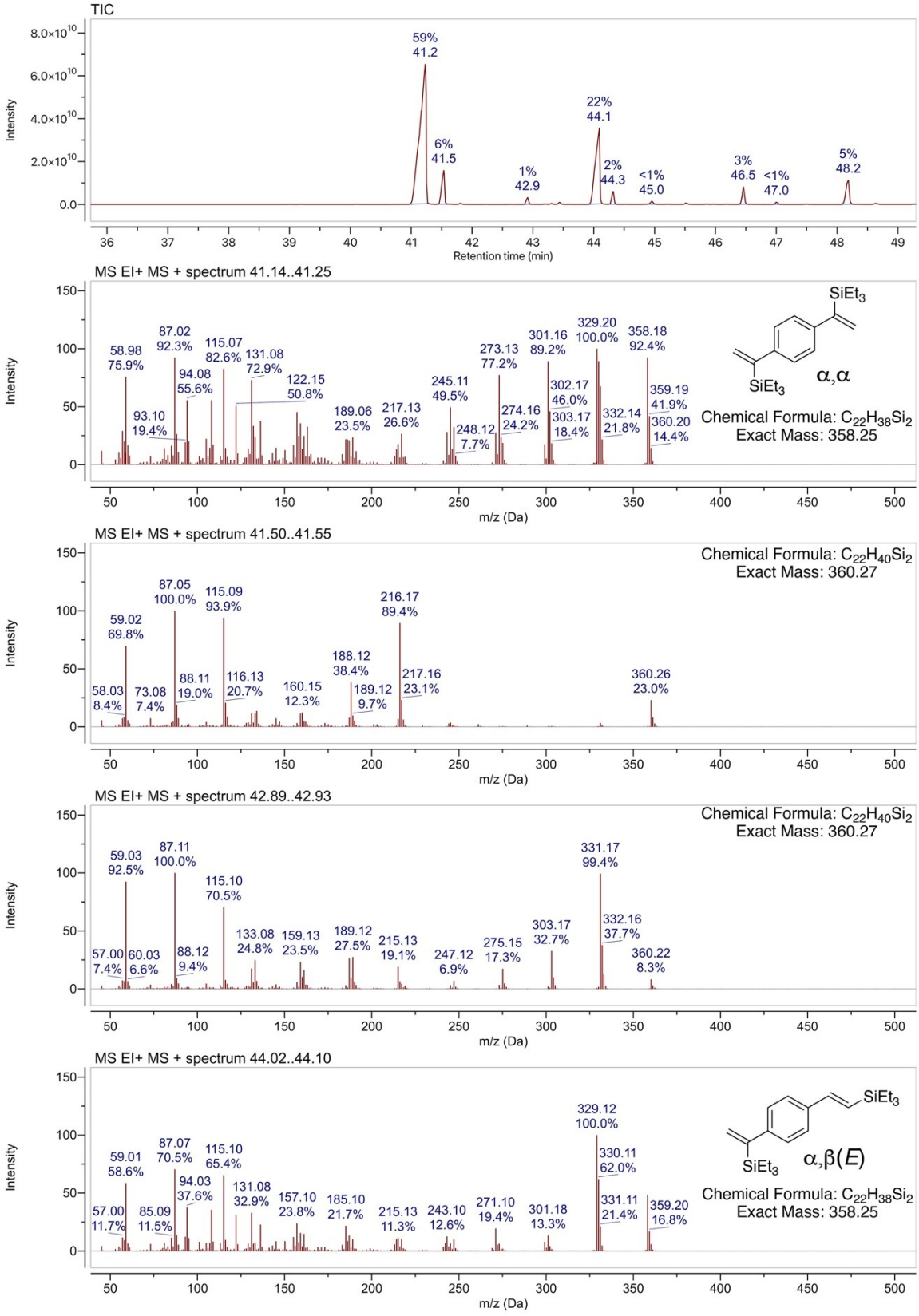

Figure S19. GC-MS traces of the reaction mixture of the hydrosilylation of 1,4-diethynylbenzene and corresponding EI MS spectra, peaks 1-4 in the chromatogram.

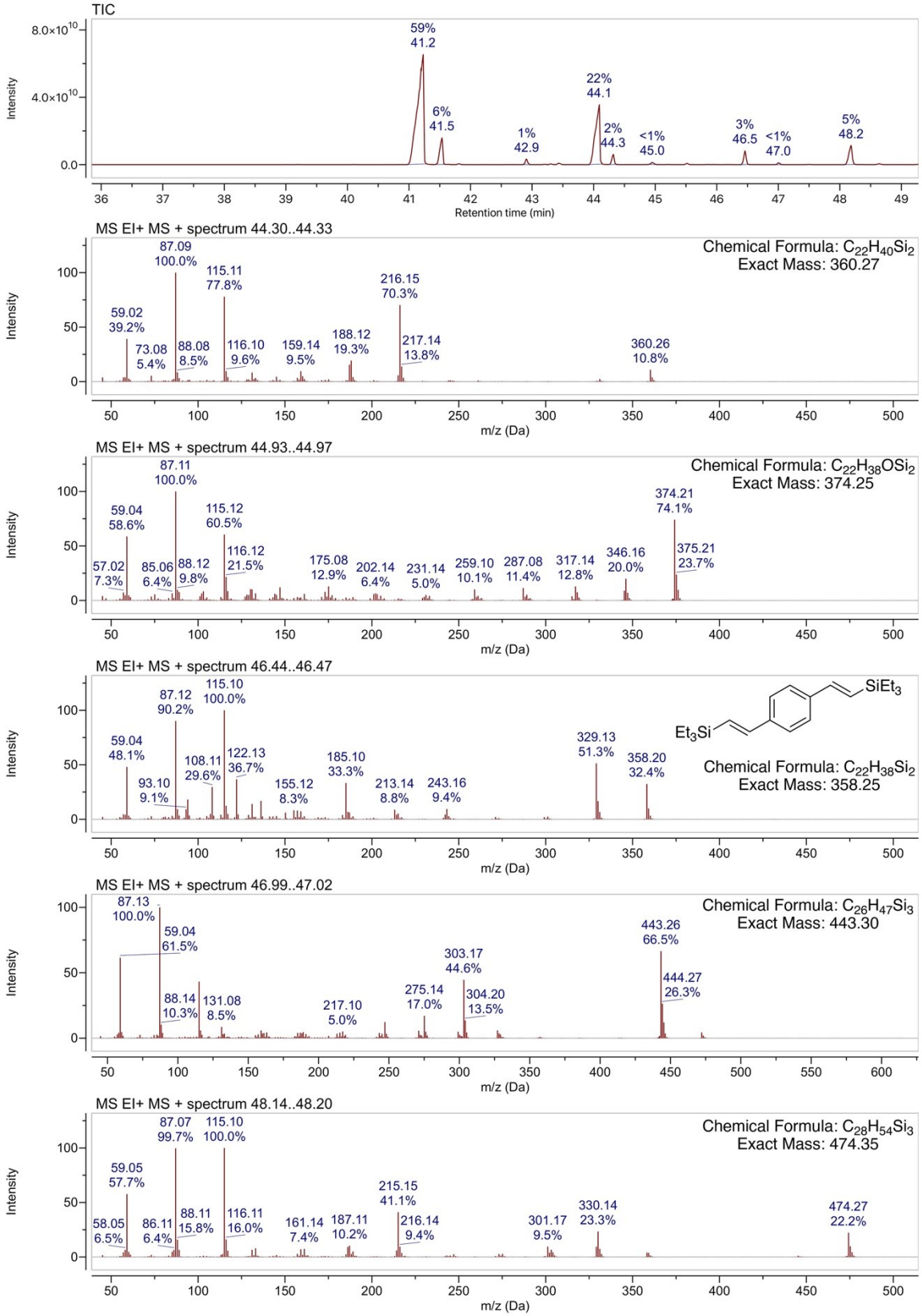

Figure S20. GC-MS traces of the reaction mixture of the hydrosilylation of 1,4-diethynylbenzene and corresponding EI MS spectra, peaks 5-9 in the chromatogram.

Hydrosilylation of Diphenylacetylene

A Schlenk tube was charged with the heterobimetallic hybrid catalyst (~ 1 mol%; Σ Rh, Ir), diphenylacetylene (15 mg, 0.08 mmol), triethylsilane (18 mg, 0.16 mmol) and the solvent (1 mL). The mixture was treated as described above.

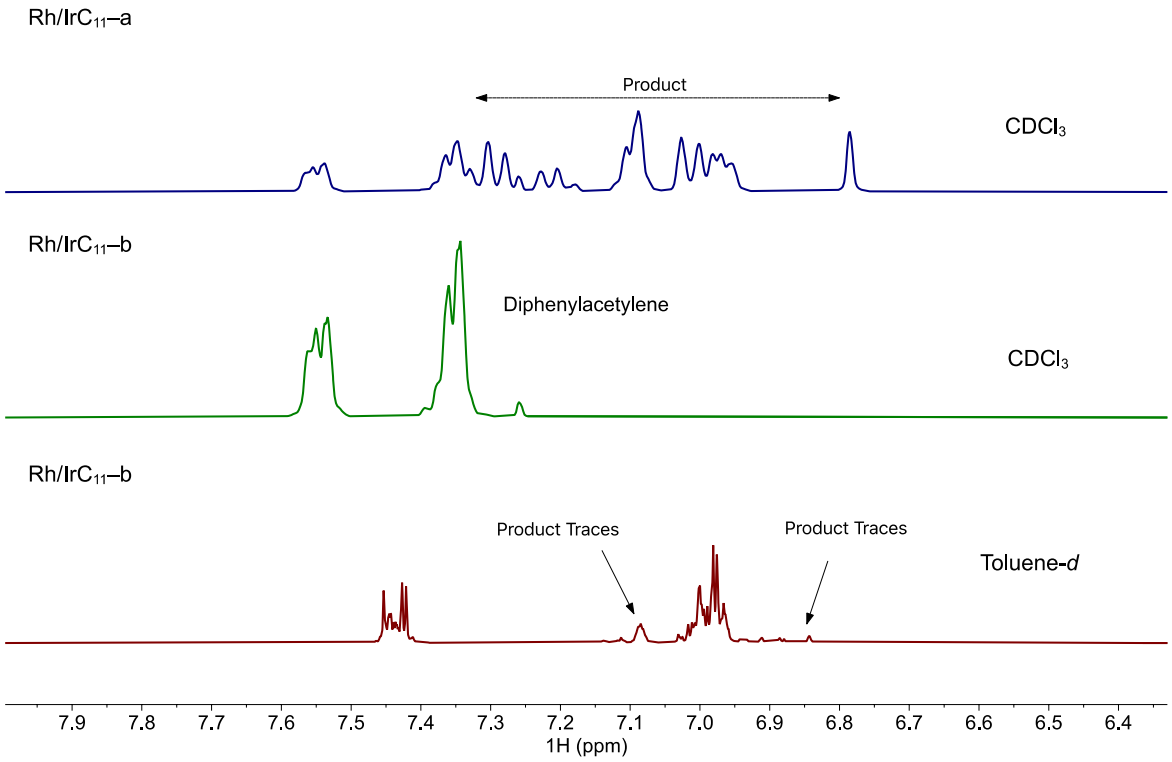

Figure S21. Selected ranges of the different catalysis experiments involving diphenylacetylene. The reaction involving **Rh/IrC$_{11}$–a** yields the hydrosilylated product, and contained some unreacted starting material (top). The reaction involving **Rh/IrC$_{11}$–b** in THF shows only unreacted starting material (middle) while in toluene-*d*^{8} traces of product are visible (bottom).

Table S23. Summary of the hydrosilylation experiments involving diphenylacetylene.

Hybrid Catalyst	Amount Catalyst	Time [min]	Solvent	T [°C]	Conversion [%]
Rh/IrC$_{11}$–a	2.3 mg	60	THF	75	80
Rh/IrC$_{11}$–b	2.6 mg	60	THF	75	-
Rh/IrC$_{11}$–b	2.6 mg	60	Toluene-*d*^{8}	120	traces

The ^{1}H NMR spectroscopic data of the product matches the literature.[2]

Hydrosilylation of 1,4-Diphenylbutadiyne

A Schlenk tube was charged with the heterobimetallic hybrid catalyst **Rh/IrC$_{11}$–a** (4.8 mg, ~ 2 mol%; Σ Rh, Ir) and 1,4-diphenylbutadiyne (18 mg, 0.09 mmol). Solvent was added (1 mL), followed by addition of triethylsilane (37 mg, 0.32 mmol). The mixture was heated under stirring for the specified amount of time (Table S24). The reactions performed in THF were worked-up as described above. Solvent evaporation and drying under high vacuum gave the product mixture as a colourless oil (27 mg for run 3, corresponding to ~ 88% for the determined ratio of E/EE, and not taking into account the minor amounts of other products which forms). Reactions in toluene-*d*^{8} were run analogously, with the following differences in the work-up: after the first centrifugation, the mixture was directly transferred to an NMR tube and analysed by ^{1}H NMR spectroscopy.

Table S24. Summary of the reactions involving 1,4-diphenylbutadiyne.

Run	Hybrid Catalyst[a]	Equiv. Et_3SiH	Time [h]	Solvent	T [°C]	Ratio E / EE	Conversion [%]
1	**Rh/IrC$_{11}$–a**	1.8	1	THF	75	88 / 12	~ 13
2	**Rh/IrC$_{11}$–a**	3.6	15	THF	75	69 / 31	95[b]
3	**Rh/IrC$_{11}$–a**	3.6	24	THF	75	73 / 27	Near Quant.
4	**Rh/IrC$_{11}$–a**	3.6	1	Toluene-*d*^{8}	120	56 / 44	100
5	**Rh/IrC$_{11}$–a**	3.6	24	Toluene-*d*^{8}	120	0 / 100	100

[a]All reactions were conducted with 4.8 mg (~ 2.0 mol%) of the hybrid catalyst. [b]Determined by ^{1}H NMR.
[b] Determined by GC-MS.

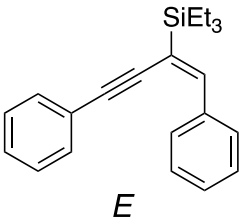

E

(*E*)-(1,4-Diphenylbut-1-en-3-yn-2-yl)triethylsilane: ^{1}H NMR (300 MHz, $CDCl_3$): δ 8.03 (m, 2H), 7.55 (m, 2H), 7.48 (m, 2H), ~ 7.41 – 7.30 (m, 4H), 6.86 (s, 1H), 1.07 (t, $J_{H\text{-}H}$ = 8 Hz, 9H), 0.86 (m, 6H) ppm. ^{13}C NMR (75 MHz, $CDCl_3$): δ 145.3, 138.0, 132.7, 131.4, 129.0, 128.6, 128.5, 128.4, 128.0, 124.6, 121.0, 91.0, 81.7, 7.5, 3.2 ppm. MS (EI): 318 (97%) $[M]^+$,

289 (49%) $[M - C_2H_5]^+$, 261 (19%) $[M - C_4H_9]^+$, 231 (77%) $[M - 3\ C_2H_5]^+$. The ^1H and ^{13}C NMR spectroscopic data is agreement with the literature.[9]

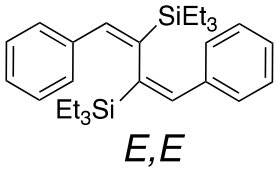

E,E

((1*E*,3*E*)-1,4-diphenylbuta-1,3-diene-2,3-diyl)bis(triethylsilane): ^1H NMR (300 MHz, Toluene-d^8): δ 7.55 (m, 4H), 7.10 – 6.97 (m, 8H), 6.81 (s, 2H), 0.96 (t, J_{H-H} = 8 Hz, 18H), 0.65 (m, 12H) ppm. ^{13}C NMR (75 MHz, Toluene-d^8): δ 145.7, 140.1, 137.5, 129.4, 128.5, 127.6, 8.4, 4.9 ppm. MS (EI): 434 (60%) $[M]^+$. The recorded ^1H and ^{13}C NMR spectroscopic data of the mixtures in $CDCl_3$ was in agreement with the literature for the *E* and *EE* compounds.[9, 10]

GC-MS analysis of the crude mixture of run 3 (Figure S22, S23) show that the mixture was composed of a minimum of three different mono-hydrosilylated isomers accompanied by two different bis-hydrosilylated isomers, and some unreacted starting material (Figures S15 and S16). The different compounds eluted in the order of starting material (38 min), mono-hydrosilylated isomers (42-44 min) and bis-hydrosilylated product (46–49 min). The major component was the mono-hydrosilylated *E*-isomer (65%), identified by comparison of the ^1H NMR spectrum to the literature.[9, 10]

GC-MS analysis of the crude mixtures of run 4 and 5 is shown in Figure S24 – S27. Again, we identified the product by comparison with reported ^1H and ^{13}C NMR spectral data.[9] Apart from the main fractions, there are also some other isomers present, which correspond to different mono products (<6%) and other bis products (27%).

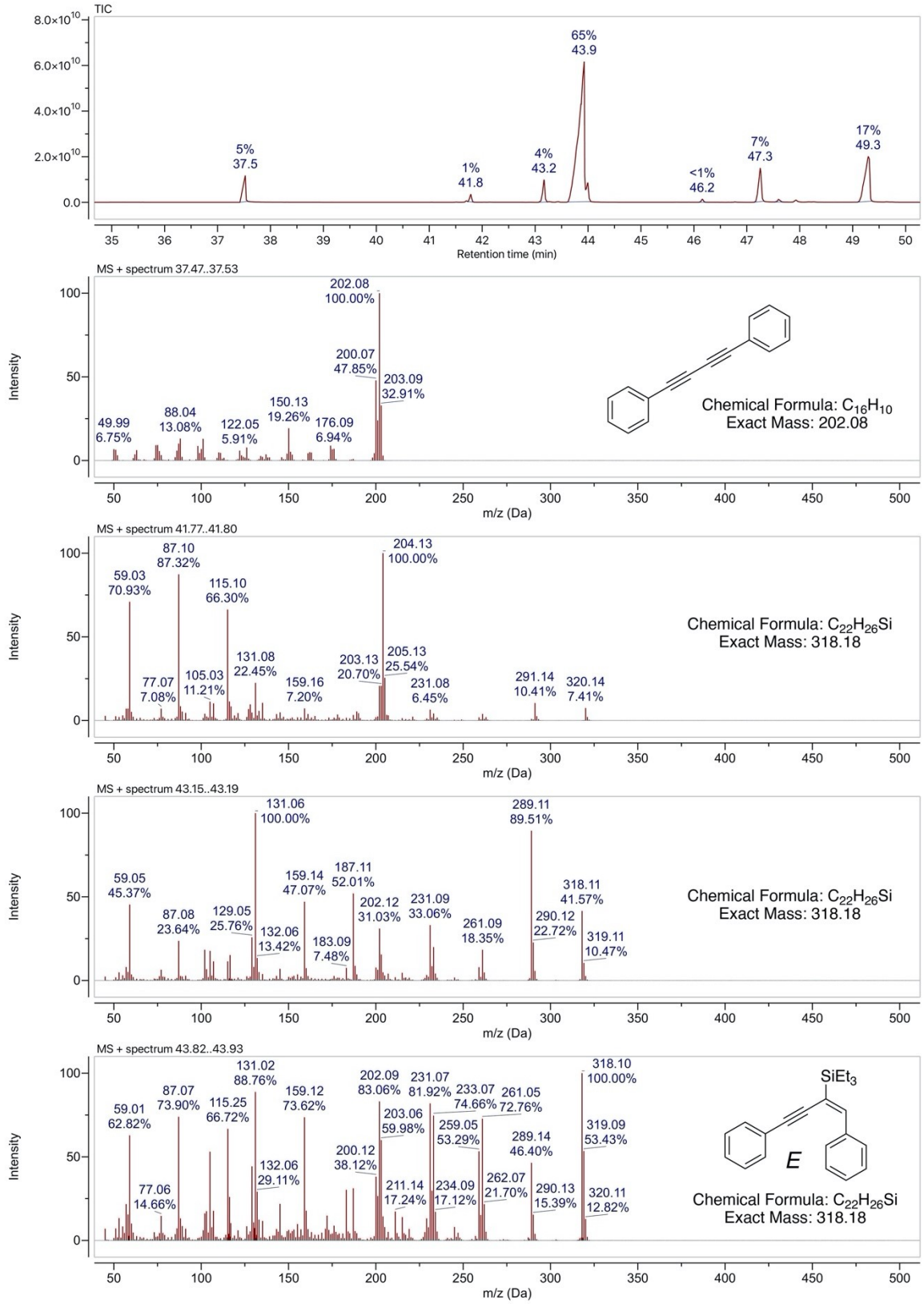

Figure S22. GC-MS traces of the reaction mixture of the hydrosilylation of 1,4-diphenylbutadiyne and corresponding EI MS spectra, peaks 1-4 in the chromatogram. Conditions: 15 h / THF / 75°C.

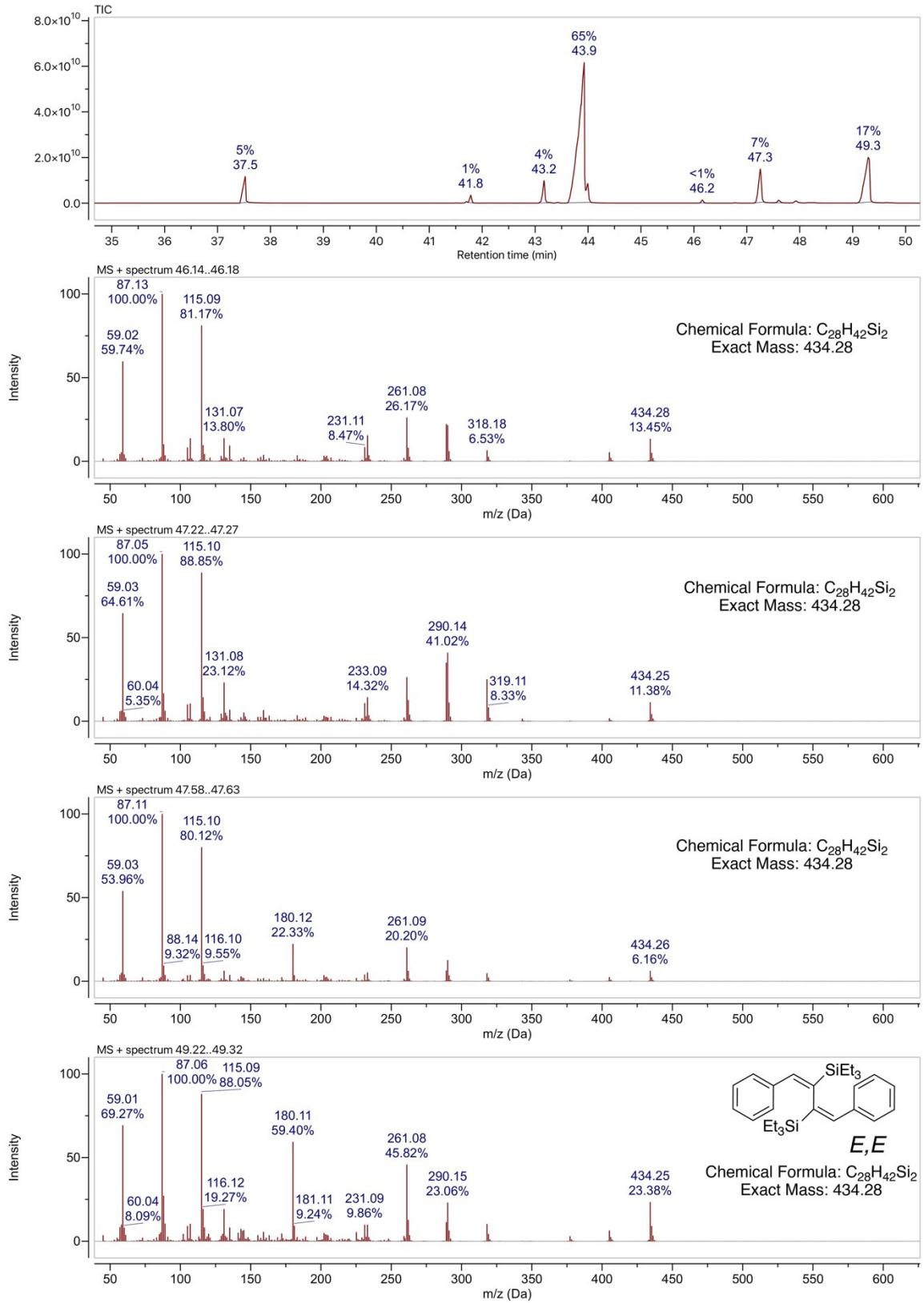

Figure S23. GC-MS traces of the reaction mixture of the hydrosilylation of 1,4-diphenylbutadiyne and corresponding EI MS spectra, peaks 5-8 in the chromatogram. Conditions: 15 h / THF / 75°C.

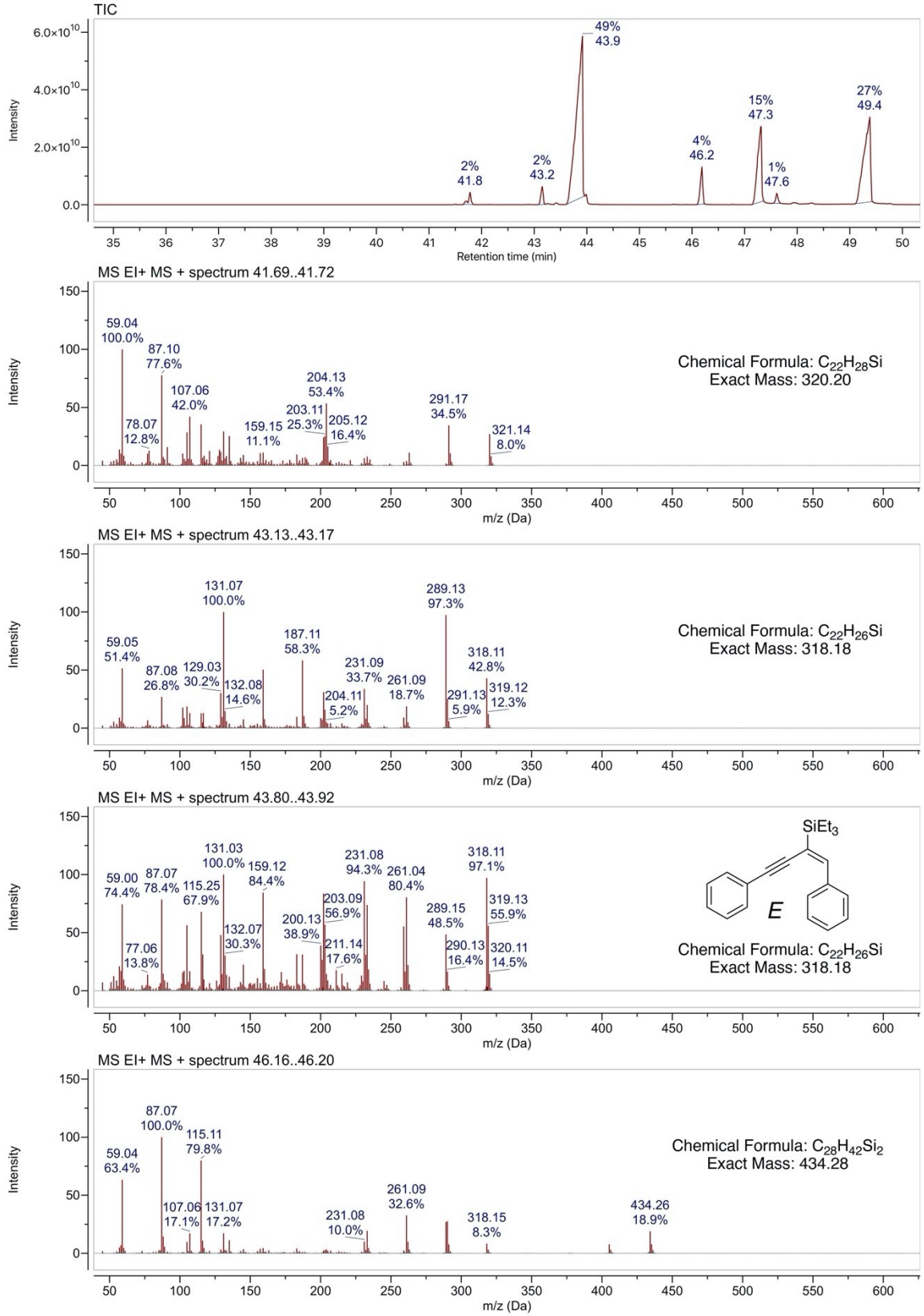

Figure S24. GC-MS traces of the reaction mixture of the hydrosilylation of 1,4-diphenylbutadiyne and corresponding EI MS spectra, peaks 1-4 in the chromatogram. Conditions: 1 h / toluene-d^8 / 120°C. Conditions: 1 h / toluene-d^8 / 120°C.

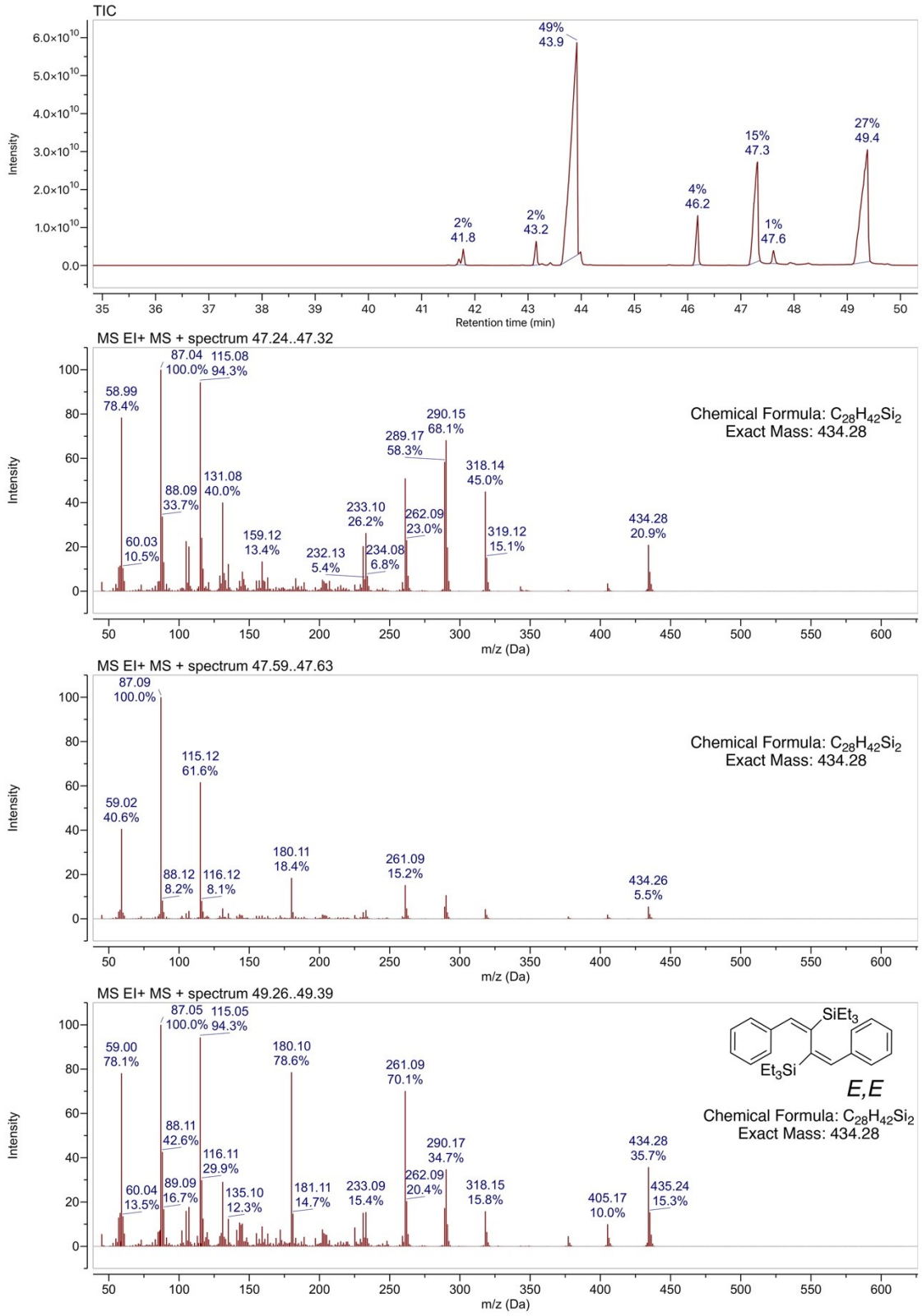

Figure S25. GC-MS traces of the reaction mixture of the hydrosilylation of 1,4-diphenylbutadiyne and corresponding EI MS spectra, peaks 5-7 in the chromatogram. Conditions: 1 h / toluene-d^8 / 120°C.

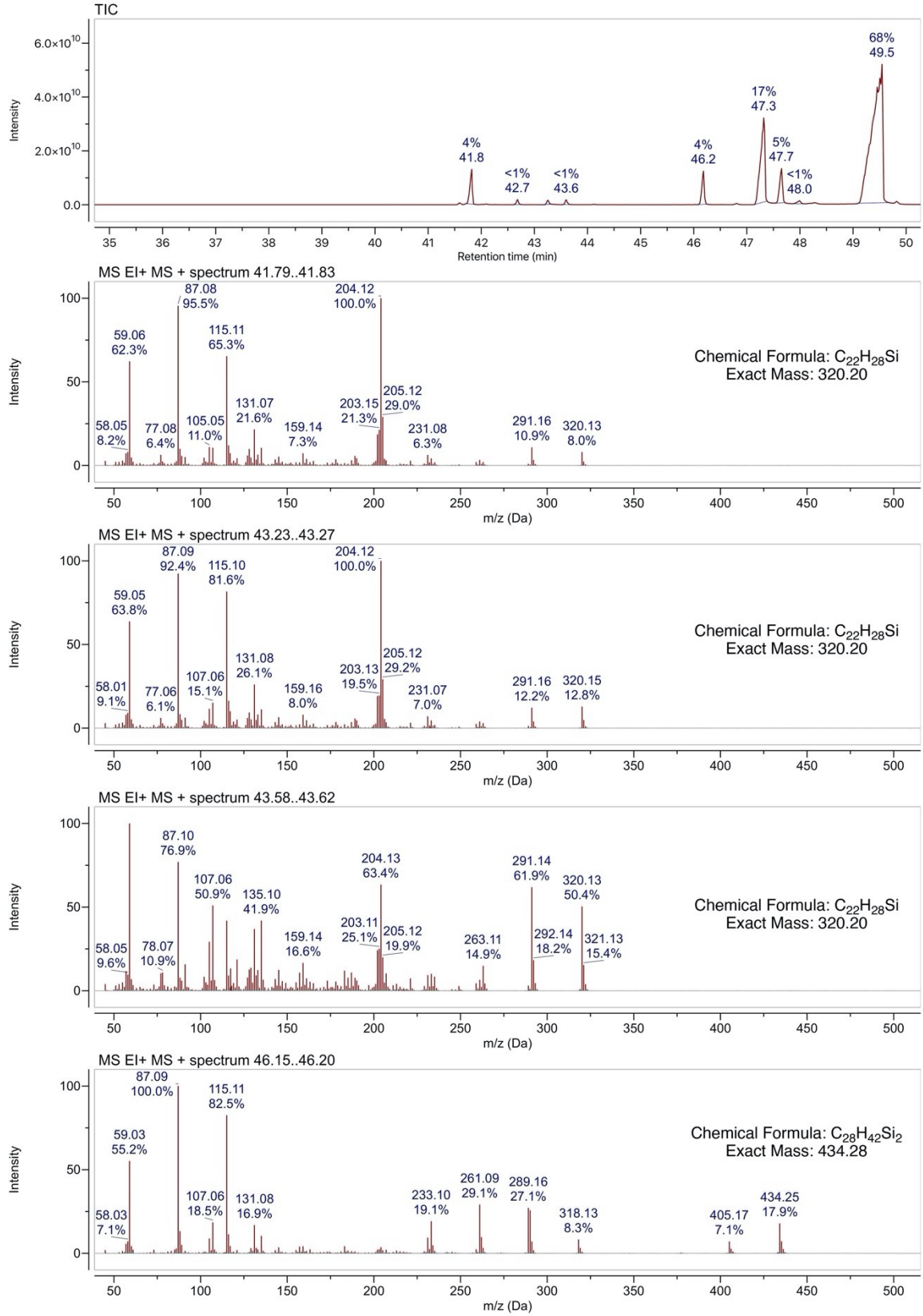

Figure S26. GC-MS traces of the reaction mixture of the hydrosilylation of 1,4-diphenylbutadiyne and corresponding EI MS spectra, peaks 1-4 in the chromatogram. Conditions: 24 h / toluene-d^8 / 120°C.

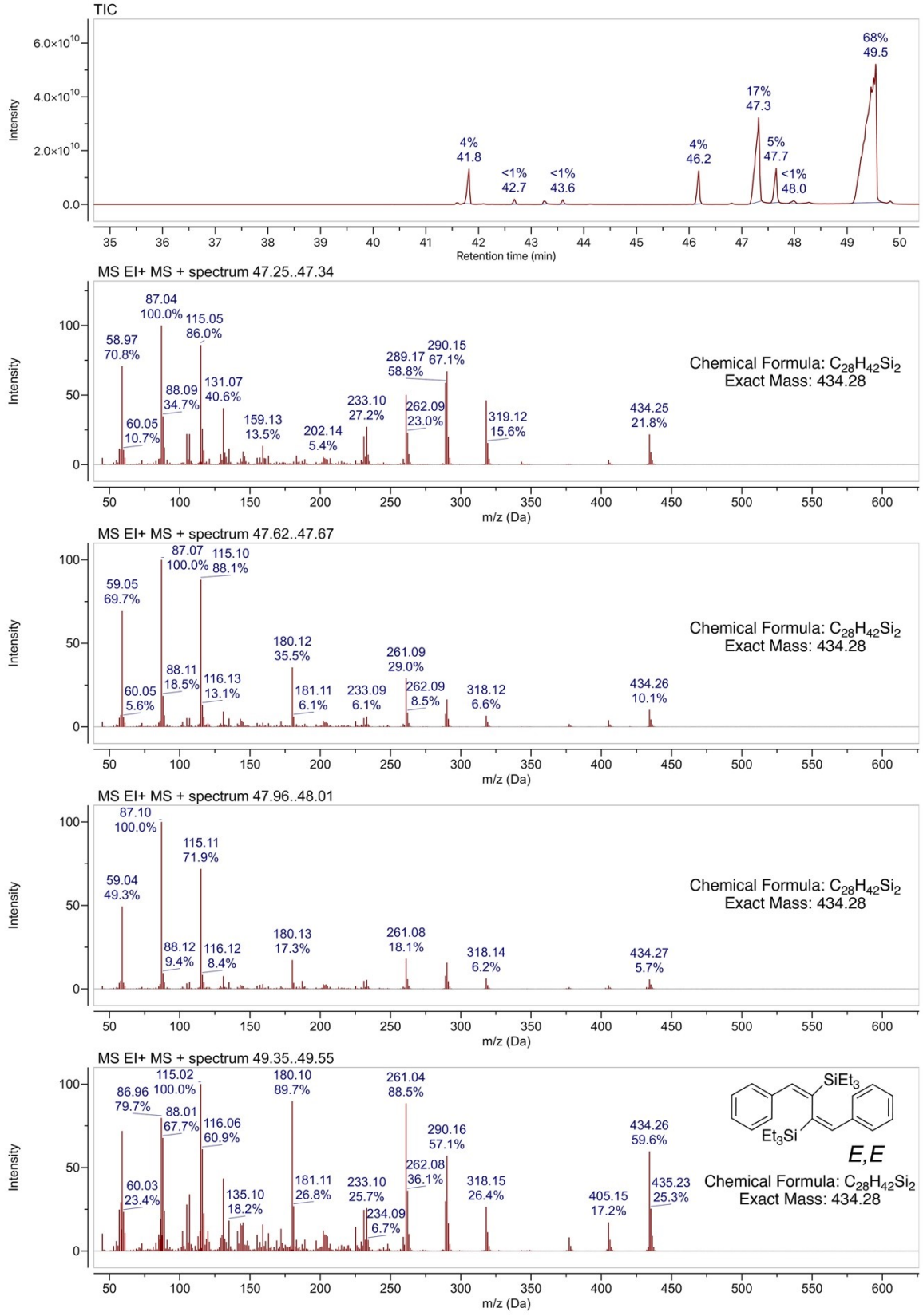

Figure S27. GC-MS traces of the reaction mixture of the hydrosilylation of 1,4-diphenylbutadiyne and corresponding EI MS spectra, peaks 5-8 in the chromatogram. Conditions: 24h / toluene-d^8 / 120°C.

4. References

1. G. R. Fulmer, A. J. M. Miller, N. H. Sherden, H. E. Gottlieb, A. Nudelman, B. M. Stoltz, J. E. Bercaw and K. I. Goldberg, *Organometallics*, 2010, **29**, 2176-2179.
2. M. Roemer, V. R. Gonçales, S. T. Keaveney, I. Pernik, J. Lian, J. Downes, J. J. Gooding and B. Messerle, *Cat. Sci. Technol.*, 2021, **11**, 1888-1898.
3. B. Ravel and M. Newville, *J. Synchrotron Rad.*, 2005, **12**, 537-541.
4. C. M. Wong, K. Q. Vuong, M. R. D. Gatus, C. Hua, M. Bhadbhade and B. A. Messerle, *Organometallics*, 2012, **31**, 7500-7510.
5. C. Hua, K. Q. Vuong, M. Bhadbhade and B. A. Messerle, *Organometallics*, 2012, **31**, 1790-1800.
6. J. W. Faller and D. G. D'Alliessi, *Organometallics*, 2002, **21**, 1743-1746.
7. D. Wang, Y. Lai, P. Wang, X. Leng, J. Xiao and L. Deng, *J. Am. Chem. Soc.*, 2021, **143**, 12847-12856.
8. A. Wang, M. Bernasconi and A. Pfaltz, *Adv. Synth. Catal.*, 2017, **359**, 2523-2529.
9. J. Walkowiak, K. Salamon, A. Franczyk, K. Stefanowska, J. Szyling and I. Kownacki, *J. Org. Chem.*, 2019, **84**, 2358-2365.
10. F. Alonso, R. Buitrago, Y. Moglie, A. Sepúlveda-Escribano and M. Yus, *Organometallics*, 2012, **31**, 2336-2342.

5. NMR Spectra

Reactions Involving Phenylacetylene

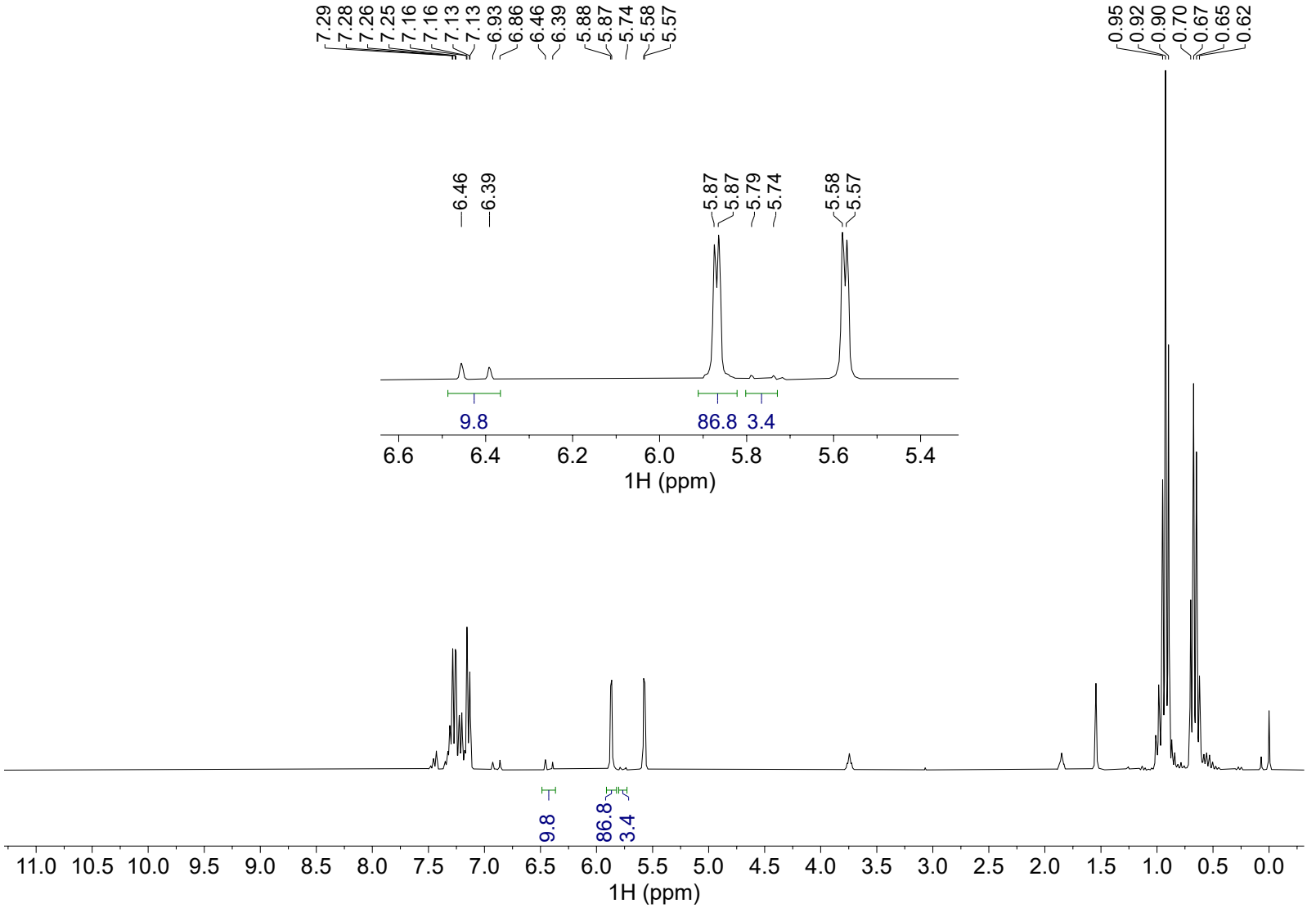

Figure S28. ^{1}H NMR spectrum (300 MHz, $CDCl_3$) of the product mixture from hydrosilylation of phenylacetylene; **Rh/IrC$_{11}$–a** / THF/ 1 h / 75°C.

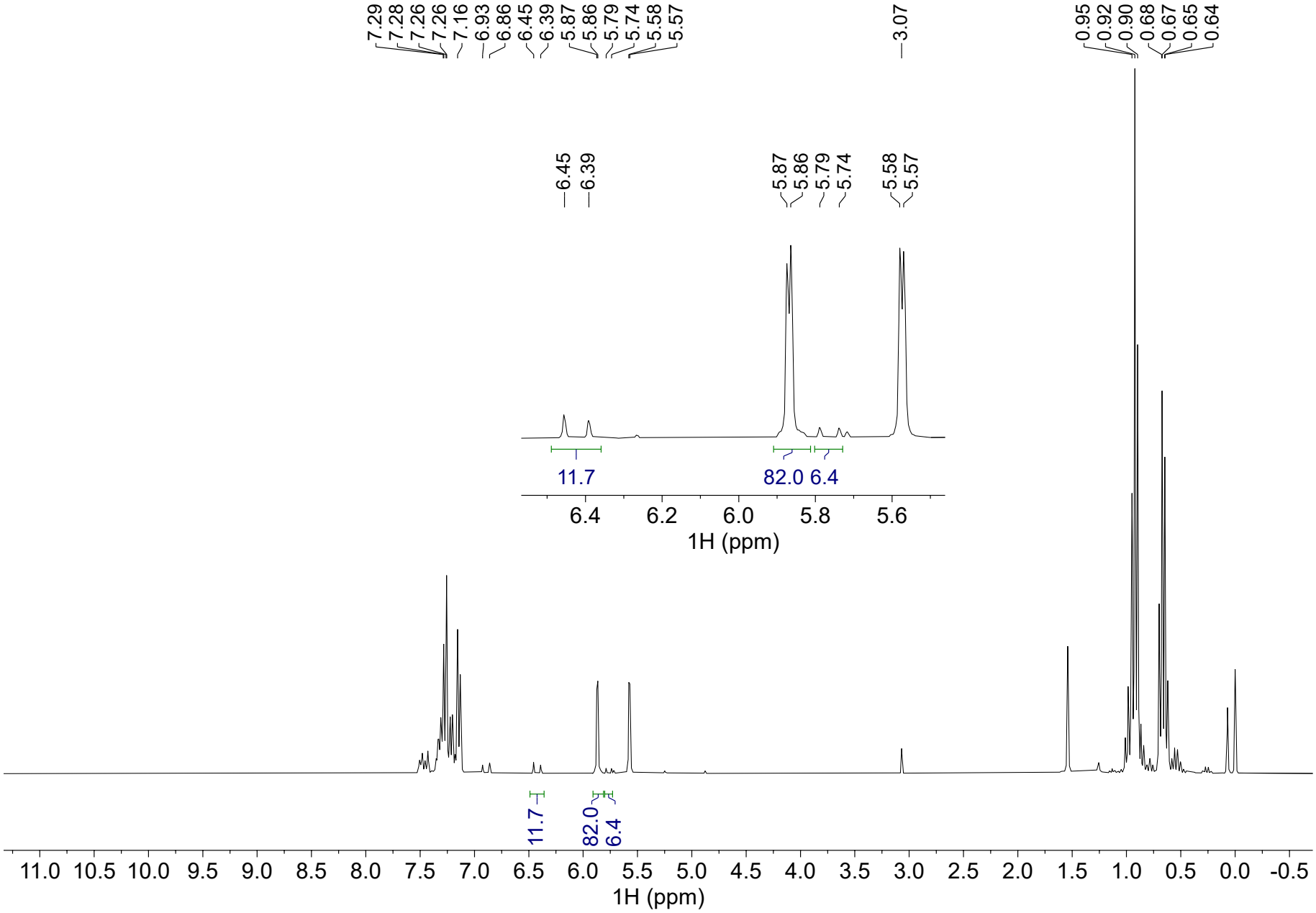
7.29
7.28
7.26
7.26
7.16
6.93
6.86
6.45
6.39
5.87
5.86
5.79
5.74
5.58
5.57
3.07
0.95
0.92
0.90
0.68
0.67
0.65
0.64
6.45
6.39
5.87
5.86
5.79
5.74
5.58
5.57
11.7
82.0
6.4
6.4
6.2
6.0
5.8
5.6
1H (ppm)
11.7
82.0
6.4
11.0
10.5
10.0
9.5
9.0
8.5
8.0
7.5
7.0
6.5
6.0
5.5
5.0
4.5
4.0
3.5
3.0
2.5
2.0
1.5
1.0
0.5
0.0
-0.5
1H (ppm)

Figure S29. ^{1}H NMR spectrum (300 MHz, $CDCl_3$) of the product mixture from the hydrosilylation of phenylacetylene; **Rh/IrC$_6$–a** / THF/ 1 h / 75°C.

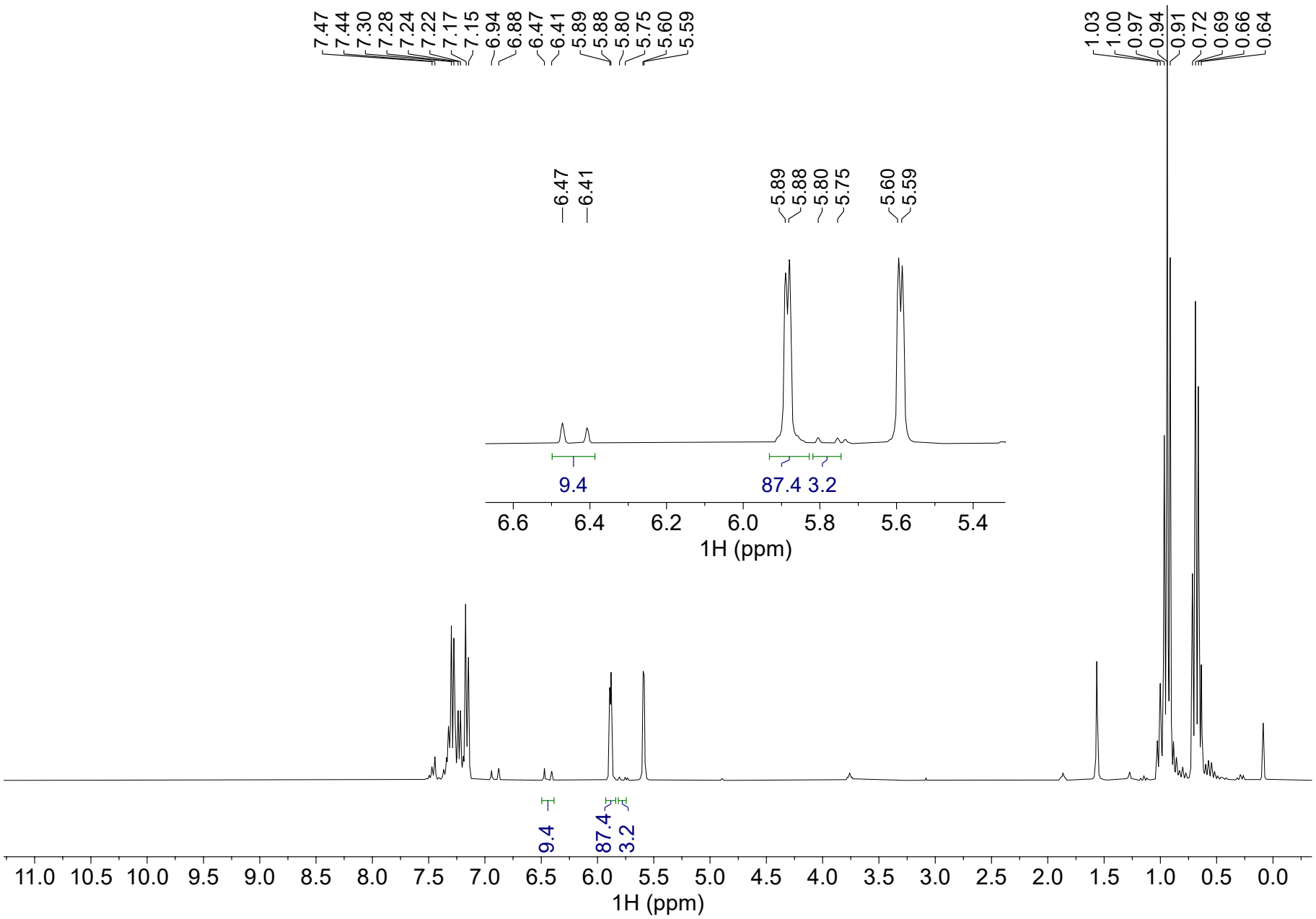
7.47
7.44
7.30
7.28
7.24
7.22
7.17
7.15
6.94
6.88
6.47
6.41
5.89
5.88
5.80
5.75
5.60
5.59
1.03
1.00
0.97
0.94
0.91
0.72
0.69
0.66
0.64
9.4
87.4
3.2
1H (ppm)

Figure S30. ^{1}H NMR spectrum (300 MHz, $CDCl_3$) of the product mixture from the hydrosilylation of phenylacetylene; **Rh/IrC$_0$–a** / THF/ 1 h / 75°C.

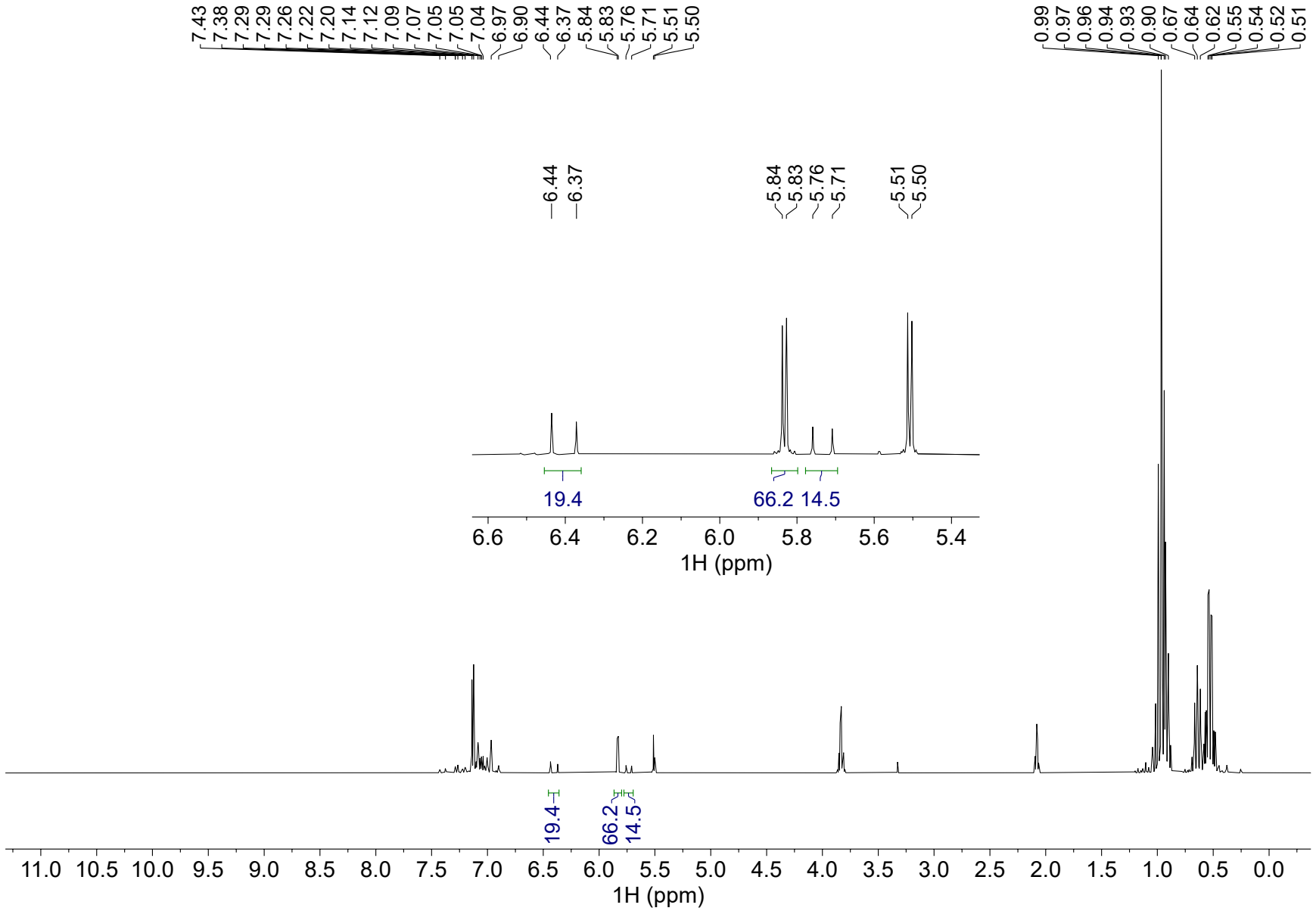

Figure S31. ^{1}H NMR spectrum (300 MHz, toluene-d^{8}) of the product mixture from the hydrosilylation of phenylacetylene; **Rh/IrC$_{11}$–a** / toluene-d^{8} / 1 h / 120°C.

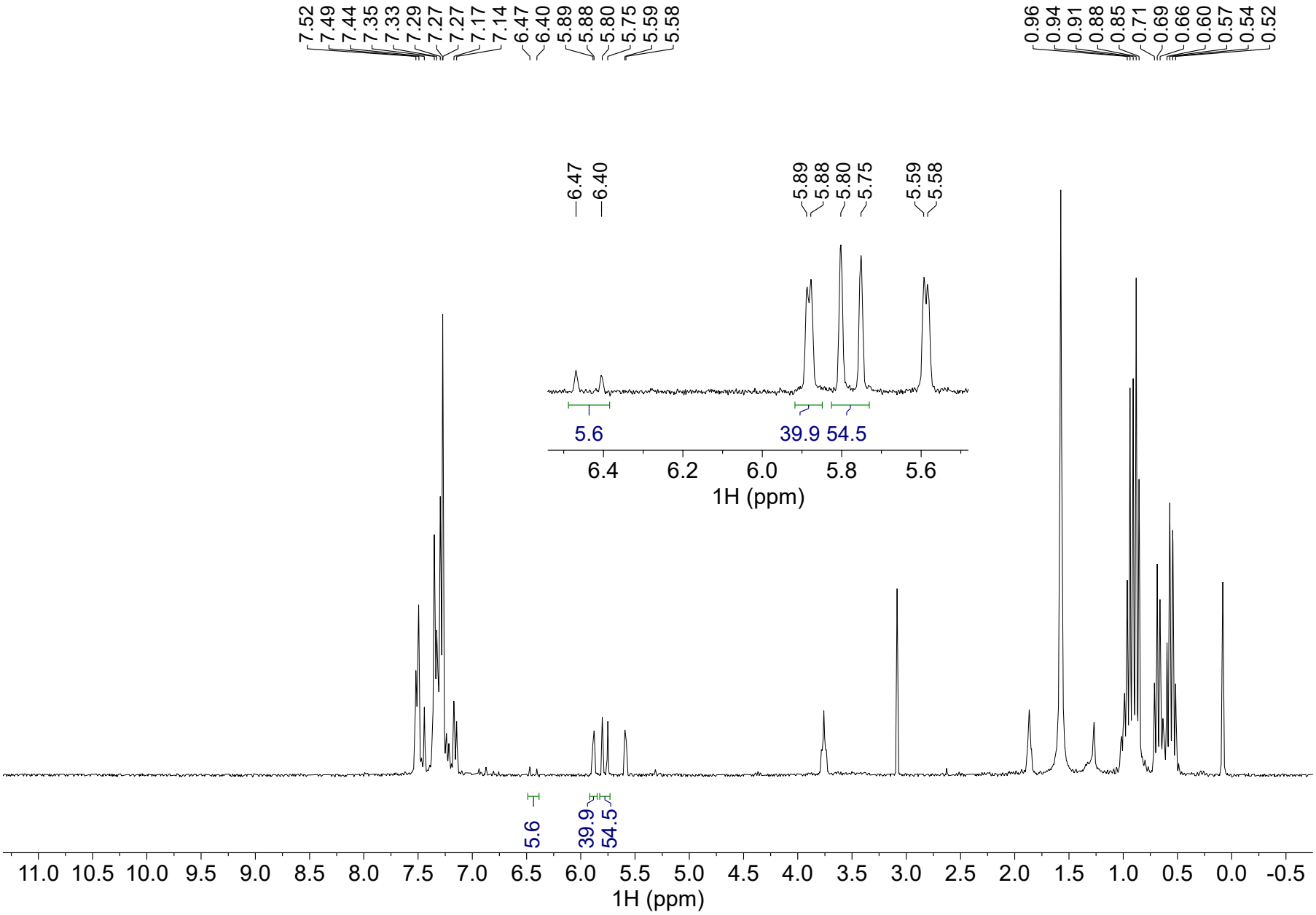
7.52
7.49
7.44
7.35
7.33
7.29
7.27
7.27
7.17
7.14
6.47
6.40
5.89
5.88
5.80
5.75
5.59
5.58
0.96
0.94
0.91
0.88
0.85
0.71
0.69
0.66
0.60
0.57
0.54
0.52
6.47
6.40
5.89
5.88
5.80
5.75
5.59
5.58
5.6
39.9 54.5
6.4
6.2
6.0
5.8
5.6
1H (ppm)
5.6
39.9
54.5
11.0 10.5 10.0 9.5 9.0 8.5 8.0 7.5 7.0 6.5 6.0 5.5 5.0 4.5 4.0 3.5 3.0 2.5 2.0 1.5 1.0 0.5 0.0 -0.5
1H (ppm)

Figure S32. ^{1}H NMR spectrum (300 MHz, $CDCl_3$) of the product mixture from the hydrosilylation of phenylacetylene; **Rh/IrC$_{11}$–a2** / THF/ 1 h / 75°C.

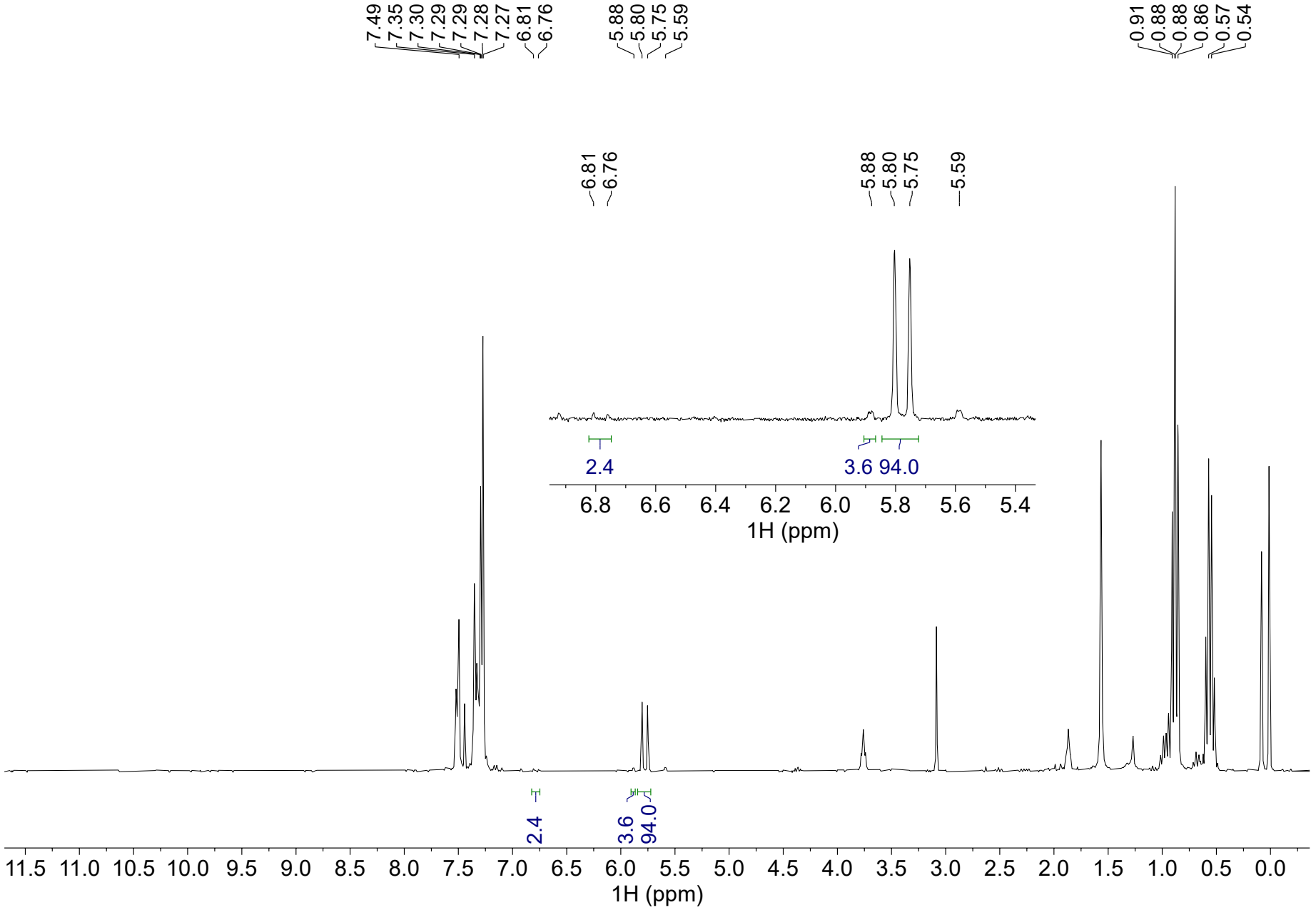
7.49
7.35
7.30
7.29
7.29
7.28
7.27
6.81
6.76
5.88
5.80
5.75
5.59
0.91
0.88
0.88
0.86
0.57
0.54
6.81
6.76
5.88
5.80
5.75
5.59
2.4
3.6
94.0
6.8
6.6
6.4
6.2
6.0
5.8
5.6
5.4
1H (ppm)
2.4
3.6
94.0
11.5
11.0
10.5
10.0
9.5
9.0
8.5
8.0
7.5
7.0
6.5
6.0
5.5
5.0
4.5
4.0
3.5
3.0
2.5
2.0
1.5
1.0
0.5
0.0
1H (ppm)

Figure S33. ^{1}H NMR spectrum (300 MHz, $CDCl_3$) of the product mixture from the hydrosilylation of phenylacetylene; **Rh/IrC$_{11}$–a3** / THF/ 1 h / 75°C.

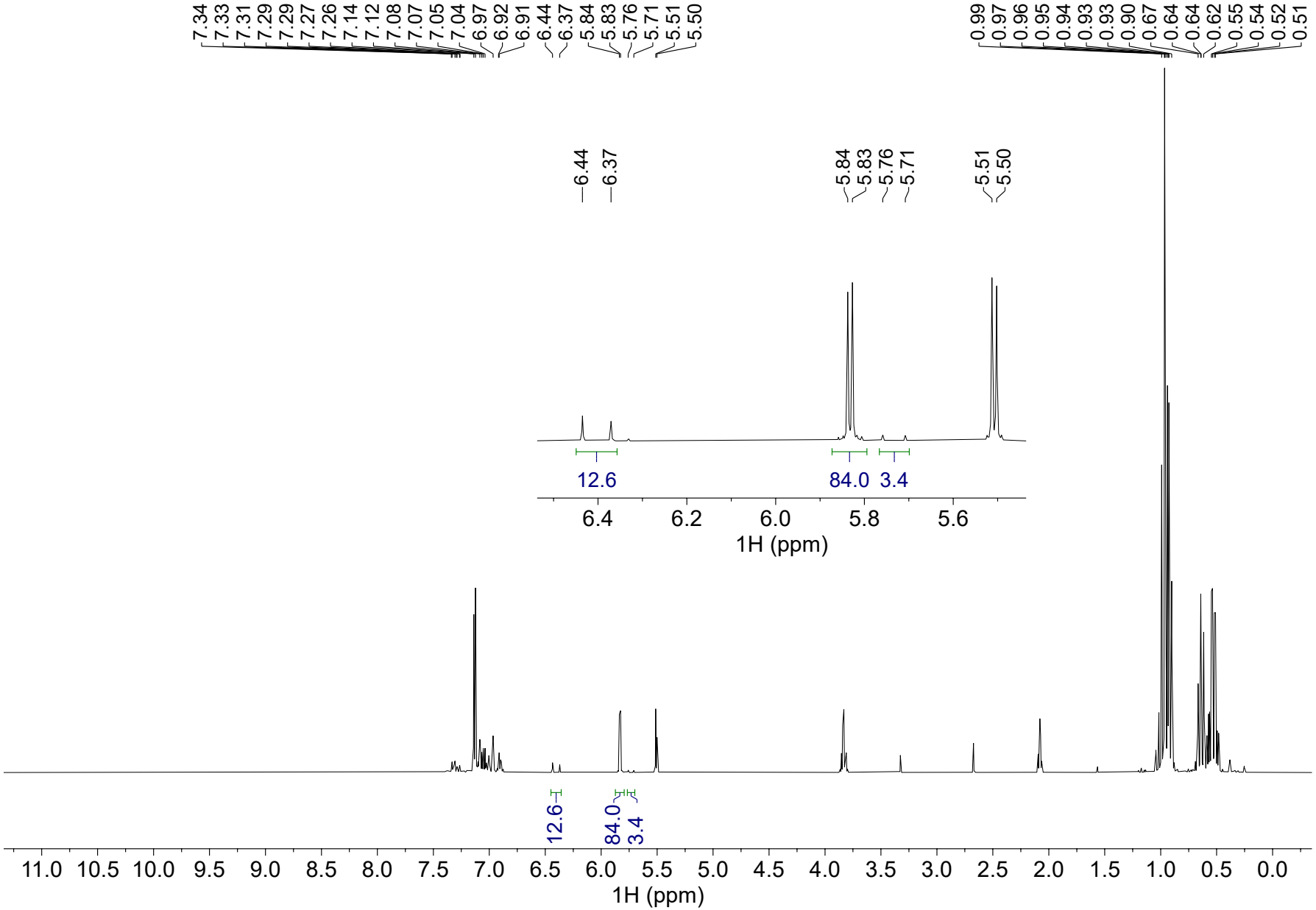
7.34
7.33
7.31
7.29
7.29
7.27
7.26
7.14
7.12
7.08
7.07
7.05
7.04
6.97
6.92
6.91
6.44
6.37
5.84
5.83
5.76
5.71
5.51
5.50
0.99
0.97
0.96
0.95
0.94
0.93
0.93
0.90
0.67
0.64
0.64
0.62
0.55
0.54
0.52
0.51
12.6
84.0
3.4
6.4
6.2
6.0
5.8
5.6
1H (ppm)
11.0
10.5
10.0
9.5
9.0
8.5
8.0
7.5
7.0
6.5
6.0
5.5
5.0
4.5
4.0
3.5
3.0
2.5
2.0
1.5
1.0
0.5
0.0
1H (ppm)

Figure S34. ^{1}H NMR spectrum (300 MHz, $CDCl_3$) of the product mixture from the hydrosilylation of phenylacetylene; **RhC$_{11}$** / toluene-d^8 / 1 h / 120°C.

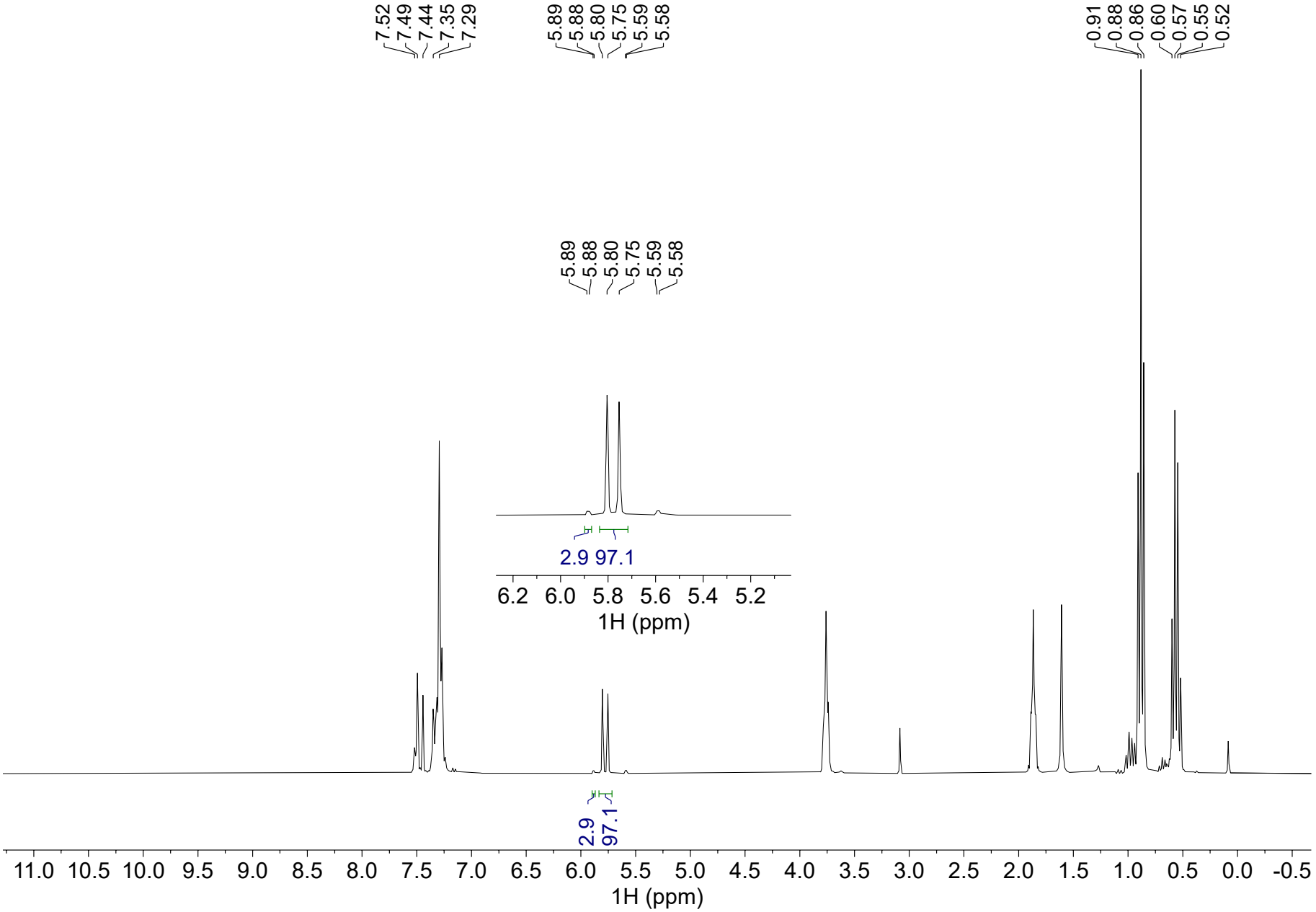
7.52
7.49
7.44
7.35
7.29
5.89
5.88
5.80
5.75
5.59
5.58
0.91
0.88
0.86
0.60
0.57
0.55
0.52
2.9 97.1
6.2 6.0 5.8 5.6 5.4 5.2
1H (ppm)
2.9
97.1
11.0 10.5 10.0 9.5 9.0 8.5 8.0 7.5 7.0 6.5 6.0 5.5 5.0 4.5 4.0 3.5 3.0 2.5 2.0 1.5 1.0 0.5 0.0 -0.5
1H (ppm)

Figure S35. ^{1}H NMR spectrum (300 MHz, $CDCl_3$) of the product mixture from the hydrosilylation of phenylacetylene; **Rh/IrC$_{11}$–b** / THF/ 1 h / 75°C.

Reactions Involving 1,4-Diethynylbenzene

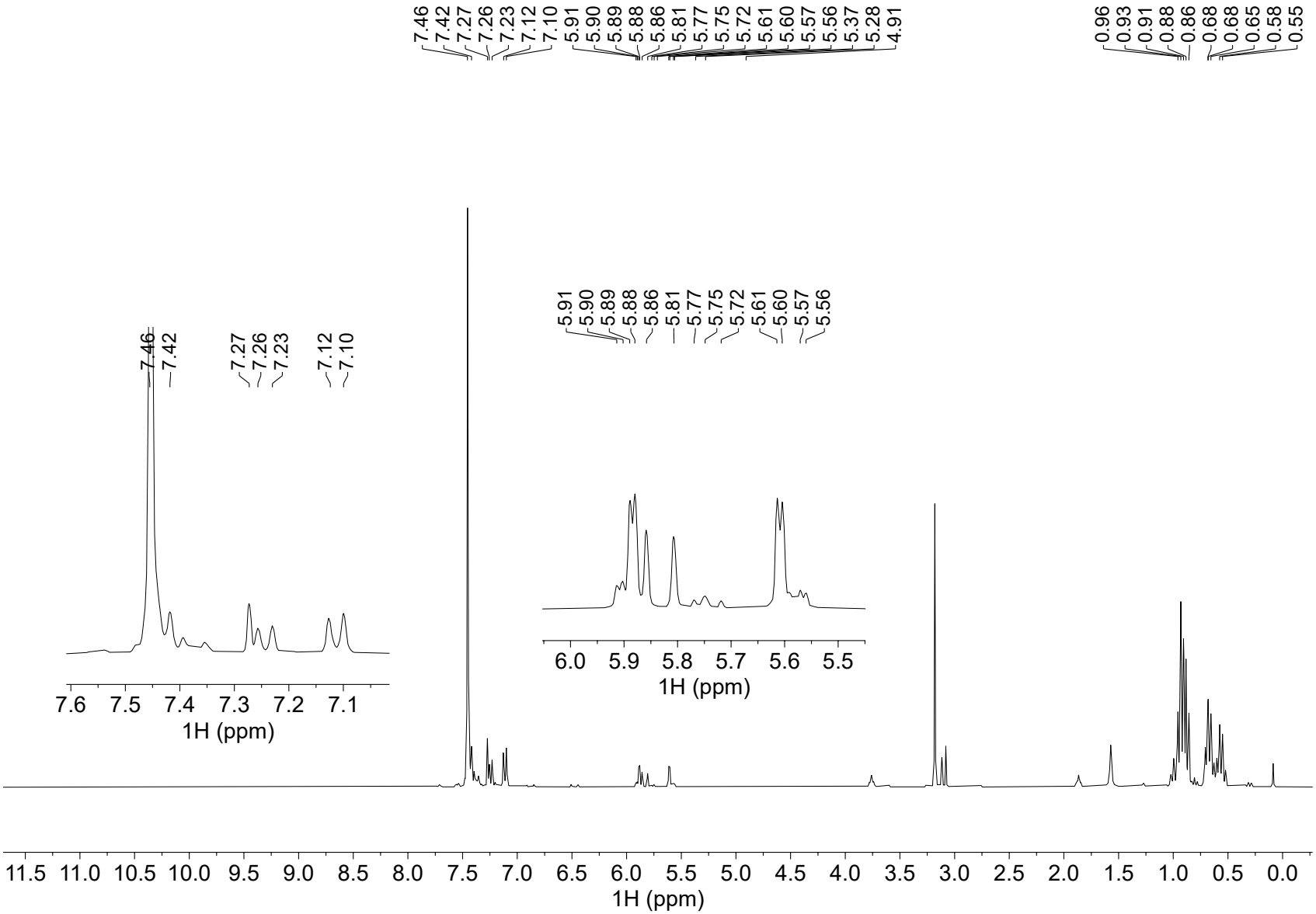

Figure S36. ^{1}H NMR spectrum (300 MHz, $CDCl_3$) of the product mixture from the hydrosilylation of 1,4-diethynylbenzene; **Rh/IrC$_{11}$–a** / THF/ 1 h / 75°C / 1.8 Eq. silane.

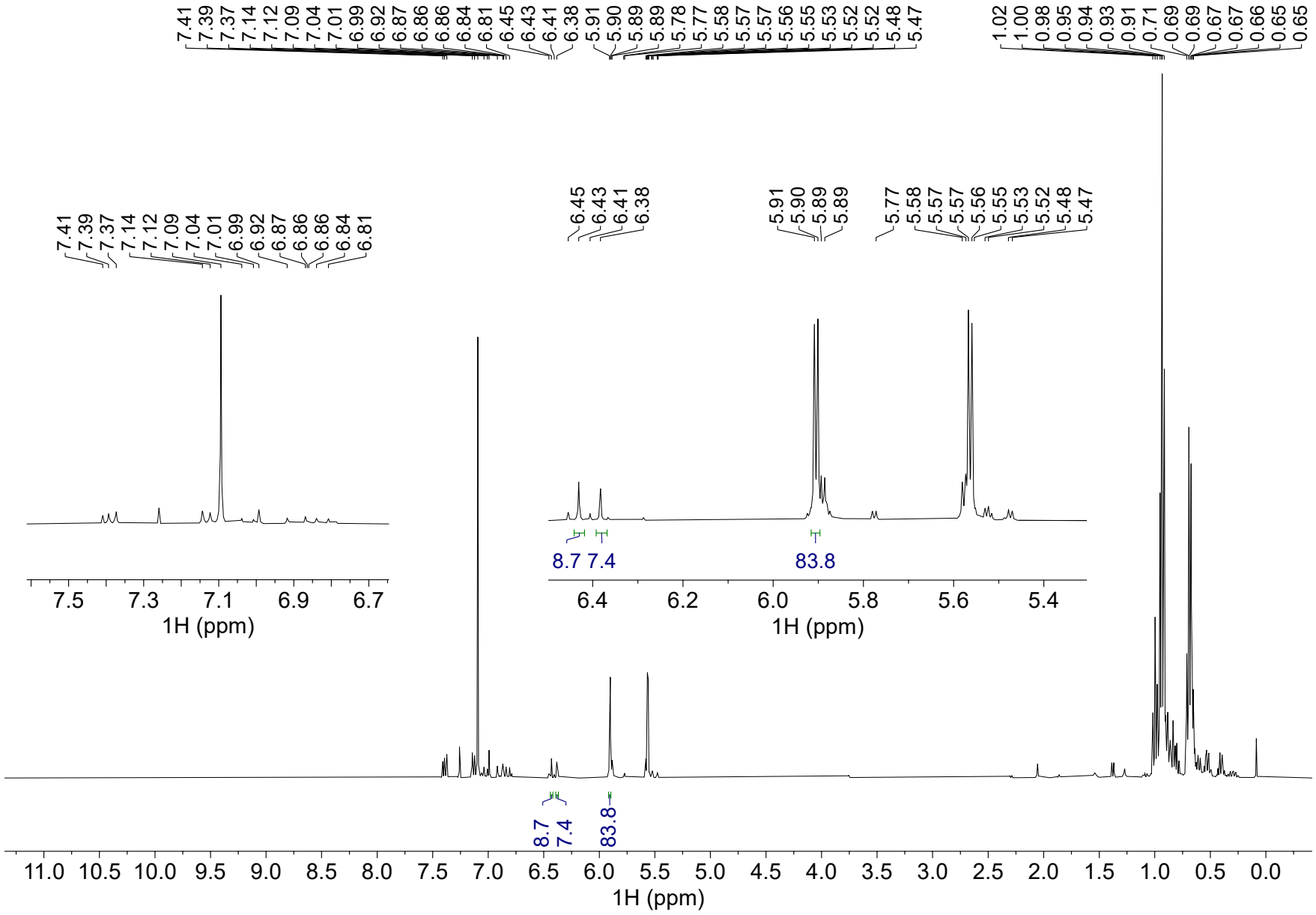

Figure S37. ^{1}H NMR spectrum (300 MHz, $CDCl_3$) of the product mixture from the hydrosilylation of 1,4-diethynylbenzene; **Rh/IrC$_{11}$–a** / THF/ 15 h / 75°C / 3.6 eq. silane

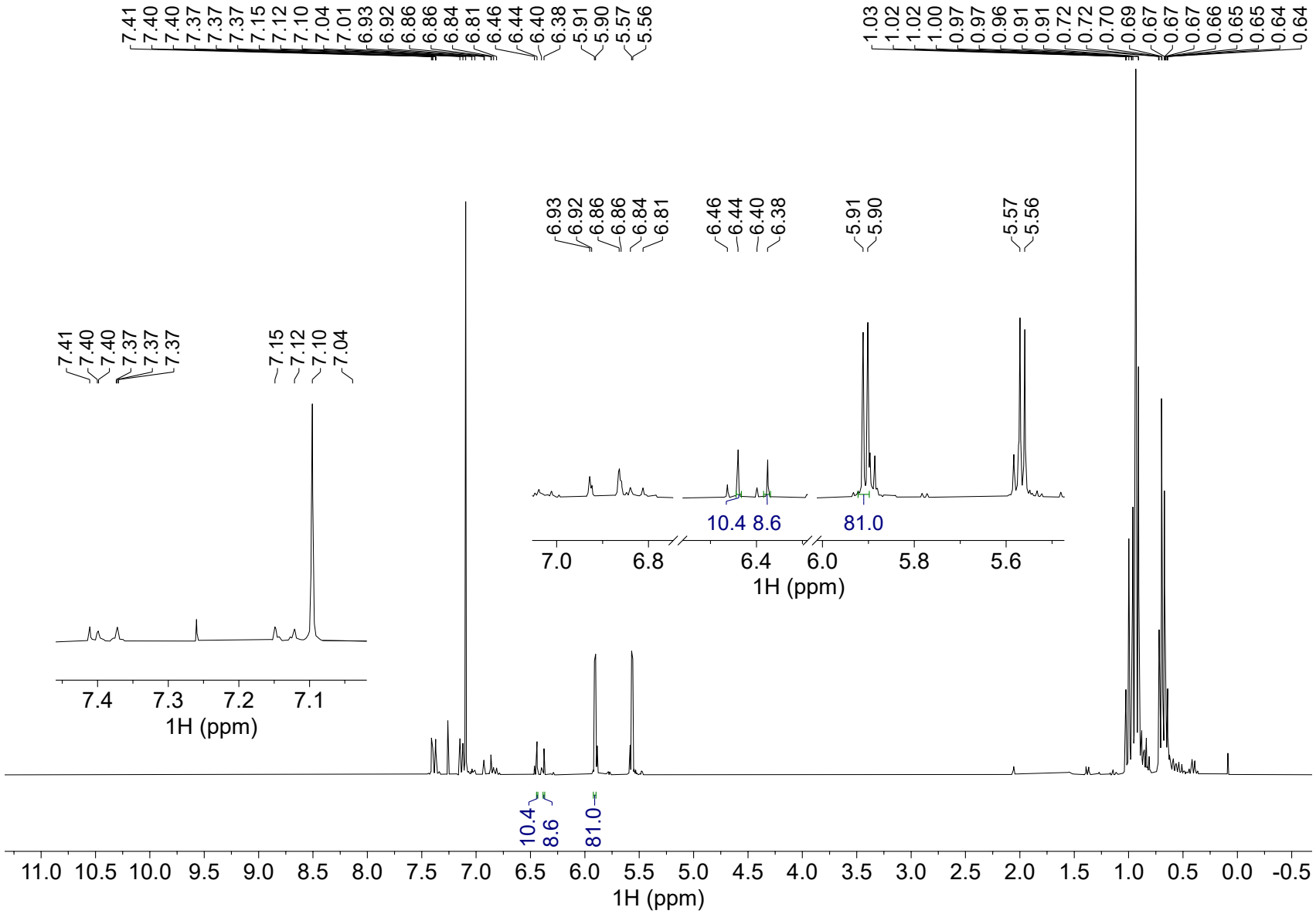

Figure S38. ^{1}H NMR spectrum (300 MHz, $CDCl_3$) of the product mixture from the hydrosilylation of 1,4-diethynylbenzene; **Rh/IrC$_{11}$–a** / THF/ 24 h / 75°C.

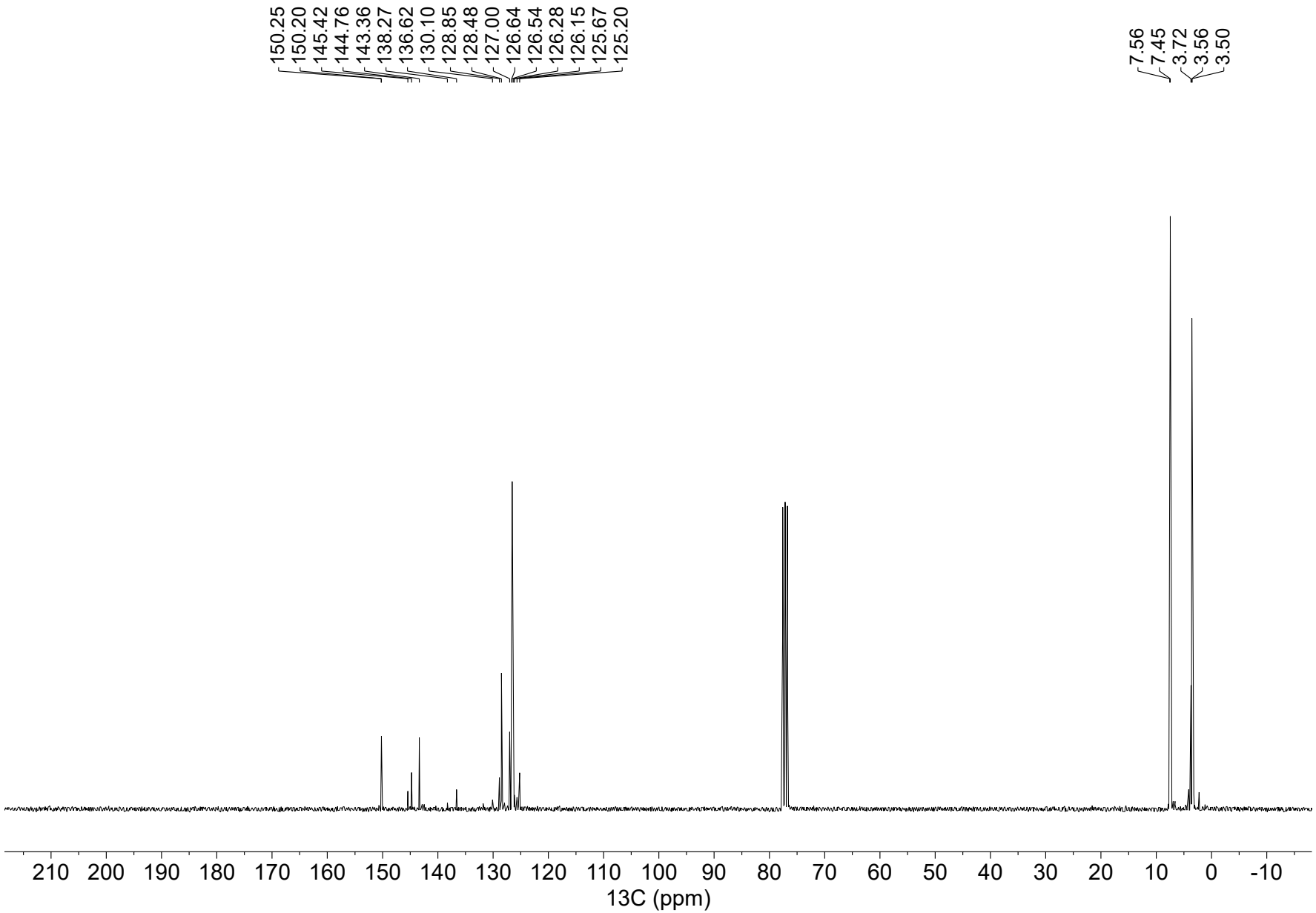
150.25
150.20
145.42
144.76
143.36
138.27
136.62
130.10
128.85
128.48
127.00
126.64
126.54
126.28
126.15
125.67
125.20
7.56
7.45
3.72
3.56
3.50
210 200 190 180 170 160 150 140 130 120 110 100 90 80 70 60 50 40 30 20 10 0 -10
13C (ppm)

Figure S39. ^{13}C NMR spectrum (75 MHz, $CDCl_3$) of the product mixture from the hydrosilylation of 1,4-diethynylbenzene.

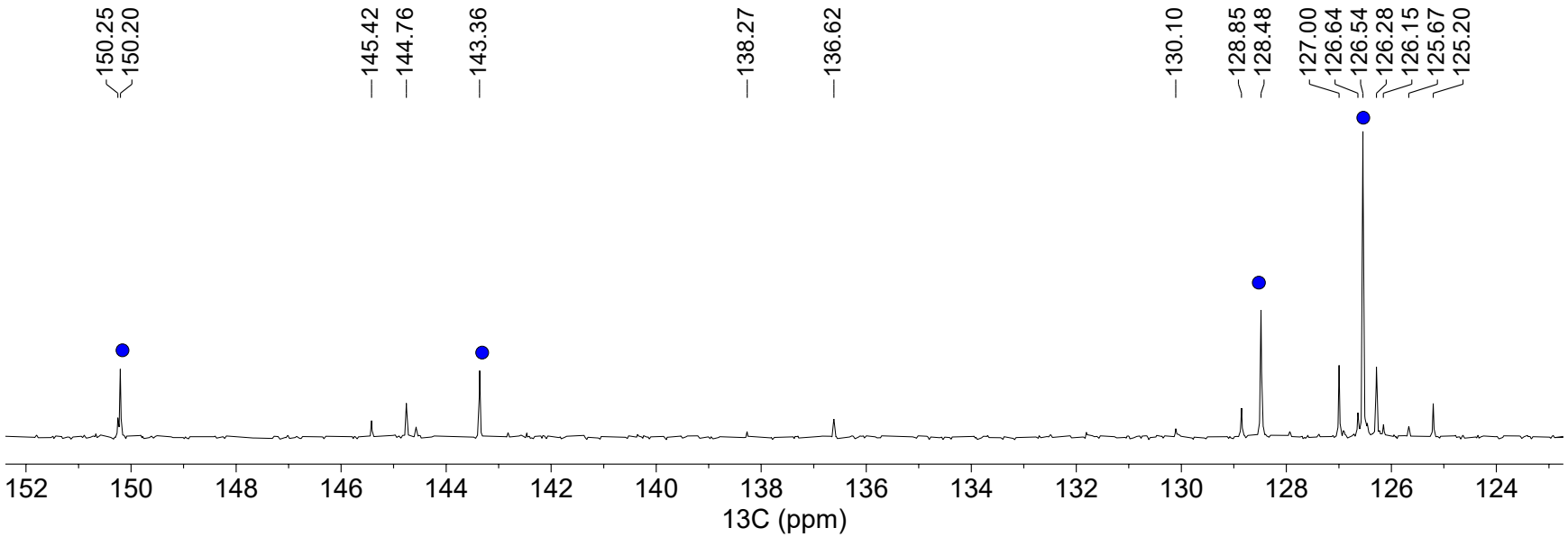
150.25
150.20
145.42
144.76
143.36
138.27
136.62
130.10
128.85
128.48
127.00
126.64
126.54
126.28
126.15
125.67
125.20
152 150 148 146 144 142 140 138 136 134 132 130 128 126 124
13C (ppm)

1H

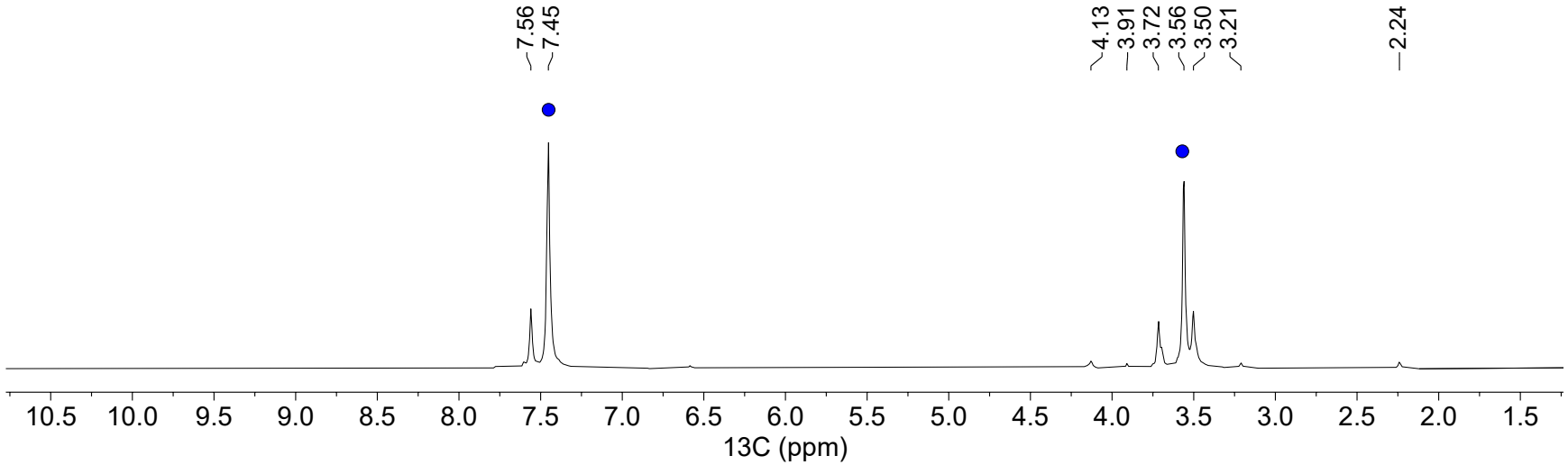
7.56
7.45
4.13
3.91
3.72
3.56
3.50
3.21
2.24
10.5 10.0 9.5 9.0 8.5 8.0 7.5 7.0 6.5 6.0 5.5 5.0 4.5 4.0 3.5 3.0 2.5 2.0 1.5
13C (ppm)

Figure S40. Selected ranges of the ^{13}C NMR spectrum (75 MHz, $CDCl_3$) of the the product mixture from hydrosilylation of 1,4-diethynylbenzene. The resonances of the α,α-product are marked with a blue indicator.

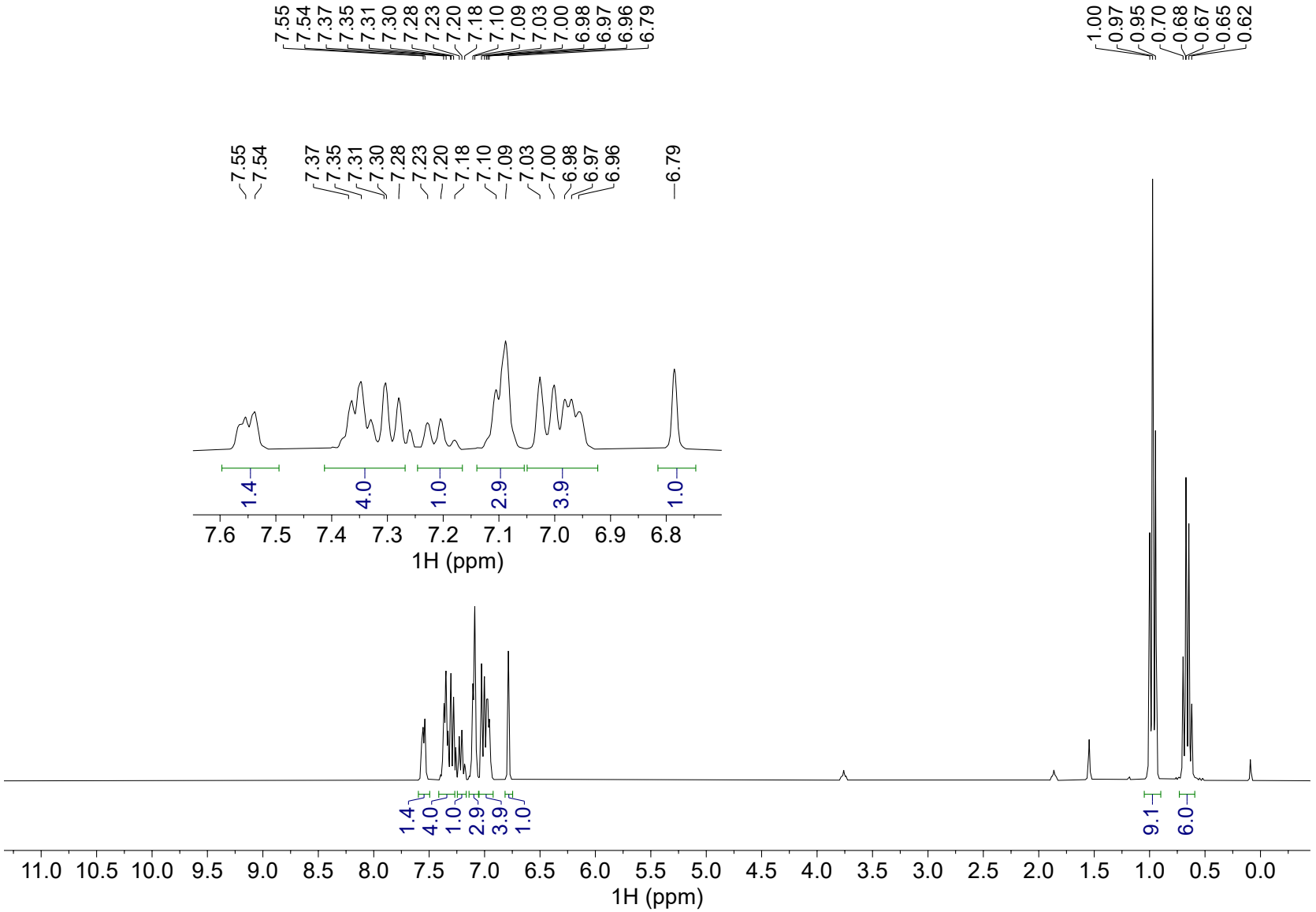
7.55
7.54
7.37
7.35
7.31
7.30
7.28
7.23
7.20
7.18
7.10
7.09
7.03
7.00
6.98
6.97
6.96
6.79
1.00
0.97
0.95
0.70
0.68
0.67
0.65
0.62
1.4
4.0
1.0
2.9
3.9
1.0
7.6 7.5 7.4 7.3 7.2 7.1 7.0 6.9 6.8
1H (ppm)
1.4
4.0
1.0
2.9
3.9
1.0
9.1
6.0
11.0 10.5 10.0 9.5 9.0 8.5 8.0 7.5 7.0 6.5 6.0 5.5 5.0 4.5 4.0 3.5 3.0 2.5 2.0 1.5 1.0 0.5 0.0
1H (ppm)

Figure S41. ^{1}H NMR spectrum (300 MHz, $CDCl_3$) of the product mixture from the hydrosilylation of diphenylacetylene; **Rh/IrC$_{11}$–a** / THF/ 1 h / 75°C.

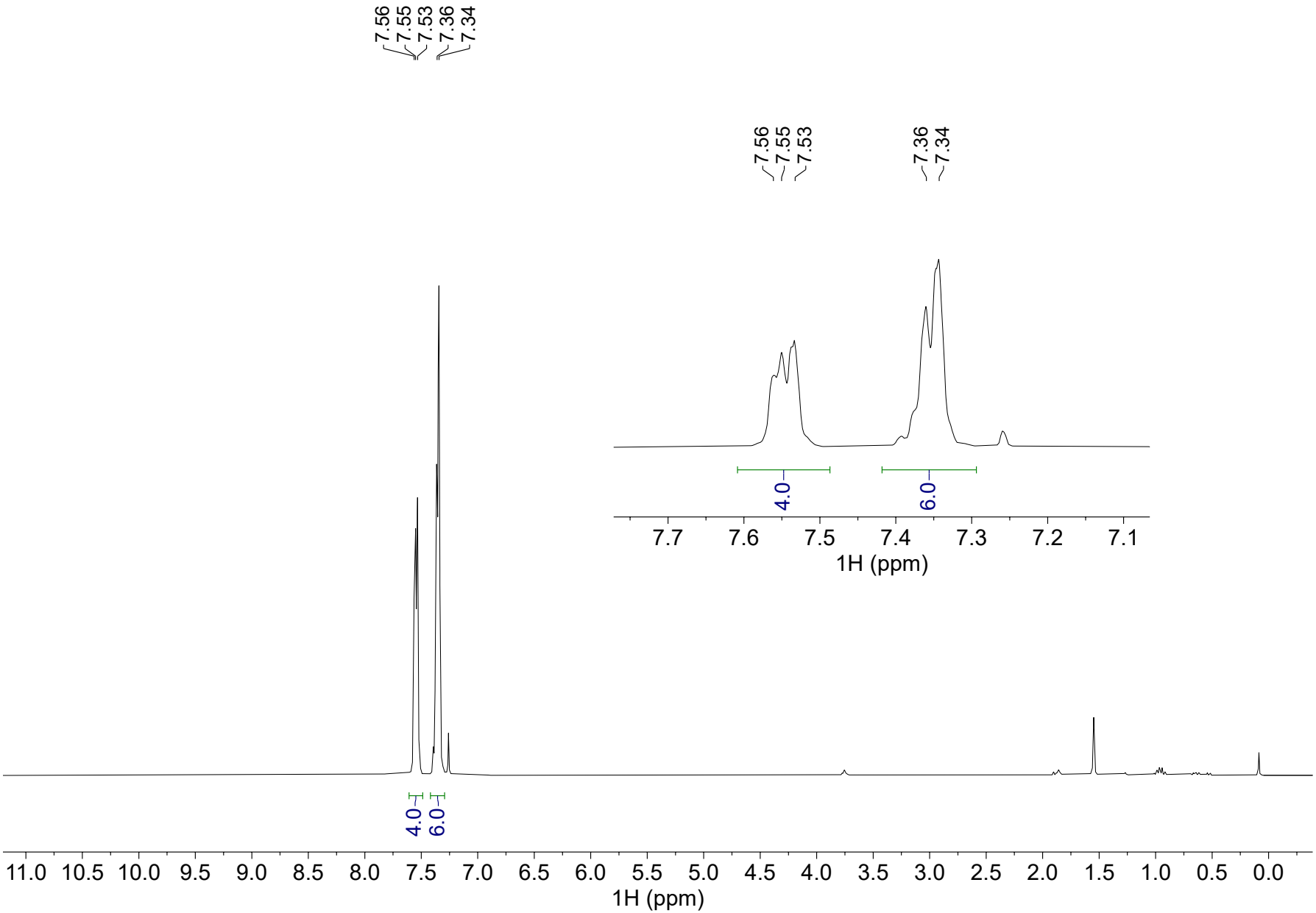
7.56
7.55
7.53
7.36
7.34
4.0
6.0
11.0 10.5 10.0 9.5 9.0 8.5 8.0 7.5 7.0 6.5 6.0 5.5 5.0 4.5 4.0 3.5 3.0 2.5 2.0 1.5 1.0 0.5 0.0
1H (ppm)
7.56
7.55
7.53
7.36
7.34
4.0
6.0
7.7 7.6 7.5 7.4 7.3 7.2 7.1
1H (ppm)

Figure S42. ^{1}H NMR spectrum (300 MHz, $CDCl_3$) of the product mixture from the attempted hydrosilylation of diphenylacetylene; **Rh/IrC$_{11}$–b** / THF/ 1 h / 75°C.

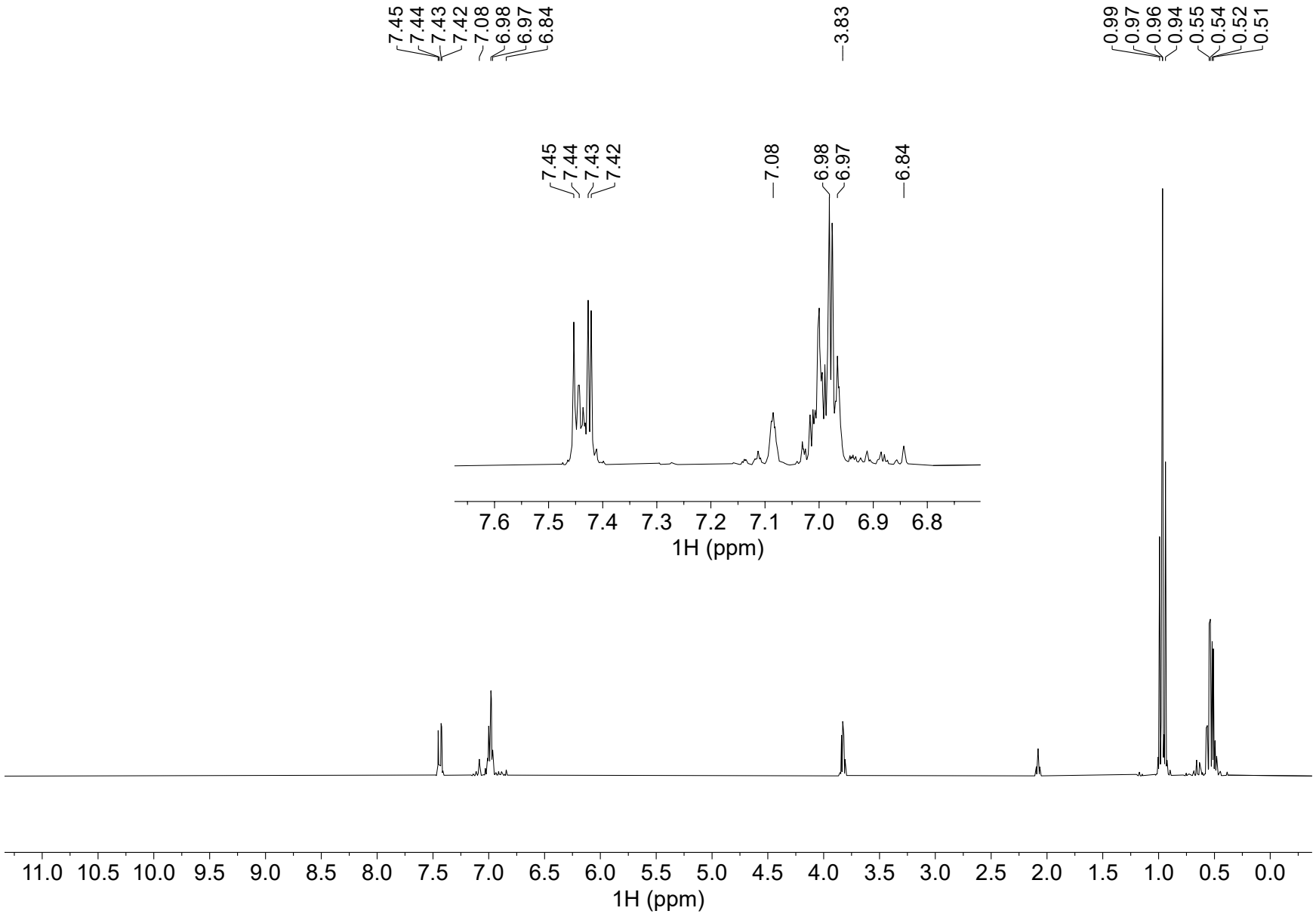

Figure S43. ^{1}H NMR spectrum (300 MHz, toluene-d^{8}) of the product mixture from the attempted hydrosilylation of diphenylacetylene; **Rh/IrC$_{11}$–b** / toluene-d^{8} / 1 h / 120°C.

Reactions Involving 1,4-Diphenylbutadiyne

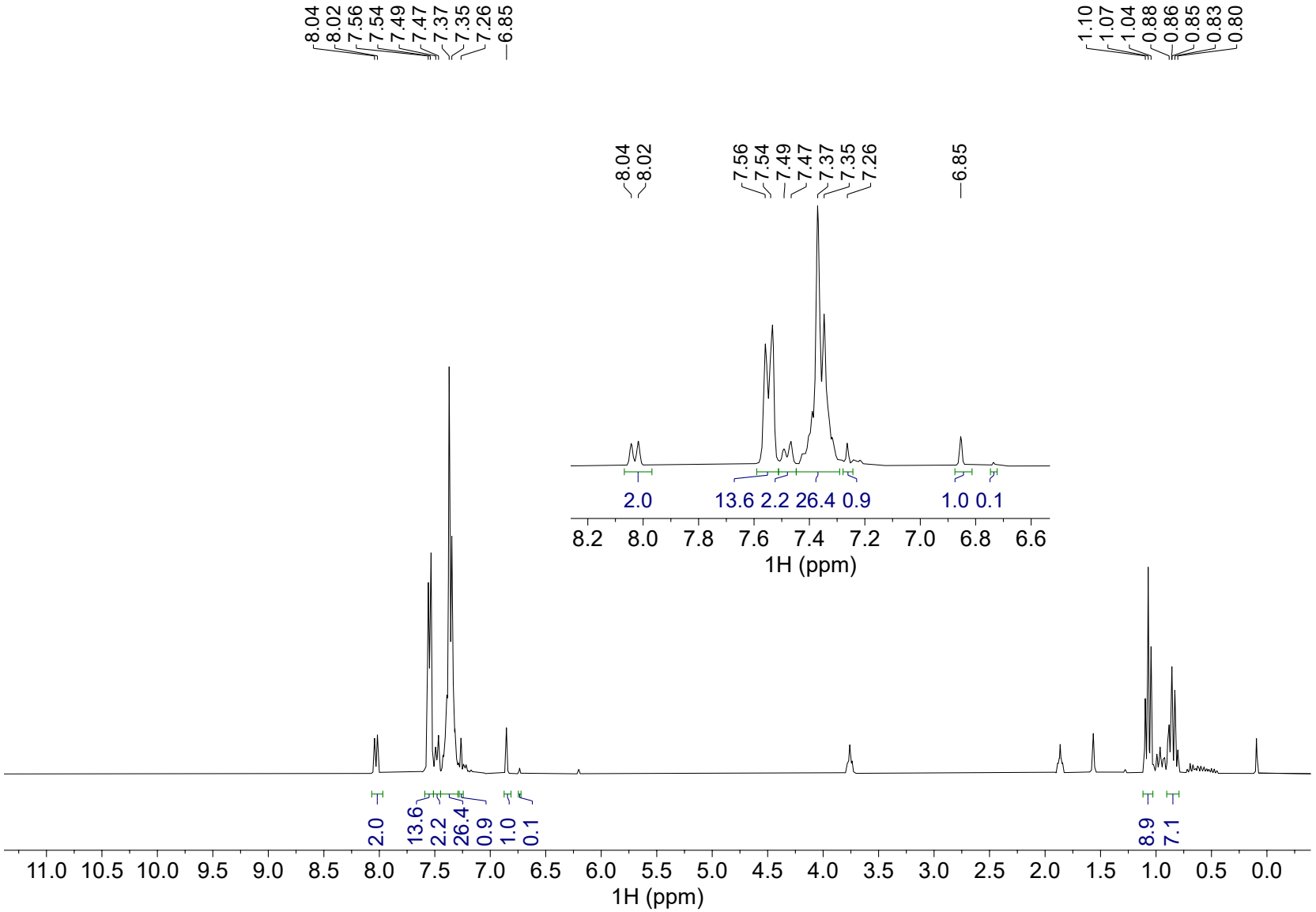

Figure S44. ^{1}H NMR spectrum (300 MHz, $CDCl_3$) of the product mixture from the hydrosilylation of 1,4-diphenylbutadiyne; **Rh/IrC$_{11}$–a** / THF/ 1 h / 75°C.

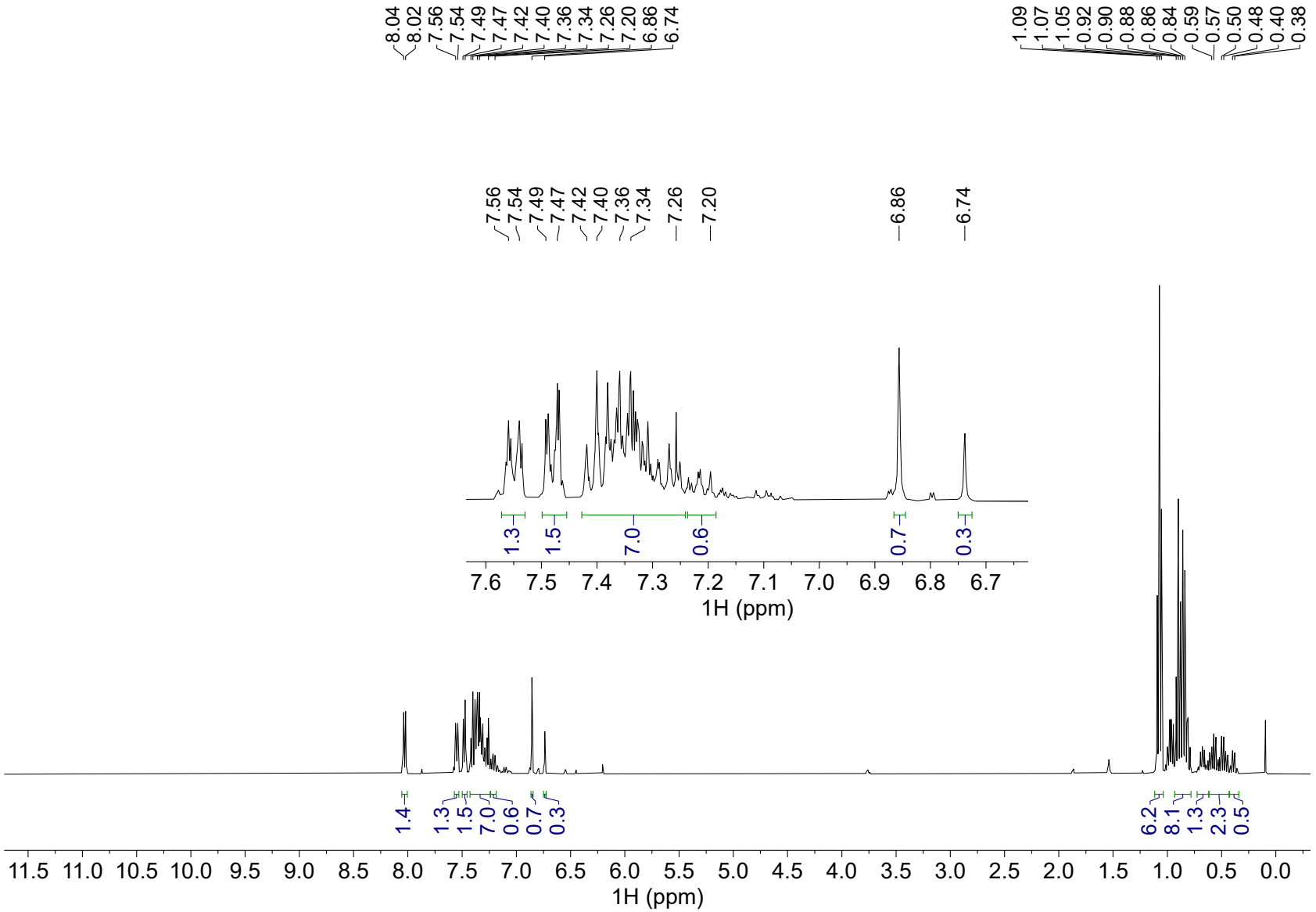

Figure S45. ^{1}H NMR spectrum (400 MHz, $CDCl_3$) of the product mixture from the hydrosilylation of 1,4-diphenylbutadiyne; **Rh/IrC$_{11}$–a** / THF/ 15 h / 75°C.

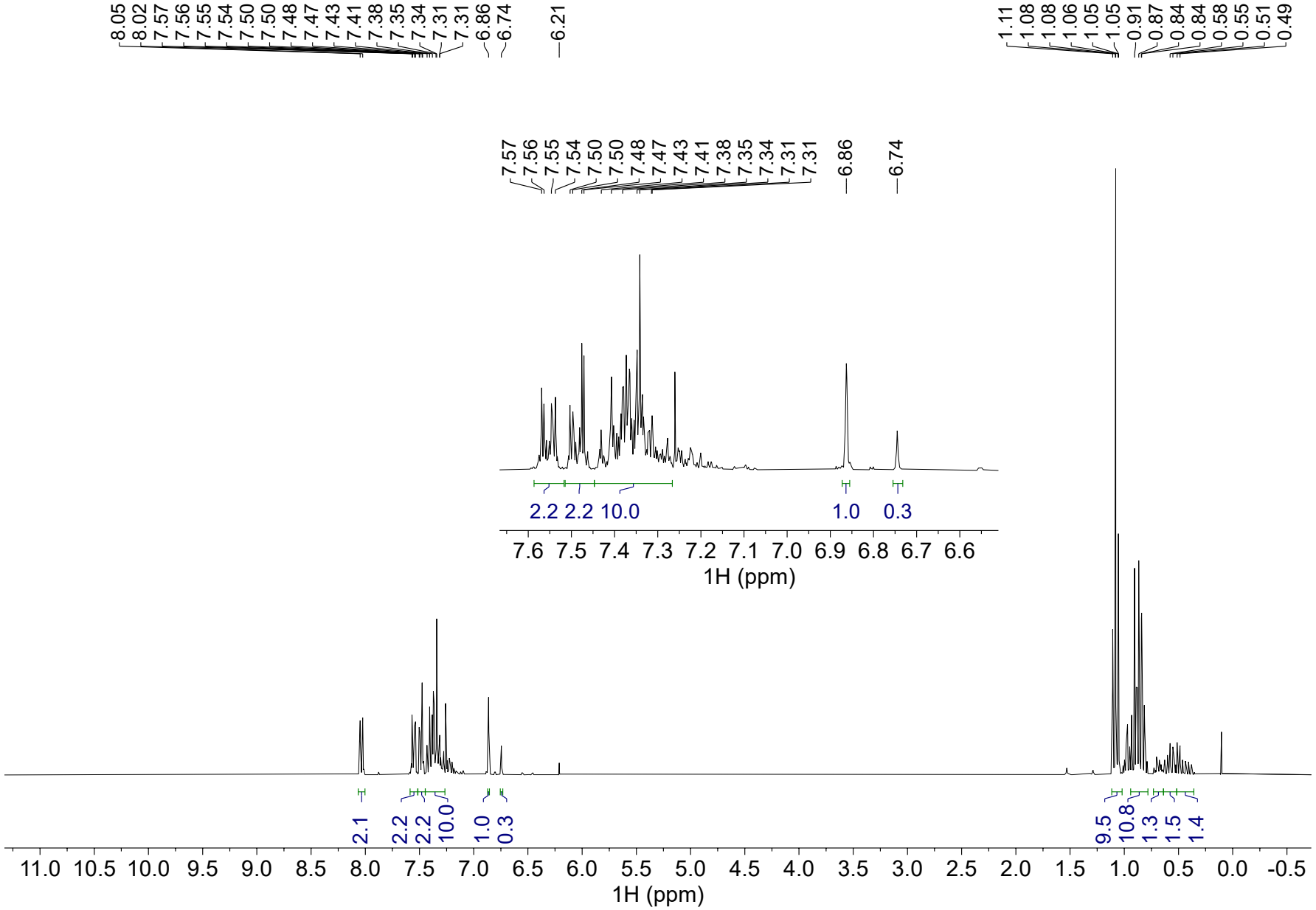
8.05
8.02
7.57
7.56
7.55
7.54
7.50
7.50
7.48
7.47
7.43
7.41
7.38
7.35
7.34
7.31
7.31
6.86
6.74
6.21
1.11
1.08
1.08
1.06
1.05
1.05
0.91
0.87
0.84
0.84
0.58
0.55
0.51
0.49
2.2 2.2 10.0
1.0
0.3
7.6 7.5 7.4 7.3 7.2 7.1 7.0 6.9 6.8 6.7 6.6
1H (ppm)
2.1
2.2
2.2
10.0
1.0
0.3
9.5
10.8
1.3
1.5
1.4
11.0 10.5 10.0 9.5 9.0 8.5 8.0 7.5 7.0 6.5 6.0 5.5 5.0 4.5 4.0 3.5 3.0 2.5 2.0 1.5 1.0 0.5 0.0 -0.5
1H (ppm)

Figure S46. ^{1}H NMR spectrum (300 MHz, $CDCl_3$) of the product mixture from the hydrosilylation of 1,4-diphenylbutadiyne; **Rh/IrC$_{11}$–a** / THF/ 24 h / 75°C.

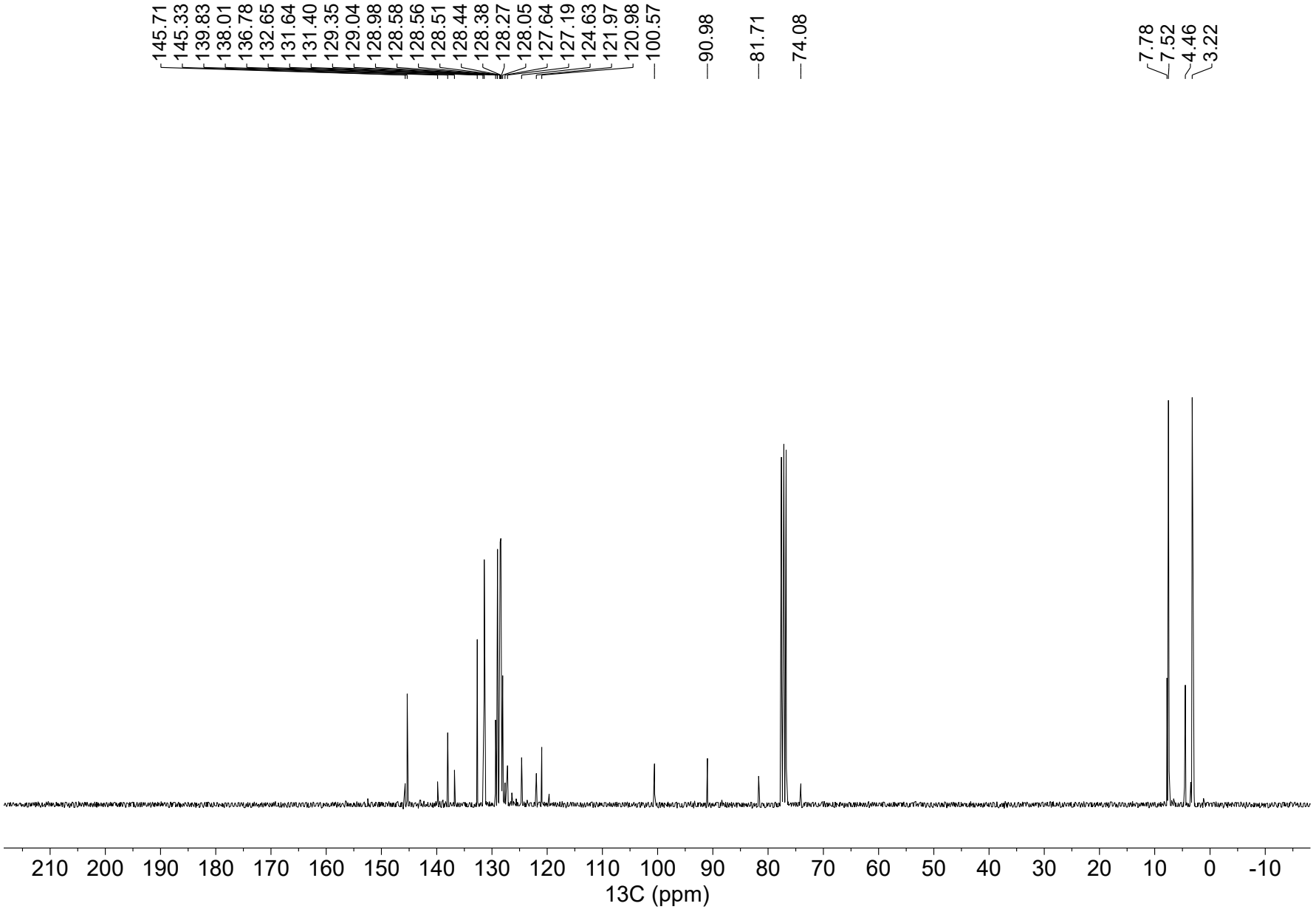
145.71
145.33
139.83
138.01
136.78
132.65
131.64
131.40
129.35
129.04
128.98
128.58
128.56
128.51
128.44
128.38
128.27
128.05
127.64
127.19
124.63
121.97
120.98
100.57
90.98
81.71
74.08
7.78
7.52
4.46
3.22
210 200 190 180 170 160 150 140 130 120 110 100 90 80 70 60 50 40 30 20 10 0 -10
13C (ppm)

Figure S47. ^{13}C NMR spectrum (75 MHz, $CDCl_3$) of the product mixture from the hydrosilylation of 1,4-diphenylbutadiyne; **Rh/IrC$_{11}$–a** / THF/ 24 h / 75°C.

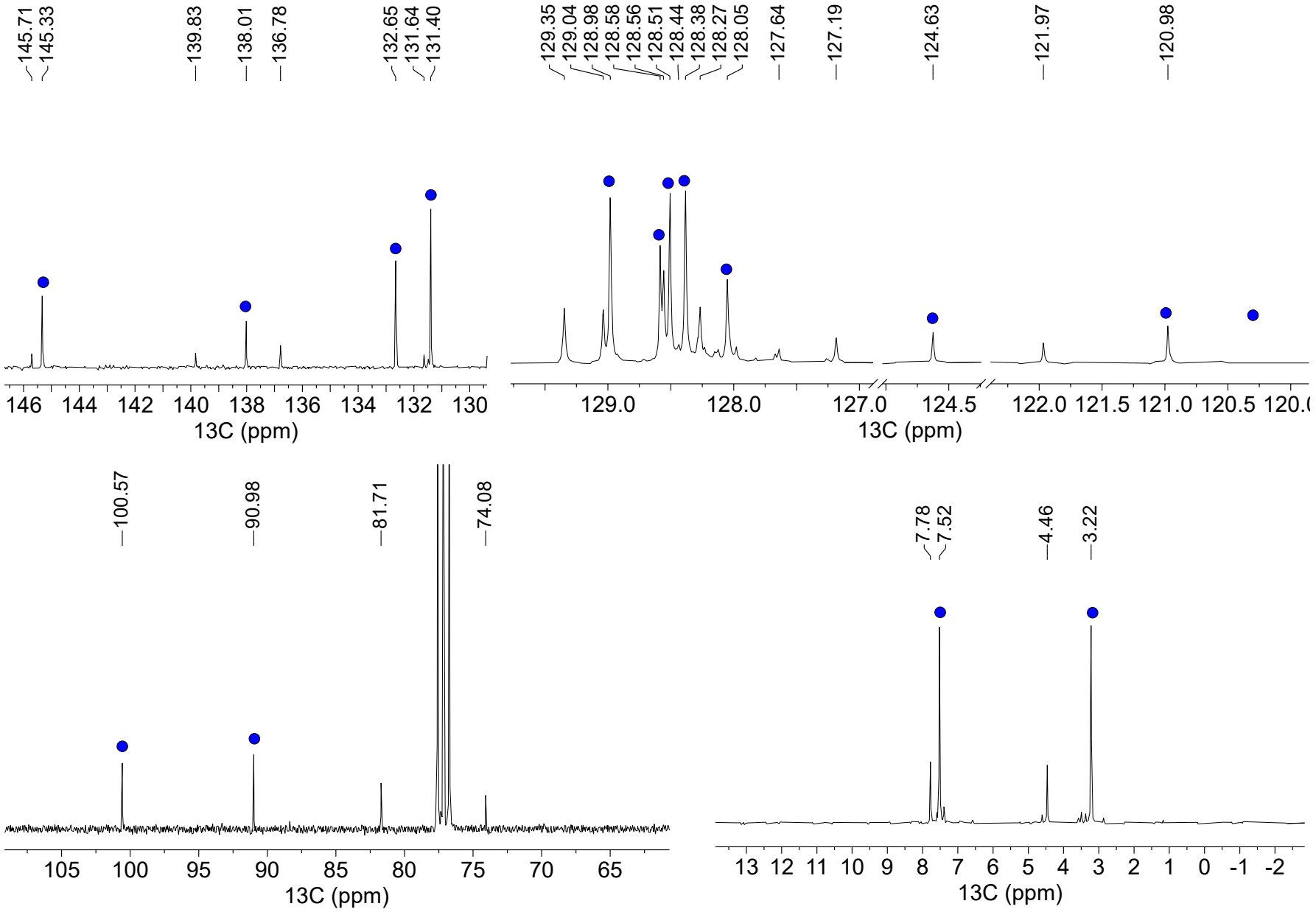
145.71
145.33
139.83
138.01
136.78
132.65
131.64
131.40
129.35
129.04
128.98
128.58
128.56
128.51
128.44
128.38
128.27
128.05
127.64
127.19
124.63
121.97
120.98
146 144 142 140 138 136 134 132 130
13C (ppm)
129.0 128.0 127.0 124.5 122.0 121.5 121.0 120.5 120.0
13C (ppm)
100.57
90.98
81.71
74.08
105 100 95 90 85 80 75 70 65
13C (ppm)
7.78
7.52
4.46
3.22
13 12 11 10 9 8 7 6 5 4 3 2 1 0 -1 -2
13C (ppm)

Figure S48. Selected ranges of the ^{13}C NMR spectrum (75 MHz, $CDCl_3$) of the product mixture from the hydrosilylation of 1,4-diphenylbutadiyne; **Rh/IrC$_{11}$–a** / THF/ 24 h / 75°C. The resonances of the *E*-product are marked with a blue indicator.

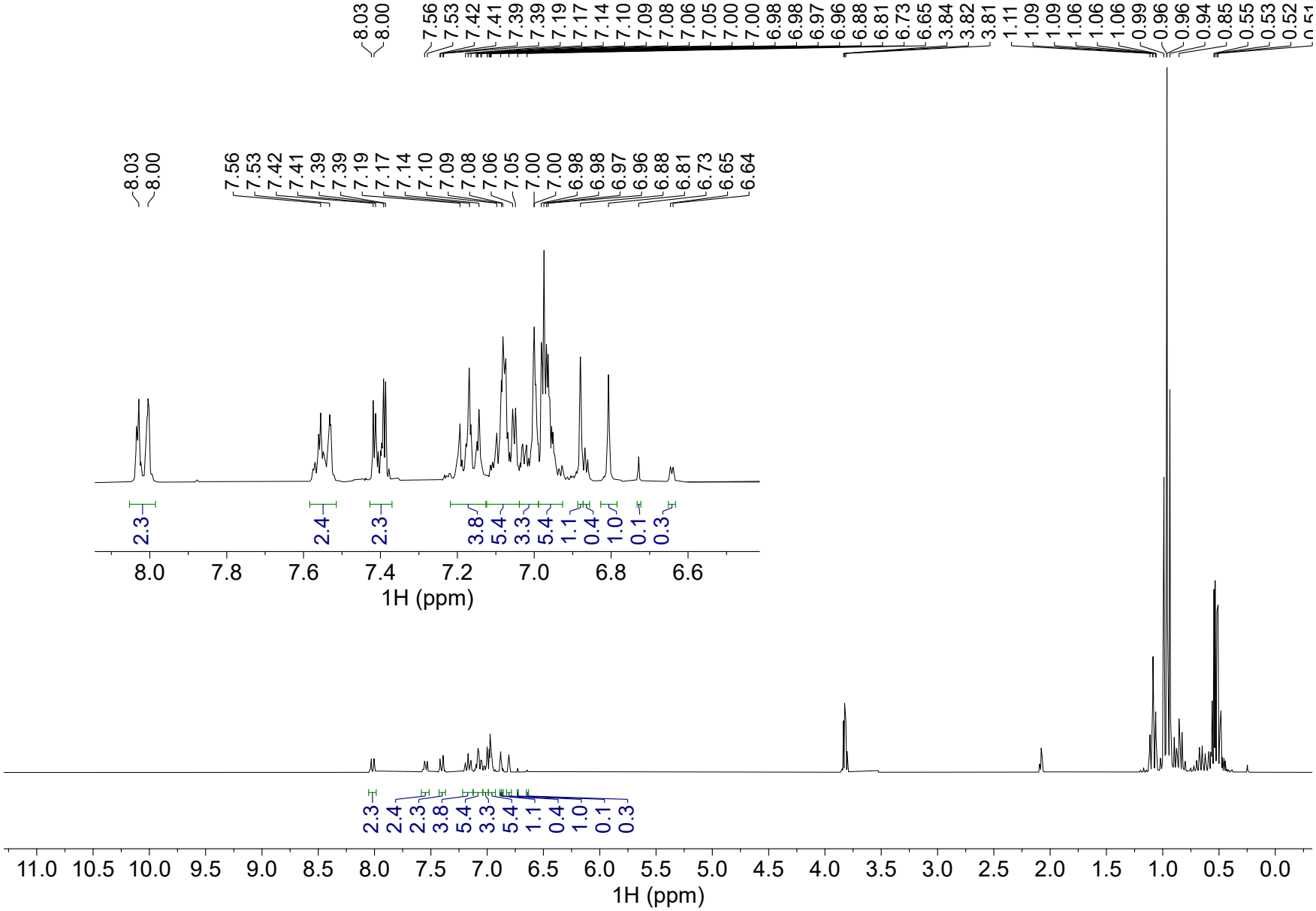
8.03
8.00
7.56
7.53
7.42
7.41
7.39
7.39
7.19
7.17
7.14
7.10
7.09
7.08
7.06
7.05
7.00
7.00
6.98
6.98
6.97
6.96
6.88
6.81
6.73
6.65
3.84
3.82
3.81
1.11
1.09
1.09
1.06
1.06
1.06
0.99
0.96
0.96
0.94
0.85
0.55
0.53
0.52
2.3
2.4
2.3
3.8
5.4
3.3
5.4
1.1
0.4
1.0
0.1
0.3
8.0
7.8
7.6
7.4
7.2
7.0
6.8
6.6
1H (ppm)
11.0
10.5
10.0
9.5
9.0
8.5
8.0
7.5
7.0
6.5
6.0
5.5
5.0
4.5
4.0
3.5
3.0
2.5
2.0
1.5
1.0
0.5
0.0
1H (ppm)

Figure S49. ^{1}H NMR spectrum (300 MHz, toluene-d^{8}) of the product mixture from the hydrosilylation of 1,4-diphenylbutadiyne; **Rh/IrC$_{11}$–a** / toluene-d^{8} / 1 h / 120°C.

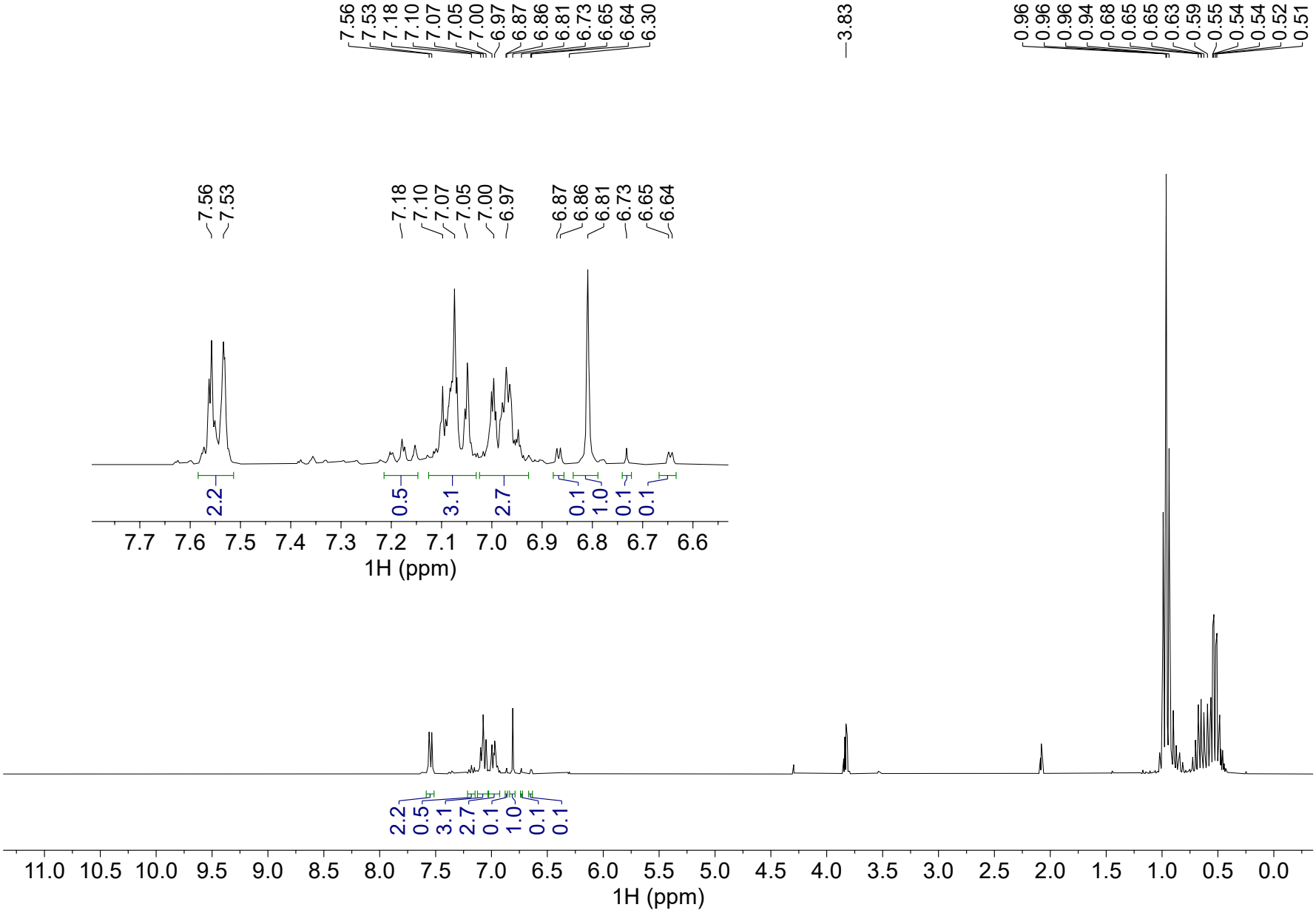
7.56
7.53
7.18
7.10
7.07
7.05
7.00
6.97
6.87
6.86
6.81
6.73
6.65
6.64
6.30
3.83
0.96
0.96
0.96
0.94
0.68
0.65
0.65
0.63
0.59
0.55
0.54
0.54
0.52
0.51
2.2
0.5
3.1
2.7
0.1
1.0
0.1
0.1
7.7 7.6 7.5 7.4 7.3 7.2 7.1 7.0 6.9 6.8 6.7 6.6
1H (ppm)
11.0 10.5 10.0 9.5 9.0 8.5 8.0 7.5 7.0 6.5 6.0 5.5 5.0 4.5 4.0 3.5 3.0 2.5 2.0 1.5 1.0 0.5 0.0
1H (ppm)

Figure S50. ^{1}H NMR spectrum (300 MHz, toluene-d^{8}) of the product mixture from the hydrosilylation of 1,4-diphenylbutadiyne; **Rh/IrC$_{11}$–a** / toluene-d^{8} / 24 h / 120°C.

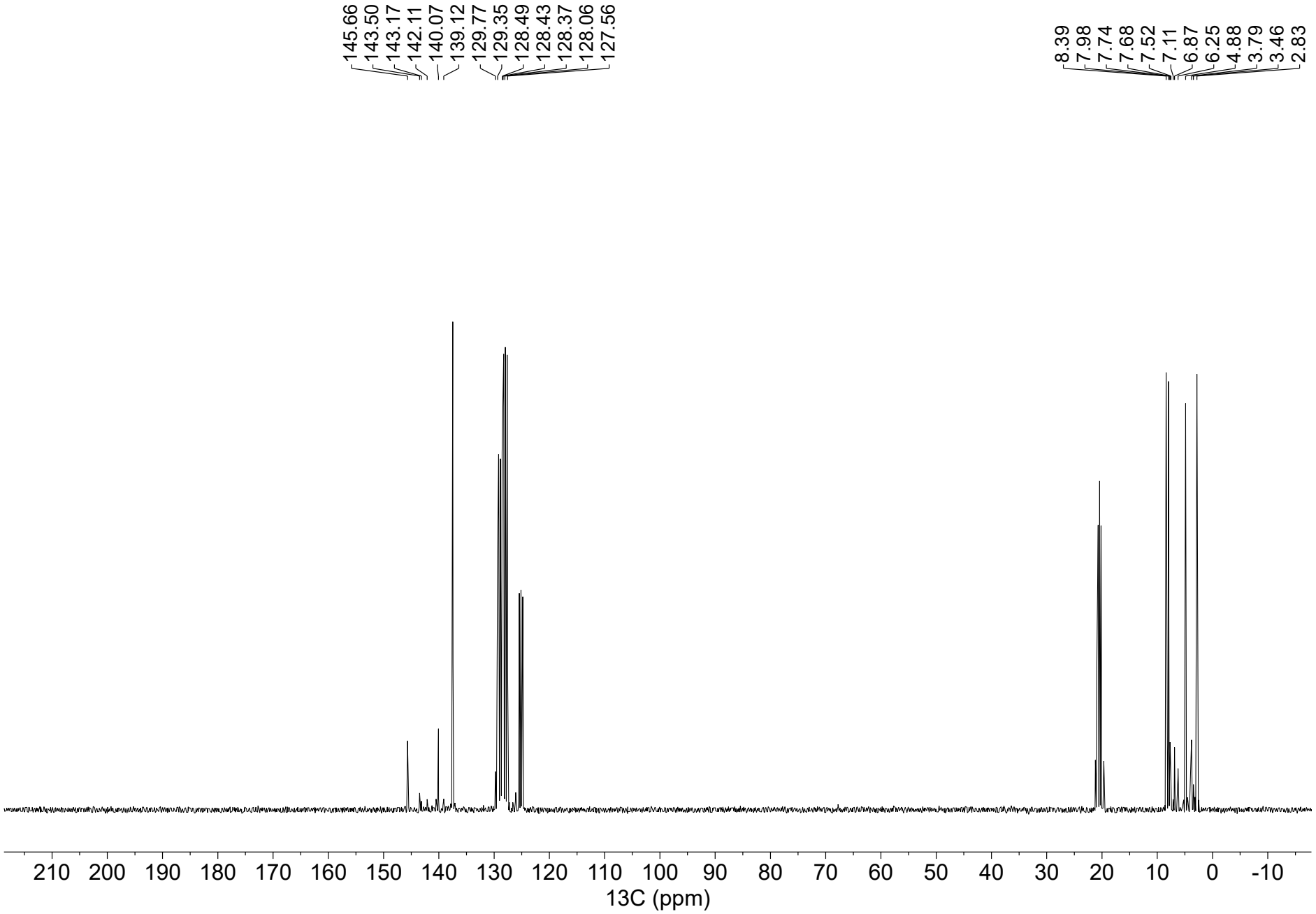
145.66
143.50
143.17
142.11
140.07
139.12
129.77
129.35
128.49
128.43
128.37
128.06
127.56
8.39
7.98
7.74
7.68
7.52
7.11
6.87
6.25
4.88
3.79
3.46
2.83
210 200 190 180 170 160 150 140 130 120 110 100 90 80 70 60 50 40 30 20 10 0 -10
13C (ppm)

Figure S51. ^{13}C NMR spectrum (75 MHz, toluene-d^8) of the hydrosilylation of 1,4-diphenylbutadiyne; **Rh/IrC$_{11}$–a** / toluene-d^8 / 24 h / 120°C.

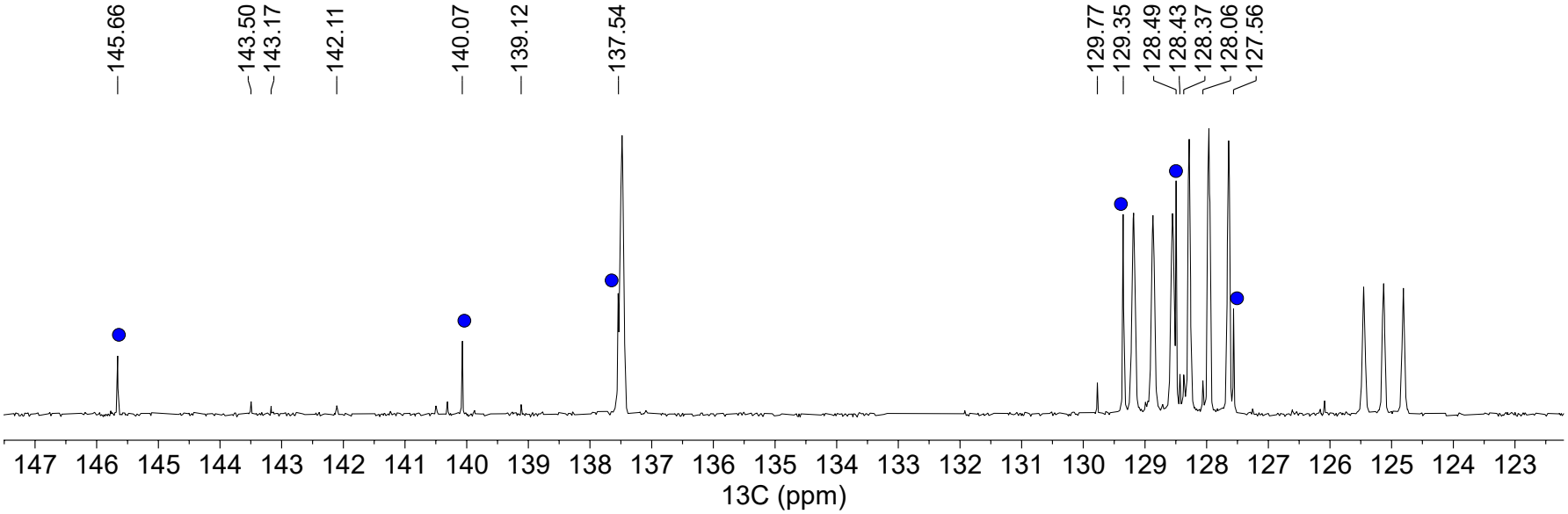
145.66
143.50
143.17
142.11
140.07
139.12
137.54
129.77
129.35
128.49
128.43
128.37
128.06
127.56
147 146 145 144 143 142 141 140 139 138 137 136 135 134 133 132 131 130 129 128 127 126 125 124 123
13C (ppm)

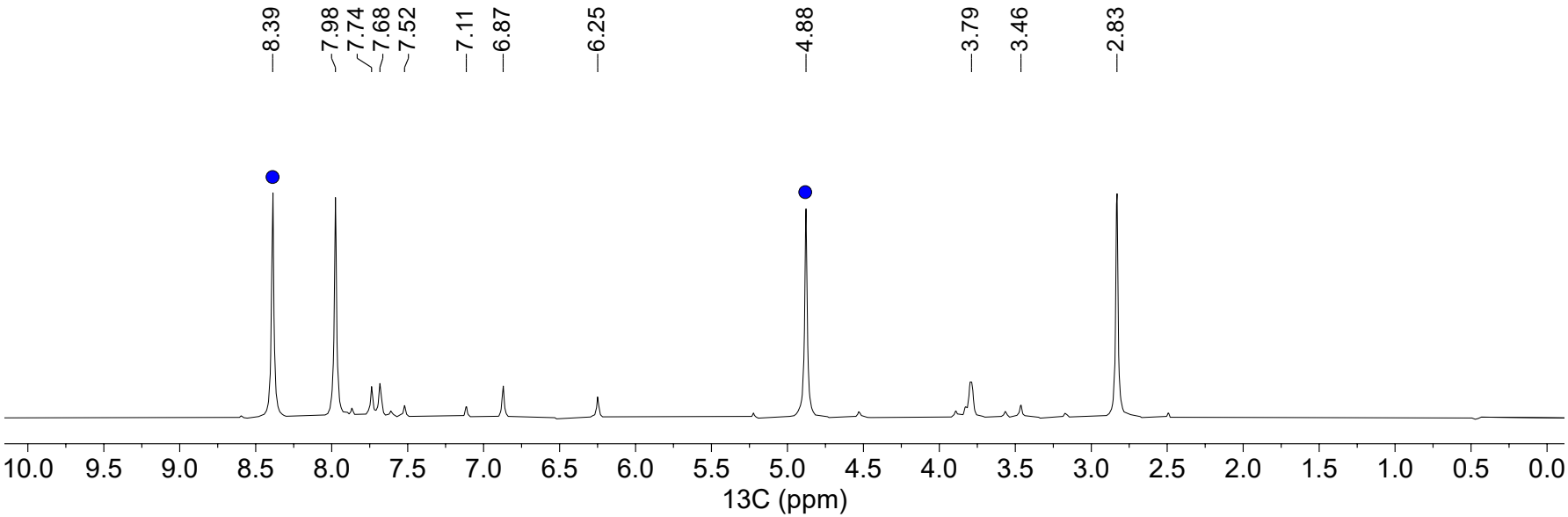
8.39
7.98
7.74
7.68
7.52
7.11
6.87
6.25
4.88
3.79
3.46
2.83
10.0 9.5 9.0 8.5 8.0 7.5 7.0 6.5 6.0 5.5 5.0 4.5 4.0 3.5 3.0 2.5 2.0 1.5 1.0 0.5 0.0
13C (ppm)

Figure S52. Selected ranges of the ^{13}C NMR spectrum (75 MHz, toluene-d^8) of the product mixture from the hydrosilylation of 1,4-diphenylbutadiyne. The resonances of the *E,E*-product are marked with a blue indicator.